Available online at www.sciencedirect.com
ScienceDirect
Advanced Drug Delivery Reviews 58 (2006) 1274–1325
Advanced DRUG DELIVERY Reviews
www.elsevier.com/locate/addr

Mathematical modeling and simulation of drug release from microspheres: Implications to drug delivery systems ☆

Davis Yohanes Arifin [a], Lai Yeng Lee [a], Chi-Hwa Wang [a,b,*]

[a] *Molecular Engineering of Biological and Chemical Systems Program, Singapore–MIT Alliance, 4 Engineering Drive 3, Singapore 117576, Singapore*

[b] *Department of Chemical and Biomolecular Engineering, National University of Singapore, 4 Engineering Drive 4, Singapore 117576, Singapore*

Received 13 July 2006; accepted 4 September 2006
Available online 26 September 2006

Abstract

This article aims to provide a comprehensive review of existing mathematical models and simulations of drug release from polymeric microspheres and of drug transport in adjacent tissues. In drug delivery systems, mathematical modeling plays an important role in elucidating the important drug release mechanisms, thus facilitating the development of new pharmaceutical products by a systematic, rather than trial-and-error, approach. The mathematical models correspond to the known release mechanisms, which are classified as diffusion-, swelling-, and erosion-controlled systems. Various practical applications of these models which explain experimental data are illustrated. The effect of γ-irradiation sterilization on drug release mechanism from erosion-controlled systems will be discussed. The application of existing models to nanoscale drug delivery systems specifically for hydrophobic and hydrophilic molecules is evaluated. The current development of drug transport modeling in tissues utilizing computational fluid dynamics (CFD) will also be described.

Keywords: Release mechanism; Polymeric system; Diffusion; Swelling; Erosion; Irradiation; Transport; Tissue; Brain; Computational fluid dynamics

Contents

☆ This review is part of the *Advanced Drug Delivery Reviews* theme issue on "Computational Drug Delivery", Vol. 58/12-13, 2006.

* Corresponding author. Department of Chemical and Biomolecular Engineering, National University of Singapore, 4 Engineering Drive 4, Singapore 117576, Singapore. Tel.: +65 6516 5079; fax: +65 6779 1936.
E-mail address: chewch@nus.edu.sg (C.-H. Wang).

0169-409X/$ - see front matter © 2006 Elsevier B.V. All rights reserved.
doi:10.1016/j.addr.2006.09.007

1. Introduction

For decades, polymeric systems have been used for pharmaceutical applications, especially to provide controlled release of drugs. Drug–polymer systems may also be useful in protecting the drug from biological degradation prior to its release. The development of these device starts with the use of non-biodegradable polymers, which rely on the diffusion process, and subsequently progresses to the use of biodegradable polymers, in which swelling and erosion take place.

Based on the physical or chemical characteristics of polymer, drug release mechanism from a polymer matrix can be categorized in accordance to three main processes (systems) [1], which are:

1. Drug diffusion from the non-degraded polymer (diffusion-controlled system).
2. Enhanced drug diffusion due to polymer swelling (swelling-controlled system).
3. Drug release due to polymer degradation and erosion (erosion-controlled system).

In all three systems, diffusion is always involved. For a non-biodegradable polymer matrix, drug release is due to the concentration gradient by either diffusion or matrix swelling (enhanced diffusion). For biodegradable polymer matrix, release is normally controlled by the hydrolytic cleavage of polymer chains that lead to matrix erosion, even though diffusion may be still dominant when the erosion is slow. This categorization allows mathematical models to be developed in different ways for each type of system.

Mathematical modeling of drug release provides insights concerning mass transport and chemical processes involved in drug delivery system as well as the effect of design parameters, such as the device geometry and drug loading, on drug release mechanism. Thus, the optimized device design for a required drug release profile can be predicted using a systematic approach with a minimum number of experimental studies.

This review presents the concepts contained in important and readily available mathematical models for controlled release primarily from microspheres. Mathematical models for cylindrical geometry, especially

for swelling- and erosion-controlled systems, will also be discussed as real systems are readily available in this geometry. It also discusses recent improvements and the major advantages and limitations of each model. The original notations are not retained in this review; instead a common notation is used to facilitate understanding and comparison between the models. The penultimate section of this review discusses the implication of phenomena at the nanoscale and the last section focuses on coupling to transport in tissue.

2. Mathematical models for diffusion-controlled systems

For diffusion-controlled microspheres, drug release profile is obtained by solving Fick's second law of diffusion subject to appropriate boundary conditions. For one-dimensional drug release from a microsphere, the second Fick's law of diffusion is given by:

$$\frac{\partial C}{\partial t} = \frac{1}{r^2}\frac{\partial}{\partial r}\left[Dr^2\frac{\partial C}{\partial r}\right] \tag{1}$$

where D and C are the diffusion coefficient and drug concentration in the polymer matrix. The boundary conditions are influenced by the mass transfer process at the surface and the volume of the surrounding system. Based on these conditions, there are three main cases which are commonly considered [2]:

1. The mass transfer resistance at the surface is negligible and the surrounding release medium is infinitely large (perfect sink condition), implying that the concentration on the surface of the matrix (C_s) is constant ($C_s = KC_b$ = constant at $r=R$). Here, C_b is the drug concentration in surrounding bulk medium and K is the drug partition coefficient between the matrix and bulk medium.
2. The mass transfer resistance at the surface is finite and the surrounding volume is in perfect sink condition, implying that the concentration of the surrounding system is constant, but the convective mass transfer coefficient (h) will determine the surface concentration $\left(-D\left(\frac{\partial C}{\partial r}\right)_{r=R} = h(C|_{r=R} - KC_b)\right)$.
3. The surrounding system is a well-stirred finite volume. This implies that the concentration of the surrounding system changes with time. The surface resistance may or may not be negligible.

Based on the matrix region where the drug diffusion primarily takes place, the diffusion-controlled system can be further categorized to reservoir and matrix systems. The reservoir system consists of a drug reservoir surrounded by the polymer matrix shell. On the other hand, in matrix system, the drug is incorporated in the polymer matrix in either dissolved or dispersed condition. The schematic illustrations of drug loading distribution for these systems are shown in Fig. 1.

2.1. Reservoir systems

The reservoir model is the simplest model of a solute of drug released from a sphere [3]. It assumes that drug is confined by a spherical shell of outer radius R and inner radius R_i; thus, the drug must diffuse through a layer of thickness $(R-R_i)$.

Fick's second law of diffusion is solved to obtain the drug distribution within the shell with boundary conditions imposed as in a hollow sphere ($R_i \le r \le R$), where the surface $r=R_i$ is kept at a constant reservoir concentration $C_r = K_r C_i$, where C_r is the reservoir drug concentration and K_r is the drug partition coefficient between the reservoir and polymer matrix. On the other hand, at the shell surface ($r=R$), drug concentration is assumed to be zero when there is no mass transfer limitation and the surrounding volume is large.

This unsteady diffusion equation is solved to give the concentration profile and the cumulative amount of drug released (M_t) as functions of time, as follows:

$$C(r,t) = C_i\frac{R_i}{r}\frac{(R-r)}{(R-R_i)} - \frac{2}{\pi}\sum_{n=1}^{\infty}\frac{C_i R_i}{n}\sin\left(n\pi\frac{r-R_i}{R-R_i}\right) \times \exp\left(-\frac{n^2\pi^2}{(R-R_i)^2}Dt\right) \tag{2}$$

$$\frac{M_t}{4\pi R_i R(R-R_i)C_i} = \frac{Dt}{(R-R_i)^2} - \frac{1}{6} - \frac{2}{\pi^2}\sum_{n=1}^{\infty}\frac{(-1)^n}{n^2}\exp\left(-\frac{n^2\pi^2}{(R-R_i)^2}Dt\right) \tag{3}$$

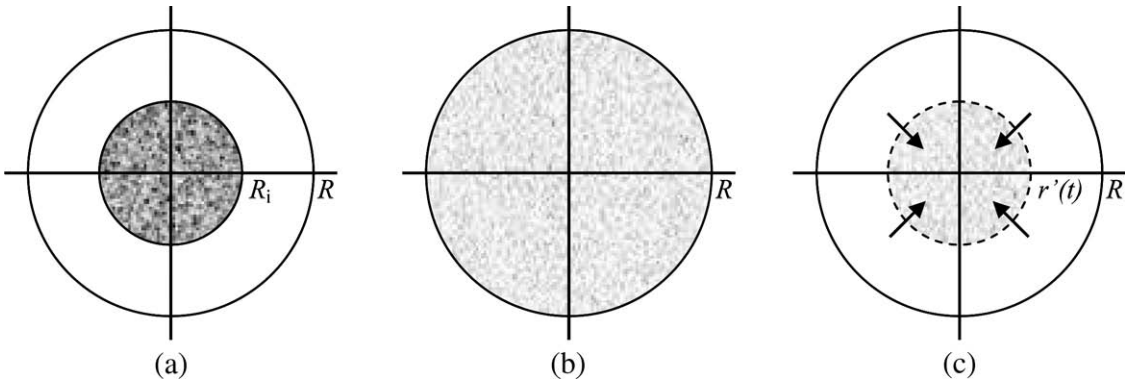

Fig. 1. Schematic illustration of cross-section of drug-loaded spheres of (a) reservoir system, (b) dissolved drug system, and (c) dispersed drug system. In reservoir system, drug is confined by a spherical shell of outer radius R and inner radius R_i; therefore, the drug must diffuse through a polymer layer of thickness $(R-R_i)$. In dissolved drug system, drug is dissolved uniformly at loading concentration C_0 in the polymeric matrix. In dispersed drug system, the radius of inner interface between "core" (non-diffusing) and matrix (diffusing) regions, $r'(t)$, shrinks with time. The "core" region is assumed to be at drug loading concentration C_0.

When the observation time is long enough ($t\rightarrow\infty$), the series term approaches zero and there is a constant diffusion rate of drug leaving the reservoir sphere; thus, the amount of drug released equation can be simplified as follows:

$$\frac{M_t}{t} = 4\pi\frac{RR_i}{(R-R_i)}DC_i \tag{4}$$

However, the use of both solutions has to be taken carefully since it seems to suggest that M_t increases without limit as time increases. One must consider that the drug content in sphere is finite and the diffusional release is only valid for a certain time range that may differ for different systems.

2.2. Matrix systems

Mathematical models for matrix systems are often valid for drug devices developed based on non-biodegradable polymers. In these models, the drug is commonly assumed to be uniformly distributed inside the non-biodegradable polymer matrix. There are two possible cases, which are (i) the initial drug loading is lower than the solubility of the drug inside the polymer matrix ($C_0<C_s$), which implies a dissolved drug system, and (ii) the initial drug loading is higher than the solubility of the drug inside the polymer matrix ($C_0>C_s$), which implies a dispersed drug system.

A very popular biocompatible, but non-biodegradable, polymer that is representative of the matrix system is *poly(ethylene-co-vinyl acetate)* (EVAc). EVAc is a hydrophobic polymer that swells less than 0.8% in water. It is commercially available with composition range of 10–40%-w/w *vinyl acetate*.

2.2.1. Dissolved drug systems ($C_0<C_s$)

Dissolved drug system prevails when initial drug loading concentration (C_0) is below the drug saturation concentration in the polymer matrix (C_s); therefore, the drug is dissolved uniformly in the polymer matrix. When the surface resistance to mass transfer at the surface is negligible, the drug concentration profile and fractional amount of drug released can be expressed as follows [3]:

$$\frac{C-C_0}{KC_b-C_0} = 1+\frac{2R}{\pi r}\sum_{n=1}^{\infty}\frac{(-1)^n}{n}\sin\left(\frac{n\pi r}{R}\right)\times\exp\left(\frac{-Dn^2\pi^2 t}{R^2}\right) \tag{5}$$

$$\frac{M_t}{M_\infty} = 1-\frac{6}{\pi^2}\sum_{n=1}^{\infty}\frac{1}{n^2}\exp\left(\frac{-Dn^2\pi^2 t}{R^2}\right) \tag{6}$$

where M_∞ is the cumulative drug released at infinite time.

In contrast, if finite convective mass transfer prevails, where $-D\left(\frac{\partial C}{\partial r}\right)_{r=R} = h(C|_{r=R}-KC_b)$, the drug

concentration profile and fractional amount of drug released can be expressed as follows [2]:

$$\frac{C-KC_b}{C_0-KC_b}=\frac{2ShR}{r}\sum_{n=1}^{\infty}\frac{1}{\beta_n^2+Sh^2-Sh}\frac{\sin\beta_n\frac{r}{R}}{\sin\beta_n}\times\exp\left(-\frac{\beta_n^2}{R^2}Dt\right) \quad (7)$$

$$\frac{M_t}{M_\infty}=1-\sum_{n=1}^{\infty}\frac{6Sh^2}{\beta_n^2(\beta_n^2+Sh^2-Sh)}\exp\left(-\frac{\beta_n^2}{R^2}Dt\right) \quad (8)$$

where Sh is Sherwood number defined as $Sh=\frac{hR}{D}$, and the β_ns are roots of the equation $\beta_n\cot\beta_n=1-Sh$. Eqs. (7) and (8) are identical to Eqs. (5) and (6) when $Sh\gg1$. It can be seen that the finite mass transfer solution depends on Sh, which is the ratio between mass transfer resistance at the surface and diffusional resistance throughout the polymer matrix.

For $Sh\gg1$, Baker and Lonsdale [4,5] also proposed two simplified solutions by using early-time and late-time approximations to explain the drug release from dissolved matrix system of a sphere during early and late-time periods respectively. The approximation results are expressed as follows:

$$\frac{M_t}{M_\infty}=6\left(\frac{Dt}{\pi r^2}\right)^{1/2}-\frac{3Dt}{r^2}\quad\text{for}\quad\frac{M_t}{M_\infty}<0.4 \quad (9)$$

$$\frac{M_t}{M_\infty}=1-\frac{6}{\pi^2}\exp\left(-\frac{\pi^2Dt}{r^2}\right)\quad\text{for}\quad\frac{M_t}{M_\infty}>0.6 \quad (10)$$

2.2.2. Dispersed drug systems ($C_0>C_s$)

Similar to the reservoir system, the polymer matrix in the dispersed drug system can be primarily divided into two regions, which are (i) the "core" (non-diffusing) region, in which the undissolved solute exists at concentration C_0, and (ii) the dissolved (diffusing) region, where all solute is dissolved and diffusion occurs. The distinct separation for these two regions is valid when $C_0>C_s$, therefore the limited application of these mathematical models must be carefully taken into account when C_0/C_s is not significantly large. Here, the "core" region is different from the reservoir region in the reservoir system since the former is a constant thickness polymer region with certain drug loading concentration (C_0), whereas the drug contained in the reservoir region does not incorporate polymer matrix. On the other hand, the "core" region is able to shrink as drug released via diffusion in the diffusion region. The necessity to involve the moving-boundary problem makes the governing equation of the mathematical model for dispersed drug system difficult to solve analytically. A schematic illustration of concentration profiles for dispersed drug system is shown in Fig. 2.

The diffusion-controlled mathematical model for dispersed drug system ($C_0>C_s$) in a planar sheet and a sphere was initiated by Higuchi [6] with the assumption that diffusion is in pseudo-steady state. In the planar system, this assumption leads to a linear concentration profile of the drug in the diffusing region, which is between the dissolution interface and the initial matrix surface. Given this assumption, the simplest and most popular version of Higuchi's equation for planar system is readily obtained:

$$M_t=S\sqrt{(2C_0-C_s)C_sDt} \quad (11)$$

Here, S is the available surface area for drug release to surrounding. For a spherical system, the pseudo-steady concentration profile in the diffusing region is $\frac{C}{C_s}=\frac{r'}{r}\frac{(R-r)}{(R-r')}$. Integration of the mass flux equation gives the relationship between the moving-boundary interface position (r') and time (t) as follows:

$$6DC_sRt=C_0(R^3+2r'^3-3Rr'^2)+C_s\left(4r'^2R+R^3\ln\frac{R}{r'}-R^3-R^2r'-2r'^3\right) \quad (12)$$

In the case of $C_0>C_s$, this solution can be further simplified to:

$$\frac{6DC_s}{C_0R^2}t=1-3\left(\frac{r'}{R}\right)^2+2\left(\frac{r'}{R}\right)^3 \quad (13)$$

The fractional cumulative release can be expressed as follows:

$$\frac{M_t}{M_\infty}=1-\left(\frac{r'}{R}\right)^3 \quad (14)$$

Koizumi and Panomsuk [7] applied Higuchi's pseudo-steady approach to obtain an approximation

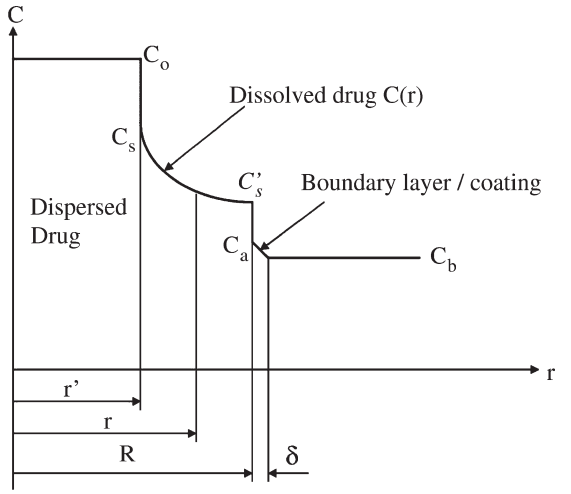

Fig. 2. A schematic diagram illustrating concentration profile in a sphere of dispersed drug system with the presence of a boundary layer in a perfect sink medium. The drug concentration at the matrix surface (C'_s) is related to drug concentration at the boundary layer interface with the matrix (C_a) with the partition coefficient K_1 ($C'_s = K_1 C_a$). If boundary layer or coating does not exist, the drug concentration at the matrix surface (C'_s) is directly related to drug concentration in the bulk medium (C_b) with the partition coefficient K ($C'_s = KC_b$) (reprinted from [15] with permission from Elsevier).

solution for drug release from a sphere. With several series simplification, a simple and explicit expression can be obtained for the amount of drug released as function of time for a perfect sink condition as follows:

$$M_t = 4\pi R^2 \left[\sqrt{2(C_0 - C_s)Dt} + \frac{4C_s}{9R} \left(\frac{C_s}{(2C_0 - C_s)} \right) Dt \right] \tag{15}$$

However, it must be noted that the solution does not suggest M_t increases to infinity as time increases as only finite amount of drug is available in the sphere.

The Higuchi approximation (Eqs. (12)–(14)) provides a good correlation of drug release profile when $C_0 > C_s$; but, in the limit of $C_0 \to C_s$, its result does not precisely match the classical diffusion solution for the dissolved drug system ($C_0 < C_s$) at the limiting case $C_0 \to C_s$. Cohen and Erneux [8] suggested a boundary layer analysis to accommodate the discrepancy that led to a simple analytical solution for the release rate with the effect of time-dependent solubility. Lee [9] applied the approximate quadratic concentration profile, $\frac{(C_s - C)}{C_s} = a_1 + a_2 \left(\frac{R-r}{R-r'} \right) + a_3 \left(\frac{R-r}{R-r'} \right)^2$, to reduce the discrepancy. Here, a_1, a_2 and a_3 are constants for the quadratic radial-dependent concentration profile to be satisfied by the perfect sink boundary conditions. When the boundary conditions are satisfied, it results in the form as follows:

$$\frac{C}{C_s} = \left[1 + \frac{C_0}{C_s} - \sqrt{\left(\frac{C_0}{C_s} \right)^2 - 1} \right] \left(\frac{R-r}{R-r'} \right) - \left[\frac{C_0}{C_s} - \sqrt{\left(\frac{C_0}{C_s} \right)^2 - 1} \right] \left(\frac{R-r}{R-r'} \right)^2 \tag{16}$$

In addition, the relationship between the moving front r' and t can be given by,

$$\frac{Dt}{R^2} = \frac{1}{12} \left[5 \left(\frac{C_0}{C_s} \right) - 4 + \sqrt{\left(\frac{C_0}{C_s} \right)^2 - 1} \right] \left(\frac{R-r'}{R} \right)^2 - \frac{1}{3} \left(\frac{C_0}{C_s} - 1 \right) \left(\frac{R-r'}{R} \right)^3 \tag{17}$$

Finally, the resulting fractional release can be written as follows:

$$\frac{M_t}{M_\infty} = \left[1 - \left(1 - \frac{R-r'}{R} \right)^3 \right] \left(1 - \frac{C_s}{C_0} \right) + 3 \frac{R-r'}{R} \left(\frac{C_s}{C_0} \right) \times \left[\left(a_1 + \frac{a_2}{2} + \frac{a_3}{3} \right) - \left(\frac{a_1}{2} + \frac{a_2}{3} + \frac{a_3}{4} \right) \right] \left(\frac{R-r'}{R} \right) \tag{18}$$

Even though Lee's solution is explicit and easy to apply, several models that provide exact solutions have also been developed to remove the discrepancy of approximate solutions. Paul and McSpadden [10] obtained the exact solution for drug release from a planar system into a perfect sink. It turns out that Lee's approximate solution agrees well with it. Abdekhodaie and Cheng [11,12] try to develop an exact solution for diffusion from a spherical matrix into both infinite and finite external medium by using a combination of variables technique. This technique allows the reduction of Fick's second law of diffusion into an ordinary differential equation. The finite external medium is assumed to have concentration of C_b. It is related to the concentration at the matrix surface ($r = R$) by the partition coefficient K ($C_s = KC_b$), implying that the

magnitude of mass transfer at the surface is finite as it depends on the bulk concentration. The effect of finite volume and the partition coefficient is lumped into an additional variable termed the effective volume ratio (λ), which is defined as $\lambda = \frac{3V_b}{4K\pi R^3}$. The solution is obtained as follows:

$$\theta = A_1 + A_2\sqrt{\pi}\left[\mathrm{erf}\left(\frac{1-\zeta}{2\sqrt{\tau}}\right) - \mathrm{erf}\left(\frac{1-\Gamma}{2\sqrt{\tau}}\right)\right] \tag{19}$$

where

$$\zeta = \frac{r}{R}, \quad \tau = \frac{Dt}{R^2}, \quad \Gamma = \frac{r'}{R}, \quad \theta = \frac{r}{R}\frac{C}{C_s}, \text{ and } \kappa = \frac{C_0}{C_s} - 1 \tag{20}$$

However, the combination variables technique fails to reduce the boundary conditions to obtain the appropriate integration constants. Therefore, even though the solution is aimed to predict drug release in a finite medium, the solution is basically valid for the cases of perfect sink condition with pseudo-steady assumption which is similar to Higuchi's approach. As a rule of thumb, the pseudo-steady approximation is considered to be valid when $\frac{C_0}{C_s} > 3$. The numerical solutions using a finite element method for slab, cylinder, and sphere matrices are available in other literatures [13]. Fig. 3a shows the concentration profile at the moving-boundary for drug release into perfect sink medium, whereas Fig. 3b depicts the influence of λ on the total amount of drug released into finite volume medium; both are shown for the case of $\frac{C_0}{C_s} = 2$. Other simpler numerical methods can be employed to solve this problem by satisfying the following boundary conditions:

$$\theta(\Gamma, \tau) = 1 \tag{21}$$

$$\frac{C_0}{C_s}(1-\Gamma) = \theta\lambda + \int_{\Gamma}^{1} \theta \mathrm{d}\zeta \qquad \text{at } \zeta = 1 \tag{22}$$

The variation of moving-boundary (Γ) with time is defined as the mass balance at the interface r' as follows:

$$\left(\frac{C_0}{C_s} - 1\right)\frac{\mathrm{d}\Gamma}{\mathrm{d}\tau} = \frac{1}{\Gamma}\left(\frac{\partial\theta}{\partial\zeta} - 1\right) \tag{23}$$

where initial condition (Γ_0,τ_0) can be adopted from the Paul and McSpadden solution [10] for small value of τ as the curvature effect in the spherical geometry can be neglected at sufficiently small τ. Here, Γ and τ are related implicitly as follows:

$$\sqrt{\pi}\frac{(1-\Gamma)}{2\sqrt{\tau}}\exp\left[\frac{(1-\Gamma)^2}{4\tau}\right]\mathrm{erf}\left(\frac{1-\Gamma}{2\sqrt{\tau}}\right) = \frac{1}{\left(\frac{C_0}{C_s} - 1\right)} \tag{24}$$

Wu and Zhou [14,15] developed a numerical solution for a finite external medium system (V_b) with an additional diffusion boundary layer incorporated on the surface of the matrix. Therefore, there are two diffusing zones, in which the drug has different diffusivities. The first diffusing zone is the polymeric matrix region between r' and R in which diffusivity is D, whereas the second diffusing zone is a constant thickness (δ) boundary layer in which diffusivity is D_a. In addition, the model accounts for the number of microspheres (N); therefore, the total drug released becomes $M_t = Nm$, where m is the cumulative amount of drug released from a single microsphere. Despite the model improvement to account for the presence of a boundary layer, the pseudo-steady-state approximation of Higuchi is assumed for both diffusing regions; therefore, the concentration profile for the diffusing region in the matrix is expressed as follows:

$$C = C_s - (C_s - C_s')\frac{R(r-r')}{r(R_0-r')} \tag{25}$$

where C_s' is the concentration at the moving interface between the dissolved and boundary layer regions ($C_s' = K_1 C_a$) and C_a is the drug concentration at the boundary layer interface with the matrix. K_1 is the partition coefficient between the matrix surface and the boundary layer. Here, it is assumed that there is no drug accumulation in the boundary layer region so the rate of drug diffusion in the matrix region of the microspheres is the same as that through the boundary layer. The schematic illustration of the drug concentration in this system is shown in Fig. 2. The cumulative drug release from a single microsphere (m) is given by:

$$\begin{aligned} m &= \frac{4\pi C_0}{3}(R^3 - r'^3) - \int_{r'}^{R} 4\pi r^2 C \mathrm{d}r \\ &= \frac{4\pi C_0}{3}(R^3 - r'^3) + \frac{2\pi}{3}\left[(2r'^3 - Rr'^2 - R^2 r')C_s \right. \\ &\quad \left. -(2R^3 - Rr'^2 - R^2 r')C_s'\right] \end{aligned} \tag{26}$$

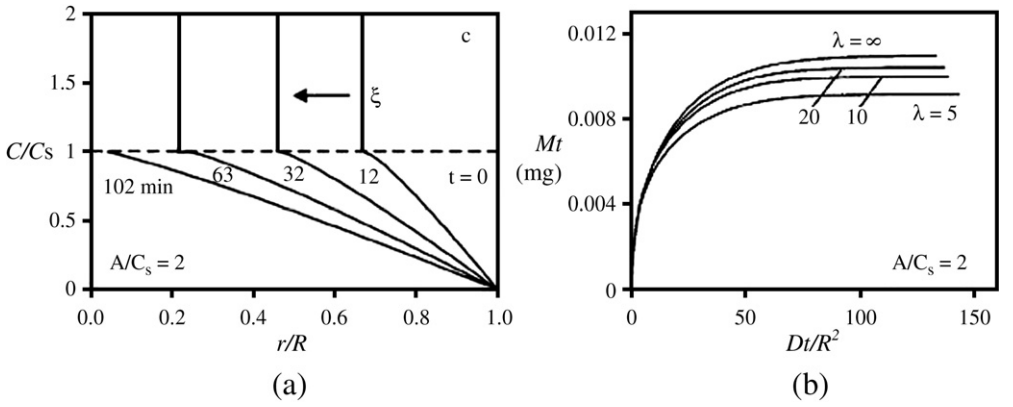

Fig. 3. (a) A moving-boundary concentration profile for a sphere of dispersed drug system in perfect sink condition with $R=1\times10^{-3}$ m, $D=1\times10^{-10}$ m^2/s, and $C_0/C_s=2$; and (b) drug release profiles into finite volume medium with various effective volume ratios (λ) with $R=1\times10^{-3}$ m, $D=1\times10^{-10}$ m^2/s, and $C_0/C_s=2$. The 100% drug release is obtained by the plateau region of release curve for $\lambda=\infty$. Both panels are obtained by solving the moving-boundary problem of dispersed matrix system using finite element method (reprinted from [13] with permission from Wiley-Liss, Inc., a subsidiary of John Wiley & Sons, Inc. Copyright © 1999).

The total amount of drug released (M_t) for a number of microspheres (N) and drug concentration in the finite external medium (C_b) are expressed respectively as follows:

$$M_t = mN \tag{27}$$

$$C_b = \frac{M_t}{V_b} = \frac{3m}{4\pi R^3}\frac{V_s}{V_b} \tag{28}$$

where V_b is the volume of the finite external medium and $V_s=W/\rho$ is the total volume of the microspheres. W and ρ are the mass and bulk density of microspheres, respectively.

Upon differentiation of the accumulative mass release with time and equating to the drug release from the microspheres, the relationship between the moving-boundary r' and time t is obtained as follows:

$$t(r') = \int_R^{r'} \frac{[-4\pi C_0 r^2 + g(r')](R-r)}{4\pi DRr(C_s - C_s')}\,dr \tag{29}$$

where $g(r')$ is a derivative function of the amount of drug that is still diffusing in the matrix diffusing zone and is defined as follows:

$$g(r') = \frac{d}{dr'}\left\{\frac{2\pi}{3}[(2r'^3 - Rr'^2 - R^2r')C_s - (2R^3 - Rr'^2 - R^2r')C_s']\right\}$$

When this relationship is simplified to the special case of $C_0 > C_s$, the amount of dissolved drug in the matrix can be ignored and the following explicit solution can be obtained:

$$t(r') = \frac{-V_b R^2}{6K_1 V_s D B_1}\left\{\ln(B_2) + 2\sqrt{3}\tan^{-1}(B_3) - 2B\left(1-\frac{D\delta K_1}{D_a R}\right)\ln\left[1-K_2\left(1-\left(\frac{r'}{R}\right)^3\right)\frac{V_s C_0}{V_b C_s}\right]\right\} \tag{30}$$

$$M_t = Nm = V_s C_0\left[1-\left(\frac{r'}{R}\right)^3\right] \tag{31}$$

where B_1, B_2, and B_3 are complex variables given by the following expressions,

$$B_1 = \left(1-\frac{C_s V_b}{C_0 V_s K_1}\right)^{1/3}$$

$$B_2 = \frac{1+B_1+B_1^2}{(r'/R)^2 + B_1 r'/R + B_1^2}\left(\frac{r'/R - B_1}{1-B_1}\right)^2 \tag{32}$$

$$B_3 = \frac{2\sqrt{3}B_1(r'/R-1)}{3B_1^2 + (2r'/R + B_1)(2+B_1)}$$

3. Mathematical models for swelling-controlled systems

The idea of using a swelling polymer is to provide more control over the release of drug, especially when its diffusivity in polymer is very low. For this purpose, a swellable device is commonly made using a hydrophilic polymer so that water is able to imbibe into the polymer matrix and cause polymer disentanglement. The level of polymer disentanglement as a function of polymer concentration is illustrated in Fig. 4. The imbibing water into the polymer matrix decreases the polymer concentration and changes the level of polymer disentanglement. The polymer matrix disentanglement also leads to matrix swelling that results in the rubbery (gel layer) region, in which there is an "enhanced diffusion" where drug mobility increases. The polymer will also dissolve at the interface when the entanglement is weak since polymer concentration is very low. Thus, in this system, the deviation from Fickian model is observed when the drug release is not only controlled by the diffusion of the drug inside the matrix, but also by the polymer matrix disentanglement and dissolution process.

For swelling-controlled system, the hydrophilic polymer is susceptible to swelling as water tends to penetrate and relax the polymer matrix. In this case, the composition of the hydrophilic polymer will determine

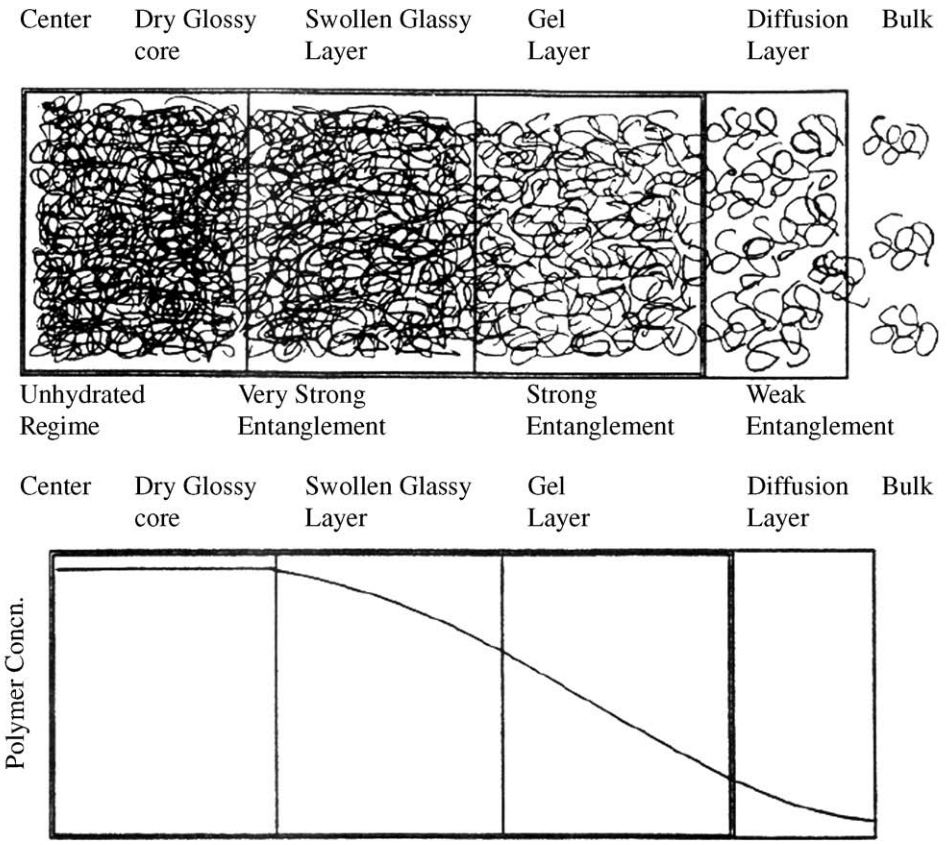

Fig. 4. A schematic illustration of level of polymer matrix disentanglement as a function of the polymer concentration in a swelling-controlled drug system. The disentanglement is due to the imbibing of water into the system that results in polymer concentration changes in the matrix. In the dry glassy core, polymer concentration is very high. In the swollen glassy layer, solvent diffusion creates a more mobile network, but with very strong chain entanglement. In the gel layer, polymer and solvent concentrations are comparable. Finally, in the high water-rich layer of diffusion layer, chain entanglement becomes weak so that the polymer can disentangle and dissolve at the interface (reprinted from [28] with permission from Wiley-Liss, Inc., a subsidiary of John Wiley & Sons, Inc. Copyright © 1995).

the extent of swelling. Typical hydrophilic polymers used for drug delivery application that exhibit swelling behavior include *hydroxypropyl methylcellulose* (HPMC), *poly(hydroxyethyl methacrylate)* or poly (HEMA), and *poly(vinyl alcohol)* (PVA). Since swelling-controlled drug delivery devices are often made as tablets and the overall drug release mechanism strongly depends on the design (composition and geometry) of the device, corresponding mathematical models for this system are commonly developed for a cylindrical geometry, while extension to other geometries is readily available with proper coordinate transformation. In addition, several studies addressing the modeling of swelling-controlled systems are also available in literatures [16–18].

A model that describes the mechanism of polymer matrix swelling is shown in Fig. 5. This model is developed by Lee and Peppas [19] by taking into account swelling moving fronts. The swelling occurs to achieve thermodynamics equilibrium when water penetrates crosslinked region inside the polymer matrix due to a water concentration gradient. As water penetrates and swelling takes place, a transformation of polymer from a glassy to rubbery state occurs and the dimension of the matrix increases. This change of state basically creates a gel layer of rubbery region for the drug to diffuse, in which the drug diffusivity increases substantially. Therefore, during the swelling, two different states, namely the glassy core and gel layer (rubbery), exist in the polymer matrix. Here, the concept of two moving fronts, namely the glassy–rubbery front (R) and the rubbery–solvent front (S), is introduced. Initially during swelling, front R moves inwards, whereas front S moves outward. When the polymer at interface S reaches its thermodynamic equilibrium with the surrounding medium, interface S will start dissolving and, therefore, front S moves inwards. Both fronts will move inwards until the front R diminishes as the glassy core disappears. Subsequently at later time, only the rubbery region is present and dissolution at interface S eventually controls the shrinking process.

Upon contact with water, the drug dissolves due to a concentration difference at interface R and diffuses out through interface S due to a concentration gradient between interface of two states. If water penetration is negligible, polymer relaxation does not occur and drug release is controlled by Fickian diffusion through the glassy polymer matrix. On the other hand, when the water mobility is dominant in penetrating the polymer matrix, a "non-Fickian Case-II transport" of drug release takes place [20]. It is characterized by the existence of a sharp interface advancing at constant velocity and the drug release is zero-order since it is controlled by the polymer dissolution process at the moving interface. Between these two extreme cases, the "anomalous transport", which has intermediate characteristics, is defined. The "anomalous" transport

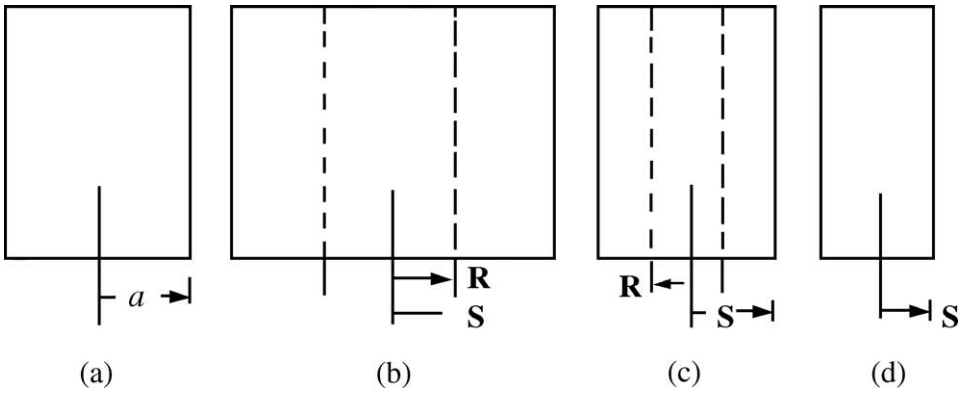

Fig. 5. Schematic illustration of one-dimensional swelling process due to solvent diffusion and polymer dissolution as proposed by Lee [19]: (a) initial thickness of the carrier, (b) early-time swelling when there are increasing position of the rubbery/solvent interface (S) and decreasing position of the glassy/rubbery interface (R), (c) late-time swelling when there are decreases of both interface S and R positions, and (d) final dissolution process when the slab only comprises rubbery region with the decrease of interface S (reprinted from [19] with permission from Elsevier).

of drug release is often identified in swelling-controlled systems since both diffusion and dissolution occur altogether and they are quite indistinguishable. Here, the drug transport is commonly modeled as the diffusion in which the diffusion coefficient depends strongly on polymer concentration since polymer swelling and relaxation enhance the drug mobility, whereas the polymer dissolution is modeled to follow first-order kinetics at the interface with surrounding medium.

In the simplest manner, Korsmeyer et al. [21,22] developed a semi-empirical equation based on a power-law expression to describe the drug release from swelling-controlled systems as follows:

$$\frac{M_t}{M_\infty} = kt^n \tag{33}$$

Here, k is a constant and n is the diffusional exponent. The power-law equation can be observed as the superposition of two processes of Fickian diffusion and "Case-II transport". It has a feature to identify the relative importance between Fickian diffusion ($n=0.5$) and "Case-II transport" ($n=1$). Aforementioned, in the latter case, the drug dissolution at the moving front due to water imbibition is the dominant step so it is characterized by a linear time dependence of drug release. In between these two processes, the "anomalous transport" takes place where phenomena of both processes are coupled ($0.5<n<1$). It is important to note that this rule of thumb is particularly valid for slab geometry. Different values of n for cylindrical and spherical geometries are available in the literature [23,24]. For spheres, the n values are 0.43 and 0.85 for diffusion and "Case-II transport" drug release, respectively. Beside the dependence on the geometry, the value of n may also be influenced by particle size distribution as observed by Ritger [23,24]. For a hypothetical mixture of 20% 20-μm, 60% 100-μm, and 20% 500-μm spheres, the n values for Fickian diffusion and the "Case-II transport" become 0.30 and 0.45, respectively. In comparison to the release profile from monodispersed particle, this mixture shows an acceleration of drug transport at early times due to the portion of particles smaller than the mean size and retardation at longer times due to the portion of particles larger than the mean size.

Modification of the Korsmeyer's semi-empirical equation by incorporating the concept of lag time was introduced by Kim and Fassihi [25] and Ford et al. [26]. Having accounted for the burst effect, the modified equation is given by:

$$\frac{M_t}{M_\infty} = k(t-t_{\mathrm{lag}})^n + b \tag{34}$$

where k is a constant and b is the total fractional drug released from the burst effect.

Another modification to the semi-empirical model was performed by Peppas and Sahlin [27] by decoupling diffusion and "Case-II transport" with the following expression:

$$\frac{M_t}{M_\infty} = k_1 t^m + k_2 t^{2m} \tag{35}$$

where k_1, k_2, and m are constants. The first term of the right-hand side is the diffusional contribution, whereas the second term is the "Case-II transport" contribution.

Ju et al. [28,29] developed scaling laws for predicting polymer and drug release profiles from hydrophilic polymer matrices. The system used is the HPMC matrix tablet in water. An anisotropic expansion model is used to account for the anisotropic expansion of the matrix when anisotropic swelling occurs. The model provides a qualitative relationship between the polymer disentanglement concentration ($\rho_{\mathrm{p,dis}}$) and the equivalent molecular weight of the polymer matrix (M_{eq}) in a HPMC/water system. The polymer disentanglement concentration ($\rho_{\mathrm{p,dis}}$) is defined as the concentration below which polymer chains start dissolving or detaching from the gel matrix, whereas the equivalent molecular weight (M_{eq}) is the weight-averaged molecular weight of the polymer matrix. Results of these studies are summarized in two scaling laws for the fractional polymer and drug releases respectively, namely $\frac{M_{p,t}}{M_{p,\infty}} \propto M_{\mathrm{eq}}^{-1.05}$ and $\frac{M_t}{M_\infty} \propto M_{\mathrm{eq}}^{-0.24}$. In these scaling laws, $\frac{M_{p,t}}{M_{p,\infty}}$ and $\frac{M_t}{M_\infty}$ are the cumulative fraction release of polymer and drug, respectively. The scaling laws are developed based on radial mass transfer model since the expansion for tablet matrix systems is mostly in the axial direction and, therefore, the dissolution surface is available mostly in the radial

direction. These results imply that drug release is less sensitive to the polymer molecular weight as compared to the polymer release. This is attributed to the assumption of infinite drug convective mass transfer coefficient at the gel–diffusion layer interface. Therefore, the outward drug release by diffusion is less influenced by the polymer molecular weight change than the polymer release that is controlled by the disentanglement and dissolution.

Since empirical models are not able to provide sufficient physical understanding on how the swelling process affects drug release, several mechanistic models have been developed to capture the swelling mechanism. The development is focused on the modeling of moving fronts of glassy and rubbery regions during the swelling, as shown in Fig. 5, and the feature of concentration-dependent diffusivity to account for the increase of drug mobility in the gel layer region. Here, the evolving polymer and drug concentrations at the moving fronts can be predicted by classical thermodynamics theories of polymer–solvent mixture [30–32,34]. Aforementioned, the first model of swelling moving fronts was developed by Lee et al. [19] for a one-dimensional swellable polymer system without any loaded drug (two-component system).

For the swelling-controlled system, Colombo et al. [31] suggested from experimental studies a new finding that the gel layer consists of two regions of dissolved and undissolved drug gel layer thickness, in which the distance of dissolved gel layer thickness is the most important parameter that influences the drug release. This is observed in several swelling systems, i.e. *diclofenac*, *diprophylline*, and *cimetidine* in HPMC, PVA, and *carboxymethyl–cellulose sodium* (CMC) polymer matrix. This is expected since dissolution process does not limit drug release from the glassy region in the undissolved region and, therefore, it is able to provide any amount of drug available at the interface R for restricted diffusion in the dissolved rubbery region. Hence, the diffusion in the dissolved rubbery layer is the controlling step for the drug release process and its distance becomes important to determine the drug release. This case is also true when the undissolved region is barely observed as the dissolution at the interface R is relatively fast. Here, the gel layer thickness becomes the important distance for drug release.

Harland et al. [32] improved Lee's moving front model to explain the mechanism of drug release from swelling tablets by adding a third component, which is the drug. Since drug is additionally incorporated in this model, three components are now taken into account, namely water (component 1), polymer (component 2), and drug (component d). In this model, the transport of drug and water components is assumed to be by Fickian diffusion and expressed in volume-fraction form. At the interface R, the polymer (v_2^*) and drug (v_d^*) volume fraction reach a thermodynamic equilibrium, whereas, at the interface S, polymer disentanglement occurs and the water ($v_{1,eq}$) and drug ($v_{d,eq}$) volume fraction are in the equilibrium with the surrounding medium. There are two periods of swelling observed from the experimental results, namely the early swelling and the front synchronization period. The early swelling period refers to the inward moving of interface R due to polymer and drug dissolution and outward moving interface S due to polymer swelling. Here, the gel layer thickness ($S-R$) increases with time. Interestingly, it is also observed from experimental results that there is a synchronization of the two fronts when ($S-R$) becomes independent of time as shown in Fig. 6a. The front synchronization period takes place after the swelling has stopped, in which both interfaces move inward at approximately the same rate. However, the mechanism of front synchronization phenomenon has not been explained in detail. It is possible that the synchronization period for swelling-controlled matrix systems only occurs in several special cases, which is probably dependent on the matrix composition, geometry, and the fabrication technique. This is supported by experimental observations, where front synchronization is observed for several polymer matrices of PVA with three drugs of different solubility (*diclofenac*, *diprophylline*, and *cimetidine*) [32], but it does not prevail for polymer matrices of HPMC with the same loaded drugs [33]. In this model, $v_{d,eq}$ and drug mass transfer coefficient at interface S (k_S) are fitted to the experimental fractional drug release curve. The fitting to experimental data is obtained for the release of *sodium diclofenac*, *diprophylline*, and *cimetidine-HCl* from PVA–*mannitol* tablets. Fig. 6b shows the cumulative release profile of *sodium diclofenac* from PVA–*mannitol* system. The application of k_S in this model may not be appropriate since drug release at the interface is essentially due to the

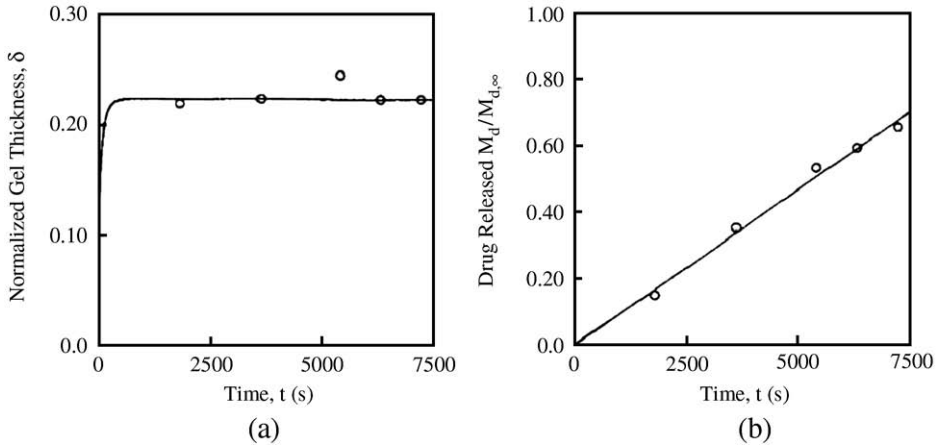

Fig. 6. The time variation of (a) normalized gel layer thickness, $\delta_{gel}=(S-R)/l$, where l is the half of slab thickness or the initial position of both interfaces R and S, with the line referring to the model prediction; and (b) cumulative fraction of *sodium diclofenac* release. The tablet consists of 30% PVA, 20% *mannitol*, and 50% *sodium diclofenac*. The release is observed at 37 °C in intestinal simulating fluid at 100 rpm. The line refers to the dissolution model proposed by Harland et al. (reprinted from [32] with kind permission from Springer Science and Business Media).

polymer dissolution and controlled by drug diffusion through the gel layer, but it is seldom limited by drug mass transfer at the interface.

Narasimhan and Peppas [34] also used Lee's moving front concept to improve Harland's model for the swelling-controlled drug device. Similar to the previous model, three components of water (component 1), polymer (component 2), and drug (component d) are taken into account. The water and drug species balances are formulated in volume-fraction form based on Fick's second law with initial conditions ($t=0$) $\upsilon_1=0$ and $\upsilon_d=\upsilon_{d,0}$. The boundary conditions are imposed as previously, where $\upsilon_2=\upsilon_2^*$ and $\upsilon_d=\upsilon_d^*$ at interface R and $\upsilon_1=\upsilon_{1,eq}$ and $\upsilon_d=\upsilon_{d,eq}$ at interface S. In this improved model, at interface S, the disentanglement (dissolution) rate of the polymer chains (k_d) is used instead of the drug mass transfer coefficient (k_S). It is predicted to be the ratio of polymer gyration radius (r_g) to its reptation time (t_{rept}), as follows:

$$k_d = \frac{r_g}{t_{rept}} \tag{36}$$

The reptation time is the time when the solvent penetration begins to disentangle the polymer chains until it is released into the surrounding medium. t_{rept} can be determined by rheological experiments, whereas r_g can be determined by light scattering experiments. This model also improves the boundary conditions estimation of volume fraction at the interfaces R and S. Here, at the interface R, the polymer and drug volume fractions are given by the free-volume theory [35–37], whereas, at the interface S, the constant volume fractions of polymer and drug are given by the Flory–Rehner equation [38].

The moving-boundary condition at the interface R is defined by applying the following mass balance equation:

$$(\upsilon_1^* + \upsilon_d^*)\frac{dR}{dt} = -\left(D_1\frac{\partial \upsilon_1}{\partial x} + D_d\frac{\partial \upsilon_d}{\partial x}\right) \tag{37}$$

The interface S initially swells outward due to polymer chain disentanglement and eventually moves inward when polymer disentanglement is limited as surface polymer concentration has reached the equilibrium state. The way of the movement of interface S is expressed as follows:

$$(\upsilon_{1,eq} + \upsilon_{d,eq})\frac{dS}{dt} = D_1\upsilon_{1,eq}\frac{\partial \upsilon_1}{\partial x} + D_d\upsilon_{d,eq}\frac{\partial \upsilon_d}{\partial x} - D_2\frac{\partial \upsilon_2}{\partial x} \tag{38}$$

The first two terms in the right-hand side account for polymer swelling due to water penetration and drug diffusion, respectively, whereas the third term accounts for polymer shrinking due to the limited chain disentanglement. It is important to note that the mass balance at interfaces R and S (Eqs. (37)

and (38)) does not conserve each species separately. When densities of polymer and drug are not similar, the flux of either one could be overestimated or underestimated based on the density difference.

Here, it is assumed that the polymer chain transport to dissolve at the interface S through a diffusion boundary layer of thickness δ_b is given by:

$$\frac{\partial v_2}{\partial t} = \frac{\partial}{\partial x}\left(D_2 \frac{\partial v_2}{\partial x}\right) - \frac{dS}{dt}\frac{\partial v_d}{\partial x} \tag{39}$$

The initial and boundary conditions at the boundary layer interface for the thin boundary layer region are as follows:

$$\begin{array}{lll} t = 0 & \forall x & v_2 = 0 \\ t>0 & x = S(t) + \delta_b & v_2 = 0 \\ 0<t<t_{rept} & x = S^+(t) & -D_2 \dfrac{\partial v_2}{\partial x} = 0 \\ t>t_{rept} & x = S^+(t) & -D_2 \dfrac{\partial v_2}{\partial x} = k_d \\ t>t_{rept} & x = S^+(t) & v_2^+ = v_{2,eq} \end{array} \tag{40}$$

There are three stages to define the boundary condition at interface S in the thin boundary layer δ_b. When $0<t<t_{rept}$, the disentanglement rate is negligible and no water is able to penetrate the interface S $\left(-D_2 \frac{\partial v_2}{\partial x} = 0\right)$. The second stage is observed when $t>t_{rept}$ as the rate of diffusion is sufficiently high and the disentanglement rate is controlling $\left(-D_2 \frac{\partial v_2}{\partial x} = k_d\right)$. The last stage indicates that the equilibrium state has been reached ($v_2 = v_{2,eq}$) when polymer is concentrated in the boundary layer since the polymer diffusion rate in the boundary layer becomes insufficient to transport the chain to the surrounding medium.

Having imposed the pseudo-steady approximation that results in linear concentration profiles of water and drug in the rubbery region, the variation of gel layer thickness variation with time is also obtained mathematically as follows:

$$-(S-R) - \alpha \ln\left[1 - \frac{(S-R)}{\alpha}\right] = Bt \tag{41}$$

The fraction of drug release from the swelling-controlled system is finally given by:

$$\frac{M_t}{M_\infty} = \frac{\sqrt{B}(v_{d,eq} + v_d^*)}{2l}\left(\sqrt{2\alpha t} + \sqrt{B}t\right) \tag{42}$$

where $2l$ is the initial slab thickness and $\alpha = \frac{A}{B}$,

$$\begin{aligned} A &= D_1(v_{1,eq} - v_1^*)\left[\frac{v_{1,eq}}{v_{1,eq} + v_{d,eq}} + \frac{1}{v_1^* + v_d^*}\right] \\ &\quad + D_d(v_{d,eq} - v_d^*)\left[\frac{v_{d,eq}}{v_{1,eq} + v_{d,eq}} + \frac{1}{v_1^* + v_d^*}\right] \\ B &= \frac{k_d}{v_{1,eq} + v_{d,eq}} \end{aligned} \tag{43}$$

It is again implied that the model accounts for the superposition of Fickian diffusion and dissolution process. The first term on the right-hand side of Eq. (42) is the diffusion-controlled release term, which has a square-root dependency on time. In contrast, the second term is the dissolution term due to the chain disentanglement, as expressed by a first-order dependency on time. The magnitude of each process is determined by the value of α, which is the dimensionless ratio of polymer dissolution at interface S to polymer and drug diffusion in the rubbery region. As α approaches zero, "Case-II transport" prevails and a linear release profile is observed. On the other hand, higher values of α indicate that the drug release is Fickian. In the former case, the gel layer thickness ($S-R$) becomes relatively flat as drug is released in a zero-order manner due to the dissolution process at the interface S.

The model is able to predict the normalized gel layer thickness variation with time for a tablet containing *cimetidine hydrochloride* (50%-wt), PVA (10%-wt), and *mannitol* (40%-wt) as shown in Fig. 7a. In addition, it can also explain the *diprophylline* release from PVA–*mannitol* tablets (Fig. 7b). In the latter case, it is important to note that the release prediction is independent of the experimental data (not a fitting). More importantly, the synchronization period is not observed, suggesting that it is likely to be a special case. Even though this concept is developed for one-dimensional system, it can later be adopted and extended to a model with any geometry of interest.

Siepmann et al. [39] developed a model for drug release from HPMC matrix by combining diffusion, swelling, and dissolution mechanisms into Fujita-type, exponential, concentration-dependent diffusivities of the solute and solvent. Drug and water diffusivities are exponentially dependent on the concentration of the swelling polymers due to their viscosity-inducing

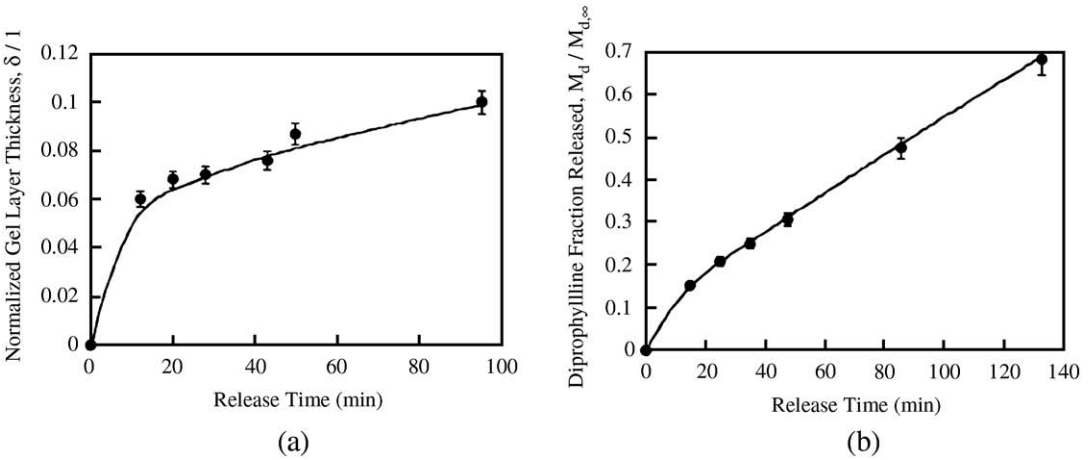

Fig. 7. The temporal variation of (a) normalized gel layer thickness, $\delta_{gel}=(S-R)/l$, where l is the half of slab thickness or the initial position of both interfaces R and S; and (b) cumulative mass release of *diprophylline*. The tablet consists of 50% *diprophylline*, 10% PVA ($\bar{M}_n = 130,000$), and 40% *mannitol*. The gel layer thickness and cumulative release profile are predicted by Eqs. (41) and (42), respectively (reprinted from [34] with permission from Wiley-Liss, Inc., a subsidiary of John Wiley & Sons, Inc. Copyright © 1997).

capabilities. In addition, the transport analysis is improved into two-dimensional (axial and radial) model and integrated with the polymer swelling and dissolution. The decrease of dry polymer matrix mass is characterized by the dissolution rate constant (k_{diss}), which is a function of the type of polymer and dissolution medium. However, in current model, the polymer dissolution is not confined at the surface boundary condition. Instead, the total polymer mass is calculated over the release period to result in time-variant matrix composition, matrix dimensions, and drug and water diffusion pathways.

The transport model applied in the cylindrical coordinate, without taking into account the variation in θ-direction, is expressed as follows:

$$\frac{\partial C_i}{\partial t} = \frac{\partial}{\partial r}\left(D_i \frac{\partial C_i}{\partial r}\right) + \frac{D_i}{r}\frac{\partial C_i}{\partial r} + \frac{\partial}{\partial z}\left(D_i \frac{\partial C_i}{\partial z}\right) \quad (44)$$

In the above equation, the concentration-dependent diffusivity can be expressed as follows:

$$D_i = D_{i,crit}\exp\left[-\beta_i\left(1-\frac{C_i}{C_{i,crit}}\right)\right] \quad (45)$$

Here, i and β_i indicate the diffusing species (i.e., 1 for water and 2 for drug) and dimensionless constants characterizing the concentration dependence of both species diffusivities, respectively. $C_{i,crit}$ and $D_{i,crit}$ are the maximum concentration and diffusion coefficient of species i in the swelling polymer matrix, respectively, at the interface between the matrix and release medium where the polymer disentanglement takes place. This model also accounts for the polymer dissolution process quantitatively. The dissolution process is characterized by a dissolution rate constant (k_{diss}) as follows:

$$M_{p,t} = M_{p,0} - k_{diss} S_t t \quad (46)$$

where $M_{p,t}$ and $M_{p,0}$ are the dry polymer matrix mass at time t and at initial time ($t=0$), respectively, and S_t is the surface area of the system at time t. It is important to note that the polymer disentanglement (dissolution) constant is defined in different ways as the previous models. In the previous models, it is defined as the polymer disentanglement rate constant (k_d) in the boundary condition at the interface with the surrounding medium.

In this model, the matrix swelling is assumed to be ideal, in which the total volume of the system is always equal to the sum of water, drug, and polymer volumes. The volume of each component is calculated at each time step, and by assuming ideal homogenous swelling and accounting for the polymer dissolution, the new volume is calculated. In this case, the system is allowed to have volume increase (swelling) and

volume decrease (shrinking) due to imbibing water into the system and polymer dissolution at the surface, respectively. However, the two moving fronts R and S in the previous models are not observed in this model as the change in volume is only attributed to change of outer boundaries. In addition, only two species (water and drug) are considered to follow the Fick's second law of diffusion as polymer dissolution process is simplified to be the overall mass decrease of the polymer. Therefore, the polymer mass balance is basically uncoupled from the drug and water transport. Since the model is later used to explain drug release from HPMC tablet, the model improvement in utilizing a two-dimensional cylindrical coordinate system is substantial. The model was able to explain the *propranolol-hydrochloride* release profile from cylindrical HPMC matrices [39]. The agreement between model and experimental data is achieved by simultaneous fitting of no more than two parameters, e.g., β_i and $D_{i,\mathrm{crit}}$. The study also shows that the effect of the initial tablet radius is more influential on drug release rather than that of initial thickness. It is expected since the former dictates more on the available surface area in the radial direction, which is the main diffusional pathline for the drug release. From a practical view, however, this model relies on computational power and does not offer an explicit mathematical solution.

By also utilizing Fick's second law in cylindrical coordinates and the Fujita-type exponential-dependence of the diffusion coefficients for both water and drug, Siepmann et al. [40,41] further developed the previous model into a "sequential layer" model (Fig. 8a), in which the tablet system is assumed to have a certain amount of single layers penetrated by water. Introducing the concept of "sequential layer", this model is performed in a computational grid and the modified structure of the grid is required for numerical analysis. An advantage of using computational grid is that it allows the modeling of inhomogeneous swelling. In contrast to the previous model, swelling is considered to take place layer by layer, in which the outermost layer swells first followed by the neighboring inner layers. Here, the model is able to capture the major feature of swelling-controlled system, which is the substantial change in volume of the system in the outer layer. This improvement is important since the substantial change in the system volume will change the concentrations of all species as well as influence the mobility of the species (increasing diffusion coefficients of water and drug). Similar to the previous model [39], only water and drug are considered in the transport model, whereas the polymer undergoes a reduction in molecular weight characterized by the constant dissolution rate constant (k_{diss}). This model has obvious improvements in accounting for the volume change in the system that affects concentration of species in the system as well as the increasing mobility of species due to water penetration. However, similar to the previous model, this model does not result in an explicit mathematical model and so it is difficult to highlight the important swelling parameters that affect the drug release. In addition, the existence of moving interface R for glassy region is neglected and diffusion of drug and water is assumed throughout the whole system. But, apparently the diffusion in the glassy core region can be negligible and the drug release is dominated by the enhanced diffusion through the gel layer.

The "sequential layer" model is able to fit the several experimental drug release profiles from HPMC tablets [40,41]. The model drugs used are *chlorpheniramine maleate*, *theophylline*, *acetaminophen*, *dicolofenac sodium*, and *propranolol-hydrochloride*. The model has also proved its capability to predict the unknown release profile in an independent experiment for *theophylline* release from HPMC tablets (Fig. 8b). In addition, the applicability of this model to fitting several model drugs from HPMC tablets with different molecular weights suggests that this model can be used to understand the effect of HPMC tablet design (e.g., initial radius, height, and size) on the drug release profile [41,42]. In concordance with the previous model's conclusion [39], simulation results also suggest that the available surface area of the device for diffusion is the most crucial parameter that determines the drug release profile, in which varying device geometry does not provide a straightforward result. The model can be improved by coupling the polymer species with drug and water species in the transport equation as has already been done before [32,34]. It would be interesting to see in the future, the development of an additional feature of glassy core region in the "sequential layer" model that may enable the observation of the variation of two moving fronts during the drug release process.

4. Mathematical models for erosion-controlled systems

Bioerodible polymers are versatile materials for a variety of biomedical applications, especially for drug delivery systems, since their chemistry and surfaces can be tailored to stabilize macromolecular agents and enhance the tissue site-targeting. More importantly, the erosion kinetics can be tailored by careful selection of polymer and a variety of techniques of encapsulation to control the drug release profile. In the simplest manner, the erosion kinetics can be altered by modifying copolymer composition or the degree of crystallinity as crystalline and amorphous polymers erode at different rates.

It is important to distinguish the two different terms commonly used in describing the polymer erosion phenomena, namely degradation and erosion. In a simplistic point of view, degradation refers to the polymer chain/bond cleavage/scission reaction (chemical process), whereas the erosion designates the loss of polymer material in either monomers or oligomers (chemical and physical process). Here, the erosion may consist of several chemical and physical steps, including degradation. Since erosion is a more general term to capture the overall mechanism of the bioerodible system, this section will mainly utilize the term erosion. But the term of degradation will still be used when specific degradation processes, e.g. polymer backbone cleavage and autocatalytic process, are involved in the model.

Since complex phenomena take place in erosion-controlled systems, physiochemical characterizations on drug devices are important to understand the possible essential mechanism of drug release. The identification of dominant drug release mechanism, in turn becomes the basis of mathematical model development. In this particular objective, transient characterizations are often necessary to conduct during drug release and erosion processes. Several characterization techniques, commonly carried out *in vitro*, have been used widely to investigate the controlled release properties of polymeric drug devices as reported in literatures [43,44]. Gel permeation chromatography (GPC) can be used to monitor the polymer molecular weight changes during the drug release and erosion. The cumulative polymer erosion and degradation, i.e. the monomer release, can be related to cumulative drug release profiles to provide insights on how polymer erosion and degradation are involved in drug release. Several mechanistic models relate the increase of drug diffusion coefficient with the decrease of polymer molecular weight due to chemical degradation which will be discussed later. Differential scanning calorimetry (DSC) can measure the degree of crystallinity and glass temperature (T_g) changes. Aforementioned in the swelling-controlled system section, T_g is important in polymeric system since above T_g, the polymer is in

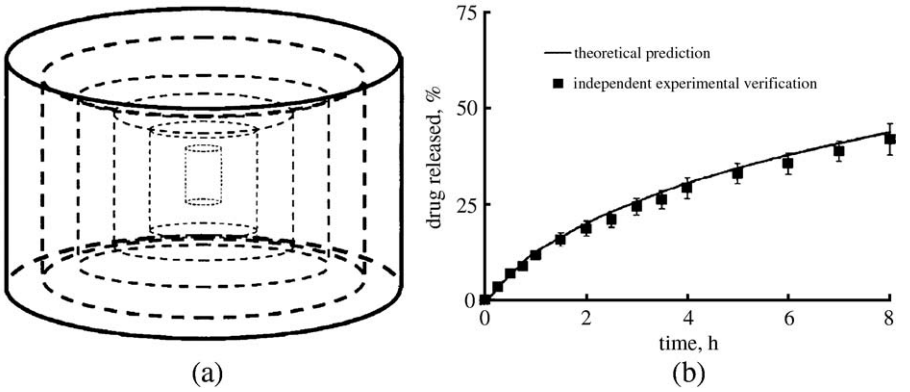

Fig. 8. (a) A schematic of "sequential layer" structure of the matrix in symmetry planes in axial and radial directions; and (b) the validation of the model by independent experiment, in which the model predicts the result before the experimental study. The theoretical prediction shows an agreement with the experimental cumulative release profile of *theophylline* from HPMC tablets with R_0=0.6 cm, Z_0=0.23 cm and 40% initial drug loading. Samples were prepared as 500-mg tablets in phosphate buffer pH 7.4 medium at 37 °C (reprinted from [40] with kind permission from Springer Science and Business Media).

rubbery state characterized by high mobility of polymer chains such that more free volume is available for drug diffusion. In contrast, below T_g, the polymer is in glassy state, where the drug diffusion is more difficult as compared to that in the rubbery region. Scanning electron microscopy (SEM) allows investigation of the microstructure of polymer surface and matrix. If the cross-section cutting of the microspheres is possible, the evolving internal morphology during the release can also be investigated using this technique.

There are two ideal scenarios for polymer erosion, namely surface (heterogeneous) and bulk (homogeneous) erosions (as shown in Fig. 9). In bulk erosion, the microsphere has a constant diameter size and external fluid is allowed to penetrate into the microsphere, during which erosion of the polymer occurs. On the other hand, in surface erosion, the microsphere has an evolving shrinking diameter as the erosion of the polymer takes place at the external matrix boundary.

It is suggested that the manner in which polymer erodes depends on the erosion number (ψ), which is the ratio of characteristic time of diffusion of water into the polymer drug to that of the degradation rate of the polymer backbone [45]. This study also implies that the types of erosion behavior depend on the types of polymer that strongly dictate the degradation rate of the polymer backbone. Therefore, polymer with reactive functional groups, e.g. polyanhydrides, is expected to degrade faster and surface erosion is expected. The most important of these polyanhydrides are *poly(1,3-bis-p-carboxyphenoxypropane-co-sebacic acid)* (p(CPP-SA)) and *poly(1,6-bis-p-carboxyphenoxyhexane-co-sebacic acid)* (p(CPH-SA)). The physiochemical characteristic of these polymers has been reviewed in literature [44]. On the other hand, polymer with less reactive functional group, e.g. polyesters, tends to degrade more slowly compared to solvent penetration rate and thus bulk erosion is expected. The most important of these esters for drug delivery application are *poly(lactic acid)* (PLA), *poly(lactic-co-glycolic acid)* (PLGA), and poly(ε-caprolactone) (PCL).

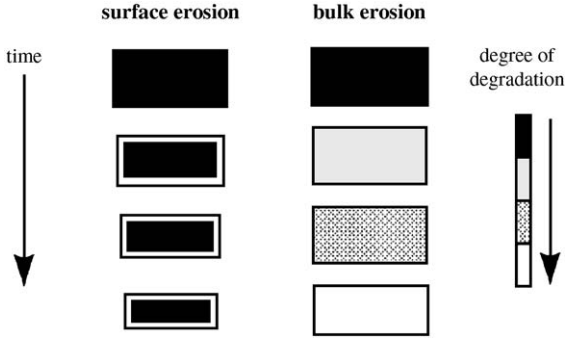

Fig. 9. Schematic illustration of surface- and bulk-erosion processes in the polymer matrix (reprinted from [45] with permission from Elsevier).

The characteristic time for water diffusion into the polymer bulk (t_{diff}) is as follows:

$$t_{diff} = \frac{\pi \langle x \rangle^2}{4} \frac{1}{D_e} \tag{47}$$

where D_e is the effective diffusivity of water inside the polymer matrix and $\langle x \rangle$ the mean distance for the diffusion. The effective Fickian diffusion is based on the continuum formulation with effective diffusion coefficient in liquid within fine pores [46]. The effective diffusion coefficient is defined as the result of hindered diffusion that may be complicated by the size, shape, and electrical charge of the solutes and pores as described in [47].The characteristic degradation time $E(t_n)$, for polymer functional groups is given by:

$$E(t_n) = \frac{1}{\lambda} \ln(n) = \frac{1}{\lambda} \left[\ln\langle x \rangle - \ln\left(\frac{\overline{M}_n}{N_A (N_p - 1)\rho} \right)^{1/3} \right] \tag{48}$$

where the pseudo first-order rate constant λ, is the kinetic rate constant that accounts for the reactivity of polymer functional groups and therefore related to the half-life of polymer bonds, $\overline{M}_n$ is the number-average polymer molecular weight, N_p is the degree of polymerization, N_A is Avogrado's number, and ρ is the density of the polymer. Thus, the erosion number (ψ) is defined as follows:

$$\psi = \frac{t_{diff}}{E(t_n)} = \frac{\pi \langle x \rangle^2 \lambda}{4 D_e \left[\ln\langle x \rangle - \ln\left(\frac{\overline{M}_n}{N_A (N_p - 1)\rho} \right)^{1/3} \right]} \tag{49}$$

If the polymer matrix characteristics and type are the same, the expression for ψ can be simplified as follows:

$$\psi = \frac{t_{diff}}{E(t_n)} = K \left(\frac{\lambda}{D_e} \right) = L(\langle x \rangle) \left(\frac{\lambda}{D_e} \right) \tag{50}$$

This analysis suggests that polymer erosion depends on the matrix geometry, i.e., shape and size, since the characteristic length (L) contributes to the magnitude of ε. If λ and D_e changes are negligible during the erosion process when erosion medium and fabricated polymer matrix characteristics (e.g. porosity and type) can be kept constant, the characteristic length (L) will be the only parameter that determines how polymer erodes. In this case, there will be a critical characteristic length (L_{crit}) that defines the boundary between two possible erosion types for each polymer type. When $L > L_{crit}$, polymer will undergo surface erosion, whereas, when $L < L_{crit}$, polymer will undergo bulk erosion. This analysis predicts that fast-eroding polymers, like polyanhydrides, are already surface-eroding at micrometer scale as $L_{crit} \approx 10^{-4}$, which is in agreement with the observation from experimental studies [44]. On the other hand, polymers like PLA and PLGA, which have relatively less reactive functional groups, tend to have bulk-eroding characteristics since they have higher L_{crit} ($\approx 10^{-2}$).

Several mathematical models have been developed to explain the drug release from the erosion-controlled systems. Theoretically, the erosion mechanism is a combination of mass transport and chemical reaction phenomena. It involves several important mechanisms, which are drug dissolution, polymer degradation, porosity creation, micro-environmental pH change due to polymer degradation, diffusion of drug in polymer matrix, and autocatalytic effect during polymer degradation. This complex interplay hinders the development of a useful and accurate mathematical model that is able to predict all the mechanism contributions on the resulting drug release kinetics from a bioerodible polymer. In the simplest manner, mathematical models for erosion-controlled systems are classified into empirical models and mechanistic models. The former does not take into account the complex physicochemical phenomena and are commonly developed for surface-eroding systems that exhibit zero-order release process. On the other hand, the latter accounts for the physicochemical phenomena that basically involve diffusional mass transfer and chemical reaction processes. Based on the approach of developing models, the latter can be sub-classified into diffusion-and-reaction models and cellular-automata models. The former models the erosion process as a transport process of combined diffusion and chemical reaction processes, whereas the latter considers the erosion process as a random event.

4.1. Empirical models

Weibull [48] provided an empirical equation that was adopted for the drug release profile by Langenbucher [49] and applied to fit the drug release by Vudathala and Rogers [50] and Dokoumetzidis et al. [51]. The Weibull equation defines the cumulative fractional drug release expression as a function of time as follows:

$$\frac{M_t}{M_\infty} = 1 - \exp\left[\frac{-(t - t_{lag})^b}{t_{scale}}\right] \tag{51}$$

In Weibull equation, t_{lag} is the lag time before the drug release takes place, t_{scale} is the time scale of the release process, and b characterizes the shape of the release curve. The case of $b=1$ gives an exponential curve, $b>1$ gives a sigmoid (S-shaped) curve, and $b<1$ gives a parabolic curve with high initial slope followed by an exponential decay.

Hopfenberg [52] developed an empirical drug release model for erosion-controlled polymer by assuming that the overall release behaves as a zero-order process. This zero-order process is essentially a combination result of dissolution and erosion processes at the polymer surface. Therefore, this empirical equation is appropriately applied for the surface-eroding particles since this model assumes that the release rate is controlled by the dissolution process on the surface. This model was also suggested by Hixson and Crowell [53] with the assumption that the shrinking spherical particle area is proportional of the cubic root of its volume. For spherical geometry, the mathematical equation is written as follows:

$$\frac{M_t}{M_\infty} = 1 - \left[1 - \frac{k_{ero,0} t}{C_0 R}\right]^3 \tag{52}$$

where $k_{ero,0}$ is the surface erosion rate constant, C_0 is the initial concentration of the drug in the matrix, and R is the initial radius of the sphere.

El-Arini and Leuenberger [54] modified the Hopfenberg model by accounting for the lag time (t_{lag}) in the

early time of drug release process. The modified drug release fraction equation is written as follows:

$$\frac{M_t}{M_\infty} = 1-\left[1-\frac{k_{ero,0}}{C_0 R}(t-t_{lag})\right]^3 \quad (53)$$

Cooney [55] considered two main steps in the polymer matrix that undergo surface erosion, which are the detachment of an atom or molecule, followed by the diffusion of this agent through a diffusion boundary layer into the bulk. For the case of surface erosion (slow dissolution rate) in a sphere, the surface dissolution/detachment controls the overall process and the mass balance is given by:

$$-\rho_s \frac{d\left(\frac{4}{3}\pi r^3\right)}{dt} = k_{ero}(4\pi r^2)\Delta C \quad (54)$$

With the assumption of constant concentration difference existing between the surface and the bulk medium (ΔC), the previous equation has a solution as follows:

$$r = R-\left(\frac{k_{ero}\Delta C}{\rho_s}\right)t \text{ or } \frac{r}{R} = \left(1-\frac{k_{ero}\Delta C}{\rho_s R}t\right) = (1-\tau) \quad (55)$$

However, even though the surface concentration can be maintained, the surface area will decrease with time leading to a lower dissolution rate. The ratio of the instantaneous dissolution rate to the initial dissolution rate (f) and the total drug release rate can be defined as follows:

$$f = (1-\tau)^2 \quad (56)$$

If the surface-eroding matrix has a uniform drug distribution, the cumulative drug release expression is similar to that of Hopfenberg, which is as follows:

$$\frac{M_t}{M_\infty} = 1-\left(\frac{r}{R}\right)^3 = 1-\left(1-\frac{k_{ero}\Delta C}{\rho_s R}t\right)^3 \quad (57)$$

The final result is basically similar to that of Hopfenberg. The only slight difference between these two models is that Hopfenberg's model does not account explicitly the contribution of concentration gradient, which is lumped to be a constant ($k_{ero,0}$).

4.2. Mechanistic models

Mechanistic models are primarily divided into two main groups based on how the erosion process is modeled. The first group is the diffusion-and-reaction model, which suggests the description of the erosion process as a combination of polymer diffusion and reaction. Until now, these models are primarily developed for the bulk-eroding microspheres with exception of several modeling efforts by Zhang et al. [56] and Larobina et al. [57]. The second group, which is the cellular-automata model, assumes the erosion process as a random event. Here, the matrix surface detachment is commonly assumed the rate-controlling step, therefore the models are best applied for surface-eroding systems. For this reason, contrary to the diffusion-and-reaction models, the cellular-automata models are primarily built to explain the surface erosion process, except for a model by Siepmann et al. [58] that utilized the Monte-Carlo technique for a bulk-eroding system.

4.2.1. Diffusion-and-reaction models

Harland et al. [59] developed the first dissolution model for a polymer matrix that undergoes bulk erosion. The model is solved for both infinite and finite mass transfer boundary conditions at the polymer surface. The model accounts for the effective Fickian diffusion and dissolution of the solute into liquid-filled pores. Aforementioned, the effective Fickian diffusion is based on the continuum formulation by applying the effective diffusivity to account the diffusion in liquid within fine pores [46]. Thus, the transport model of the drug solute is expressed as follows:

$$\frac{\partial C}{\partial t} = D_e\left(\frac{\partial^2 C}{\partial r^2}+\frac{2}{r}\frac{\partial C}{\partial r}\right)+k(\varepsilon C_s - C) \quad (58)$$

Here, C and D_e are the drug concentration and effective diffusivity in liquid-filled pores respectively, k is the drug dissolution rate constant, ε is the porosity of the polymer matrix and εC_s is the equivalent drug saturation concentration in the solution found in the pores. The second term in the right-hand side is the dissolution term and is negligible when the drug loading (C_0) is smaller than the solubility concentration (εC_s). In case of a non-constant diffusivity, the diffusion coefficient is assumed to be exponentially concentration-dependent and the boundary condition at the surface is the infinite convective mass transfer under a perfect sink medium.

Performing dimensionless analysis by scaling naturally so that all variables are bounded between 0 and 1, a new dimensionless number, the dissolution/diffusion number (*Di*), is defined as follows:

$$Di = \phi_s^2 = \frac{kR^2}{D_e} \tag{59}$$

Following a chemical engineering point of view, *Di* is the square of Thiele modulus (ϕ_s) since similar phenomenon is observed when reaction and diffusion take place altogether inside a catalyst.

The solution of fractional drug release for infinite mass transfer at the surface is as follows:

$$\frac{M_t}{\varepsilon C_s \frac{4}{3}\pi R^3} = 6\sum_{n=1}^{\infty} \frac{(Di+n^2\pi^2)Di\tau + n^2\pi^2\{1-\exp[-(Di+n^2\pi^2)\tau]\}}{(Di+n^2\pi^2)^2} \tag{60}$$

where the dimensionless time (τ) is defined as $\tau = D_e t/R^2$.

On the other hand, for the release under a finite convective mass transfer condition, the Sherwood number (*Sh*), which is the ratio of the rate of convective mass transfer to that of diffusion, appears in the solution. The solution is as follows:

$$\frac{M_t}{\varepsilon C_s \frac{4}{3}\pi R^3} = 6Sh^2\sum_{n=1}^{\infty} \frac{(Di+\alpha_n^2R^2)Di\tau - \alpha_n^2R^2\{\exp[-(Di+\alpha_n^2R^2)\tau]-1\}}{(Di+\alpha_n^2R^2)^2[\alpha_n^2R^2+Sh(Sh-1)]} \tag{61}$$

where $Sh = hR/D_e$ and α_n are the roots of the transcendental equation of $\alpha_n R\cot(\alpha_n R) + Sh - 1 = 0$.

Interestingly, the simplified solution for longer times of drug release, during which dissolution controls the process, reveals that that the amount of drug release is simply a first-order function of time as follows:

$$M_t = \frac{2\pi R^3 \varepsilon C_s}{\sqrt{k}}\left[\sqrt{\frac{D_e}{R}}\coth\left(R\sqrt{\frac{k}{D_e}}\right) - \sqrt{k}\csc^2 h\left(R\sqrt{\frac{k}{D_e}}\right)\right] + 8\pi R D_e \varepsilon C_s \times\left[\frac{kR}{2D_e}\sqrt{\frac{D_e}{k}}\coth\left(R\sqrt{\frac{k}{D_e}}\right) - \frac{1}{2}\right]t \tag{62}$$

This relationship takes places as long as undissolved drug in the microparticles still exists.

Heller and Baker [60] used the classical Higuchi model as a basis to develop a mathematical model for bulk-eroding polymers. The main process that controls drug release is assumed to be the hydrolytic backbone cleavage before the drug is solubilized in the medium. The modified Higuchi model is as follows:

$$\frac{dM_t}{dt} = \frac{S}{2}\left(\frac{2PC_0}{t}\right)^{1/2} \tag{63}$$

In this equation, *S* is the surface area on both sides of the planar film, C_0 is the initial drug concentration (loading) in the polymer, and *P* is the permeability of the drug inside the polymer matrix.

Contrary to the classical Higuchi model, this model accounts the effect of the drug permeability in the biodegradable polymer, which is not constant, but increases with time, as more pores are created during the erosion. The following equation was used to account for the change of permeability with time as a function of number of remaining bonds.

$$\frac{P}{P_0} = \frac{\text{initial number of bonds}}{\text{remaining number of bonds}} = \frac{N}{N-Z} \tag{64}$$

where *N* is the initial number of bonds and *Z* is the number of bonds that have undergone cleavage.The bond cleavage process is assumed to follow a first-order kinetics that can be expressed as follows:

$$\frac{dZ}{dt} = K(N-Z) \tag{65}$$

where *K* is the first-order kinetic rate constant for bond cleavage process.The final equation for the rate of drug released from the system is as follows:

$$\frac{dM_t}{dt} = \frac{S}{2}\left(\frac{2P_0\exp(Kt)C_0}{t}\right)^{1/2} \tag{66}$$

Thombre and Himmelstein [61] developed a mathematical model for a bulk-eroding polymer matrix of *poly(orthoester)* (Fig. 10). The model is based on slab geometry and a perfect sink condition is assumed. In this model, the acid generation from acid hydrolytic

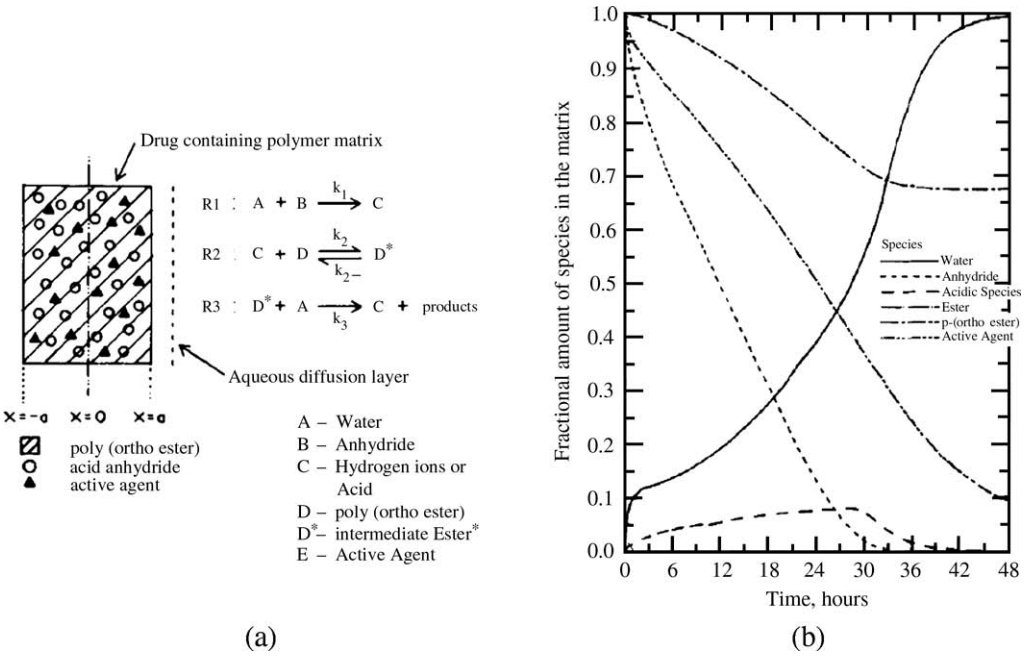

Fig. 10. (a) Schematic illustration of the diffusion-reaction model for *poly (orthoester)* drug delivery system by Thombre and Himmelstein; and (b) fractional release of each species as a function of time based on the proposed model (reprinted from [61] with permission from Wiley-Liss, Inc., a subsidiary of John Wiley & Sons, Inc. Copyright © 1985).

reaction is taken into account. The resulting species mass balance is as follows:

$$\frac{\partial C_i}{\partial t} = \frac{\partial}{\partial x}\left(D_{e,i}(x,t)\frac{\partial C_i}{\partial x}\right) + \upsilon_i \tag{67}$$

In this equation, υ_i is the net sum of synthesis and degradation rate of species i, whereas A, B, C, and E denote water, acid generator, acid, and drug, respectively.The diffusion coefficient of each species is also updated during the erosion as an exponential function of the respective species concentration as follows:

$$D_{e,i} = D_{i,0}\exp\left[\mu\frac{(C_{i,0}-C_i)}{C_{i,0}}\right] \tag{68}$$

where $D_{i,0}$ and $C_{i,0}$ are initial diffusion coefficient and concentration of component i when the polymer is yet hydrolyzed, and μ is a constant.

Several models prefer to apply the simple Fick's second law, but define the molecular weight dependence of drug diffusivity in the polymer matrix to account for increase in drug release during erosion. The advantage of these models is the variation of polymer molecular weight with time due to erosion and the dependence of drug diffusivity on polymer molecular weight can be independently determined and therefore, the number of fitted parameters is minimized. Here, however, it is important to note that the pore creation that enhances the drug diffusion is not mechanistically modeled.

Charlier et al. [62] assumed that the polymer degradation, which is quantitatively regarded as the polymer molecular weight, follows a first-order kinetic process of polymer chain cleavage. However, the model is developed to quantify drug released from PLGA film with planar geometry.

$$\frac{dM_w}{dt} = -k_{degr}M_w \rightarrow M_w = M_{w,0}\exp(-k_{degr}t) \tag{69}$$

The drug diffusion coefficient in polymer matrix during erosion is assumed to correlate inversely to the polymer

molecular weight, which suggests the following equation:

$$\frac{D_e}{D_0} = \frac{M_{w,0}}{M_w} \rightarrow D_e = D_0 \exp(k_{degr} t) \tag{70}$$

This model assumes a linear concentration gradient as predicted in the classical Higuchi model. The final expression for the rate of drug release is as follows:

$$M_t = S\left(\frac{2C_0 C_s D_0 (e^{k_{degr} t} - 1)}{k_{degr}}\right) \tag{71}$$

At early times, the resulting equation can be reduced into Higuchi's solution for $C_0 > C_s$ as $e^{k_{degr} t} \approx 1 + k_{degr} t$, whereas, at longer times, the exponential term will control the drug release and Eq. (71) still holds. The solution for the former case is expressed mathematically as follows:

$$M_t = S\sqrt{2C_0 C_s D_0 t} \tag{72}$$

Raman et al. [63] used the simple diffusion model for spherical geometry with diffusivity dependence on molecular weight to explain the *piroxicam* release from bulk-erosion *poly(lactide-co-glycolide)* (PLG) microspheres. The molecular weight loss due to the erosion is expressed as follows:

$$M_w = \begin{cases} M_{w,0} & \text{when } t < t_{lag} \\ M_{w,0} e^{k_{degr}(t - t_{lag})} & \text{when } t \geq t_{lag} \end{cases} \tag{73}$$

Here, t_{lag} is the lag time before the polymer matrix erodes. The diffusivity dependence on molecular weight is estimated to be an empirical cubic polynomial fit that relates $\ln(D_e)$ and $\ln(M_w)$. Another important feature of the model is the effect of non-uniform drug distribution using data from confocal fluorescence microscopy. Here, intensity plots obtained from confocal microscopy are converted to initial radial distribution of drug.

He et al. [64] also used a similar approach by combining Baker and Lonsdale's model [4] for diffusion-controlled release and the concept of increased diffusion coefficient due to polymer chain scissions. In their model, similar to Charlier's approach, the variation of D_e with time is defined as an exponential function. However, the overall fraction drug release is obtained from a combination between Baker and Lonsdale's diffusion solution (Eqs. (9) and (10)) and the pure matrix erosion (F_E) of Fitzgerald and Corrigan [65]. For drug release from a sphere, this is expressed as follows:

$$\frac{M_t}{M_\infty} = 4\sqrt{\frac{D_e t}{\pi r^2}} - 3\frac{D_e t}{r^2} + F_E\left[\frac{\exp(k_{degr}(t - t_{max}))}{1 + \exp(k_{degr}(t - t_{max}))}\right] \tag{74}$$

where t_{max} is the time to maximum matrix erosion rate.

This model is able to describe the triphasic drug release profile that comprises: (i) initial "burst" due to the short diffusion pathways, (ii) intermediate phase of zero-order release due to simultaneous drug diffusion and polymer degradation, and (iii) second rapid drug release due to final matrix erosion that releases the remaining drug. The resulting release profile is similar to the "S" erosion model for bulk erosion by Zhang et al. [56] that will be described later in this section.

A similar approach was also used by Siepmann et al. [66] to explain the 5-*fluorouracil* (5-FU) release from bulk-erosion PLGA microspheres. However, this model requires two different constants to express the evolving drug diffusivity as the diffusivity is not a simple ratio relationship as in Charlier et al. [62]. A similar approach was previously done by Wada et al. [67] for *aclarubicin hydrochloride* (ACR) release from PLA-based microspheres. The variations of drug diffusivity with molecular weight and molecular weight with time are expressed as follows:

$$D_e = D_0 + \frac{k}{M_w} \tag{75}$$

$$M_w(t) = M_{w,0} \exp(k_{degr} t) \tag{76}$$

In addition, the difference with previous models is that the amount of drug release utilized the approximate explicit solution by Koizumi and Panomsuk [7] for spherical delivery system. The amount of drug released equation is expressed as follows:

$$M_t = 4\pi R^2 \left[\sqrt{2(C_0 - C_s) C_s D_e t} + \frac{4 C_s D_e t}{9R} \times \left(\frac{C_s}{2C_0 - C_s} - 3\right)\right] \tag{77}$$

Ehtezazi and Washington [68] combined the percolation theory and classical Crank diffusion model to study the macromolecule (FITC-*dextran*) release from porous PLA microspheres. Here, the kinetic model is basically lumped in the evolving drug diffusion coefficient through the percolation theory. In this approach, the pores are divided into conducting (accessible) and discrete (isolated) regions. The accessible pore region is connected to the exterior surface that allows mass transport from the system to the surrounding. On the other hand, the isolated pore space is disconnected from the surrounding medium. It is assumed that, below the percolation threshold (ρ^{C}), the accessible porosity is not available and, thus, the porosity equals to the isolated porosity. The Bethe lattice theory relates the percolation threshold with the coordination number z, which is given by:

$$\rho^{C} = \frac{1}{(z-1)} \tag{78}$$

Having determined the Bethe lattice coordination number for molecule of which the diameter is smaller than the porous diameter, the effective diffusion coefficient is related to the transport coefficient of the porous structure (ε^{E}) that is determined as follows:

$$D_e = D_0 \varepsilon^{E} \tag{79}$$

For a Bethe lattice model, ε^{E} can be calculated as follows:

$$\varepsilon^{E} = -\left(\frac{z-1}{z-2}\right)\frac{C'(0)}{D_0} \tag{80}$$

where $C'(x)$ is the derivative of a non-linear integral equation defined in Ehtezazi and Washington [68].

After determination of D_e, the fraction of drug released is calculated using the classical Crank model for diffusion in microspheres. Furthermore, in order to take into account the non-uniform distribution of microsphere sizes, the equation is slightly modified by introducing the fraction of microspheres with certain size ranges.

Siepmann et al. [69] provided a hypothesis to incorporate the autocatalytic effect to explain the *lidocaine* release from PLGA microspheres. The PLGA polymer is known to undergo the bulk-erosion process, where its polyester chains are cleaved into shorter chains of alcohols and acids throughout the matrix due to contact with water. The resulting acids will diffuse out of the microparticles to get neutralized. On the other hand, bases also diffuse into the microparticles to neutralize the acids. However, since both diffusional processes are comparably slower than the rate of acids generation, the micro-pH inside the system still drops during the bulk-erosion process. Here, the hypothesis is that, with the increasing microparticles size, the diffusion pathways for acids and bases increase and thereby, the neutralization process is less pronounced. This will lead to a drop in micro-pH inside the matrix and the accelerated polymer degradation. When polymer degradation is assumed to follow first-order kinetics, the experimental results are fitted into the equation to obtain the polymer degradation rate constant (k_{degr}).

Having assumed the drug release as a diffusion-controlled process with effective diffusivity (Eq. (58) without the dissolution term in the right-hand side of the equation) into a perfect sink medium with a finite convective mass transfer coefficient (h), the fitting shows that the effective diffusivity (D_e) increased substantially with increasing microsphere diameter. This is modeled by defining the effective diffusivity as a function of microsphere diameter. This observation suggests that the simulation results without autocatalytic effect fail to predict the *lidocaine* release profile (Fig. 11). It is explained by the autocatalytic effect that causes the increasing polymer degradation rate with increasing microsphere diameter so that it allows higher mobility of the drug to be released into the medium. This is confirmed by SEM study that shows the smaller microspheres were more resistant to degradation than larger microspheres [69] as shown in Fig. 12. In this case, using the classical diffusion model, it is initially assumed that the dissolution of the drug in this bulk-eroding system is negligible, whereas the autocatalytic effect is more significant. Though it is often acceptable that for a hydrophobic agent, like *lidocaine*, since the dissolution contribution is marginal, the fitting could have been done better by assuming both dissolution and diffusion processes take place together using a Harland model [59]. If the magnitude of the dissolution term turns out to be negligible, it can be confirmed that the drug was released dominantly by the diffusion process. Nevertheless, this finding unveils an interesting discussion on how important the size effect on the drug release rate.

Batycky et al. [70] developed a model to predict the water-soluble glycoprotein released from bulk-eroding

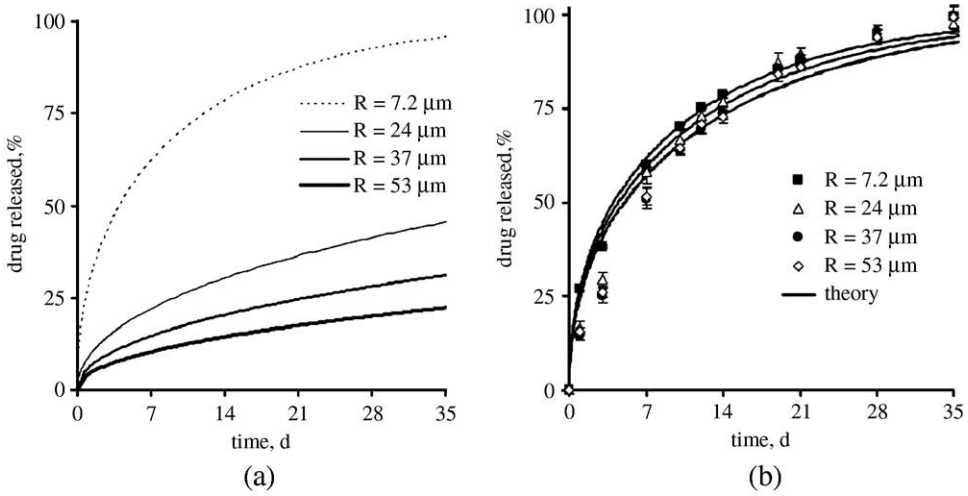

Fig. 11. (a) Theoretical *lidocaine* release profiles for different sizes of PLGA microspheres without autocatalytic effects ($D_e = 4.6 \times 10^{-14}$ cm^2/s); and (b) experimental (symbols) and theoretical (solid lines, with autocatalytic effects) *lidocaine* release profiles for different sizes of PLGA microspheres in phosphate buffer pH 7.4 (reprinted with permission from [69]. Copyright 2005 American Chemical Society).

system of PLGA and PLA by taking into account the evolving populations of micro- and mesospores and the possible fractional drug release due to the initial burst (Fig. 13). Since the protein is water-soluble and has a relatively large size, the model incorporates the induction phase that takes place when the available

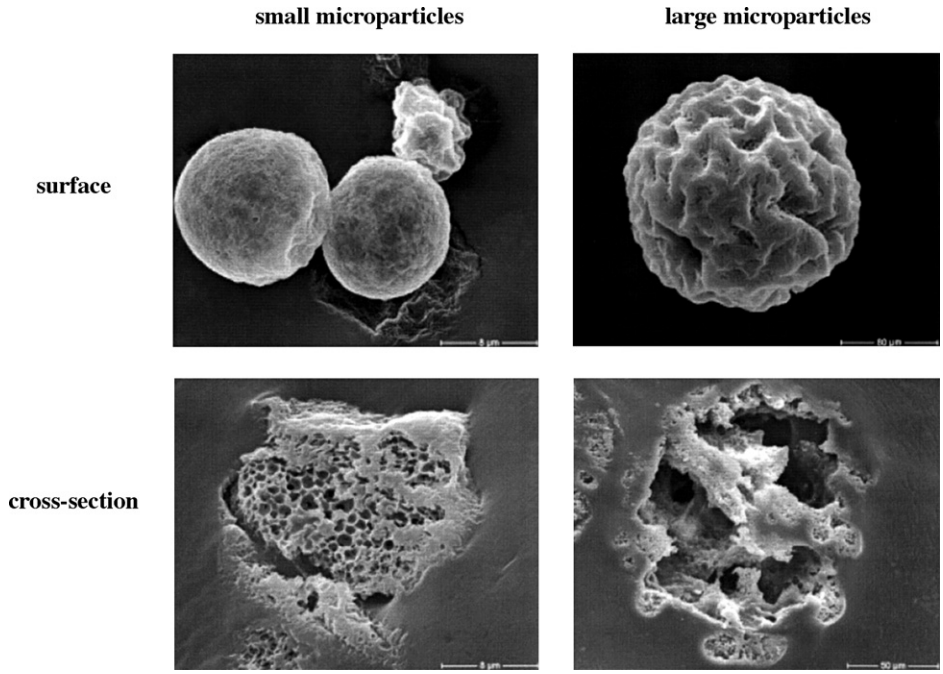

Fig. 12. SEM pictures (surfaces and cross-sections) of small ($R = 8$ μm) and large ($R = 80$ μm) *lidocaine*-loaded PLGA microspheres in phosphate buffer pH 7.4 at day 7 (reprinted with permission from [69]. Copyright 2005 American Chemical Society).

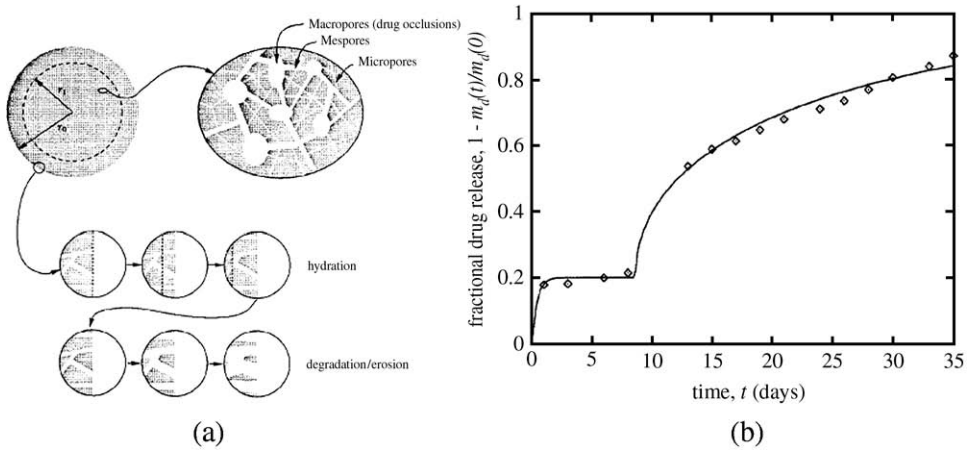

Fig. 13. (a) Schematic illustration of a microsphere that undergoes hydration, degradation, and erosion in bulk-erosion system; and (b) experimental (symbols) and model fitting (solid lines) of fractional release profile of MN rgp 120 protein (reprinted from [70] with permission from Wiley-Liss, Inc., a subsidiary of John Wiley & Sons, Inc. Copyright © 1997).

initial porosity is low, and thus prevents release of the protein via diffusion until mesoscopic pores are available in sufficient quantity. This also suggests that there is an initial burst before the induction time (t_d) due to the water-soluble protein because of the protein desorption in mesospores connected to external surface of the microsphere. The model involves an explicit evolving microstructural model of pores development during the erosion. This is related to the mass and molecular weight change of the polymer that was described by a combined model of random end-scission. The fractional protein release from the microspheres is expressed as follows:

$$\frac{M_t}{M_\infty} = 1-b[\exp(-k_{\text{degr}}t)] - (1-b)\frac{6}{\pi^2}\sum_{i=1}^{\infty}\frac{\exp\left(\frac{-i^2\pi^2 D_e(t-t_d)}{R}\right)}{i^2} \quad (81)$$

In this equation, b is the drug fraction release in the initial burst. The last term will be negligible when $t<t_d$ as the drug is not available to diffuse yet. Following the induction time ($t>t_d$), the drug undergoes Fickian diffusion through the porous microspheres.

This model has a good agreement with the experimental data in terms of polymer mass loss fraction and protein release fraction. However, there are several limitations in this model. For instance, drug diffusivity is assumed to be constant, which may not be true as the bulk erosion increases the porosity and therefore, the drug diffusivity should increase during the erosion. The model also does not account for the effects of variable pH on the degradation constants as the acidic monomers are produced during the erosion. More importantly, the fraction of drug release from the burst effect must be obtained experimentally through the fitting of release curve. Therefore the model can actually be considered as a semi-empirical model though the diffusion-and-reaction concept is still retained after the induction period. However, this effort illustrates the difficulties of modeling the release of hydrophilic drug, i.e. protein from hydrophobic polymer, i.e. PLA and PLGA, and justifies the use of a semi-empirical equation to fit the experimental data. The unique problem of modeling the hydrophilic drug released from nanospheres will also be discussed later in Section 6.

Zhang et al. [56] developed mathematical models for bulk- and surface-eroding polymeric microspheres by considering diffusion, dissolution, and erosion processes altogether. The bulk-erosion models are solved for both infinite and finite mass transfer cases, whereas the boundary movement in surface erosion model is assumed to be a first-order process with time. This study also includes the sensitivity analysis of several parameters that may affect the drug release. The drug release profiles are fitted to several experimental data, even though it is mainly performed for the bulk-erosion case.

For the bulk-erosion model, the concept of effective (V_1) and virtual (V_0) solid phases was proposed. The effective solid phase is the volume of solid that is eroding, in which the change pattern is related to the type of erosion. Erosion reduces the part of the effective solid phase and causes drug release from matrix entrapment. As a result, the drug concentration in effective solid phase is reduced. The virtual solid phase is the initial volume of microspheres before erosion occurs. Therefore, three phases are taken into account in this model, which are the liquid phase that has constant volume of V_0, the virtual solid phase that has constant volume of V_0, and the effective solid phase that has a variable volume of V_1. At the initial time, the volume of the effective solid phase V_1 is equal to that of the virtual solid phase V_0. The concentration in virtual solid phase is expressed as follows:

$$C_S = \left(\frac{V_1}{V_0}\right) C_{SE} \tag{82}$$

where C_S and C_{SE} are drug concentrations in virtual and effective solid phases, respectively.

In the effective solid phase, concentration decreases only due to the dissolution process. When the liquid phase concentration is higher than this concentration, the drug will deposit back to the effective solid phase. In addition, the diffusion coefficient varies with the changes of polymer porosity and tortuosity. Here, the tortuosity changes are proportional to the volume change of effective solid phase.

Three types of erosion are modeled, namely linear erosion, "S" erosion, and hyperbolic erosion. The pattern the polymer matrix erodes depends on several physical properties, such as degree of crystallinity (the amorphous region is more prone to degradation), molecular weight distribution (wide distribution would accelerate the degradation rate), the portion of *glycolide* (more *glycolide* monomer increases the degradation rate), and glass transition temperature (polymer chains in the rubbery state are more responsive to erosion with the presence of liquid water). For linear erosion, the ratio of amorphous region to crystalline region and free chains to rigid chains are comparable. For hyperbolic erosion, most of the polymer is in the amorphous state and the polymer chains are loose. This causes fast degradation at the initial stage followed by slow degradation at the later stage due to the presence of crystalline region. For "S" erosion, it is possible that the amorphous part is blocked by the crystalline domain, which makes the degradation rate slow at the beginning. When the crystalline region is hydrolyzed, the amorphous polymer chains are free to degrade therefore both degradation and drug release rates are accelerated.

For surface-erosion model, two compartments are considered, namely the solid and pore (liquid) compartments. The latter refers to the available compartment for water penetration. The size of the microsphere subsequently decreases, but the average polymer molecular weight does not change appreciably. This suggests that erosion is confined at the external boundary. The model assumed that the amount of water penetrating the microspheres is low so it does not cause erosion in the interior of microspheres. The dissolution from the solid phase to the liquid phase is taken into account in the Fick's second law for the liquid phase as proposed in Eq. (58) by Harland et al. [59]. Under an infinite convective mass transfer condition, the initial and boundary conditions for the equation are given by:

$$\begin{array}{ll} t = 0 \text{ and } 0 \le r \le R_0 & C_L = C_b \\ t > 0 \text{ and } r = 0 & \dfrac{\partial C_L}{\partial r} = 0 \\ t > 0 \text{ and } r = R_0(1 - k_{ero}t) & C_L = C_b \end{array} \tag{83}$$

where C_L is the drug concentration in the liquid phase and the constant rate of movement of erosion boundary is given as k_{ero}.

On the other hand, the governing equation and initial condition for solid phase that only accounts for the dissolution term can be expressed as follows:

$$\frac{\partial C_S}{\partial t} = -k(\varepsilon C_{sat} - C) \tag{84}$$

$$t = 0 \text{ and } 0 \le r \le R_0 \quad C_S = C_0 \tag{85}$$

where R_0 is the initial radius of the moving front of the eroding interface.

The dissolution term is set to zero when no driving force is present ($C_L = C_{sat}$ or $C_S = C_b$), in which case dissolution does not take place anymore. C_{sat} is the drug saturation concentration. This condition applies for both governing equations of liquid and solid phases. These equations are solved by the transformation technique to convert the moving-boundary problem to a fixed-boundary problem, which is computationally easier to handle. In this surface erosion model, even though the model is assumed to be a two-compartment model, the

solid and liquid compartment equations are actually uncoupled. In the liquid compartment, the additional drug concentration is attributed to the dissolution term and also washed away to the surface due to its concentration gradient.

Larobina et al. [57] developed a new model for surface-eroding polymer system based on the polymer phase separation phenomenon observed by Shen et al. [71]. This phenomenon is observed in the system of CPP–SA and CPH–SA when the fraction of one component is in excess of ~80%-mol. In this system, SA is the fast-eroding phase with rate constant k_A, whereas CPP or CPH is the slow-eroding phase with rate constant k_B. In addition, t_A and t_B are the times required for both fast-eroding and slow-eroding phases to degrade, respectively. The surface erosions for both species are described by zero-order reactions. Since the drug will be released when the polymer phase that entraps it degrades, the drug partitioning into either of these phases influences the drug release from this polymer system. Due to the inability of the whole polymer system to entrap the entire drug in compatible domains, in which the over-saturation condition occurs, this model also accounts for the burst effect. The cumulative drug release from this model can be expressed as follows:

$$\frac{M_t}{M_\infty} = (1-b)\frac{(x_A(t)\phi_{A,0} + x'_B(t)\phi_{B,0}P)}{\phi_{A,0} + \phi_{B,0}P} + b \qquad (86)$$

In this equation, x_A and x'_B are the released mass fractions of fast- and slow-eroding monomers, respectively, $\phi_{A,0}$ and $\phi_{B,0}$ are the surface fractions of fast- and slow-eroding domain, respectively, b is the fraction of drug released in the burst, and P is the ratio of drug concentration in the slow-eroding phase to that in the fast-eroding phase. Here, k_A is fitted to the monomer release data, whereas the other three constants (k_B, t_A, and t_B) are calculated after k_A is determined. Then, the experimental drug release data is fitted to Eq. (86) to estimate P.

Here, the model has shown good agreements in terms of drug release profile with experimental results [71]. However, P is a semi-empirical parameter that is difficult to obtain experimentally and may vary with time as erosion progresses with time. The fitting should suggest whether the estimated P is reasonable.

4.2.2. Cellular-automata models

Zygourakis [72] first developed a cellular-automata model to simulate the drug release from surface-eroding polymer matrices. The model used a two-dimensional grid. Each pixel in the grids represents drug, polymer, filler, or pore. The erosion process relies on the "life expectancy" that is defined for each type of pixel. The lifetime starts counting when the solvent is in contact with the polymer, which makes the pixels in surface more prone to polymer erosion rather than any other site. But, this model does not consider the mass transport phenomena, such as the water and drug diffusion inside the polymer matrix during erosion. The cross-sections of the matrix grid for 0, 25, 50, and 75% drug released are shown in Fig. 14. The dissolution rates of the drug (R_d) and polymer (R_p) are defined as:

$$R_d \equiv \frac{dV_d}{dt} = \frac{k_d S_d (C_{d,s} - C_{d,b})}{\rho_d} = \frac{k_d S_d \Delta C_d}{\rho_d} \qquad (87)$$

$$R_p \equiv \frac{dV_p}{dt} = \frac{k_p S_p (C_{p,s} - C_{p,b})}{\rho_p} = \frac{k_p S_p \Delta C_p}{\rho_p} \qquad (88)$$

When the diffusion resistance is assumed to be negligible, the drug release rate is equal to the drug dissolution rate. Therefore, the drug release rate in a constant volume medium (V_0) is given as follows:

$$\frac{dM_t}{dt} = \frac{1}{V_0}\frac{dV_d}{dt} = \frac{1}{V_0}\frac{k_d S_d \Delta C_d}{\rho_d} \qquad (89)$$

These equations are solved using cellular automata and discrete iterations by updating the lifetime of each pixel for each time point.

Zygourakis and Markenscoff [73] improved the model by analyzing the effect of several structural parameters on the erosion and release rates. The parameters that are analyzed in this model are given by:

1. The ratio of dissolution rate constant (χ), which is defined as $\chi = \nu_1/\nu_2$.
2. The initial loading of the first component (λ_1), which is defined as $\lambda_1 = V_{1,0}/(V_{1,0}+V_{2,0})$, where $V_{1,0}$ and $V_{2,0}$ are the initial volumes of components 1 and 2, respectively.

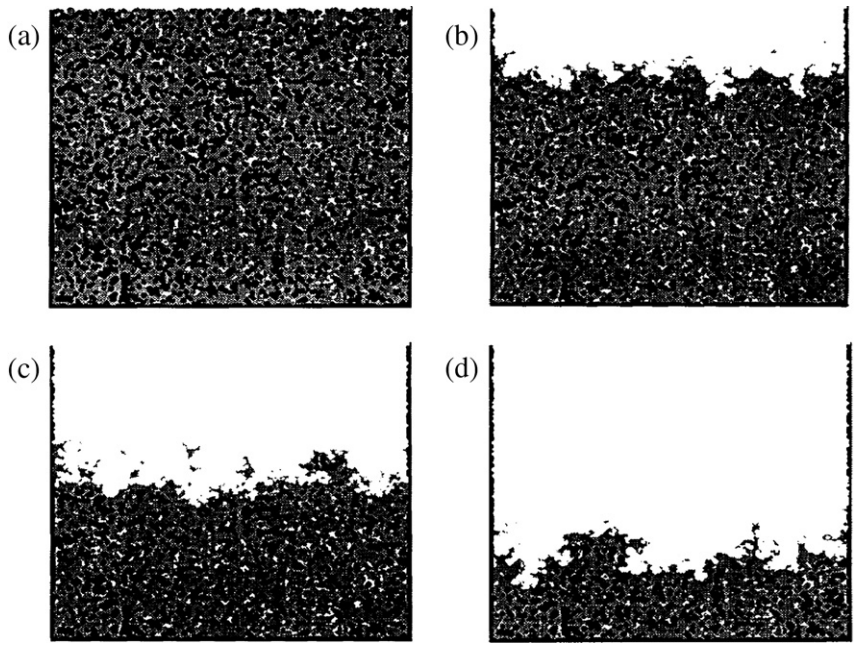

Fig. 14. Zygourakis cellular-automata model [72] for surface-eroding system simulation. The pixel types are drug, polymer, filler, and pores. There are four stages of surface erosion as shown, referring to the time points when the drug released is (a) 0%, (b) 25%, (c) 50%, and (d) 75% (reprinted from [72] with permission from Elsevier).

3. The dispersion parameter (ξ), defined as the aspect ratio $\xi = d/h$, where d is the characteristic length of component 1 and h is the characteristic length of the device.
4. The porosity of the device (ε).
5. The pore size parameter (γ), whose length is defined as $\gamma = l/h$, where l is the pore size.

The first two parameters are already incorporated in the previous model [72], whereas the remaining three parameters are new to account for the characteristic geometry of the device as well as the dynamics of erosion process that affects the porosity of the matrix. The simulation results show the effect of these parameters on the release profile of surface-erosion matrix system.

Gopferich and Langer [74] utilized the Monte-Carlo technique to build a mathematical model for the polymer matrix erosion. The model takes into account several parameters that are correlated with how the polymer erodes, such as crystallinity, geometry, and porosity. The degree of crystallinity is important as the crystalline region erodes slower than the amorphous region as observed experimentally [75]. Similar to the Zygourakis model, the simulation is conducted in the two-dimensional grid. In the subsequent modeling development, this model was also used as the basis for the three-dimensional erosion of polymer cylinder [76]. Each pixel is assigned its initial lifetime. The initial lifetime expectancy for each pixel is assigned randomly according to Erlang distribution. To account the effect of crystallinity, the crystalline and amorphous pixels are assigned different Erlang distribution constants (e):

$$e(t) = \lambda e^{-\lambda t} \tag{90}$$

where λ is the first-order degradation rate constant.

Pixels that are in contact with either water or the eroded neighbor pixels will start to erode and its lifetime is calculated from that point. The pixel will be removed from the grid when its lifetime ends. The

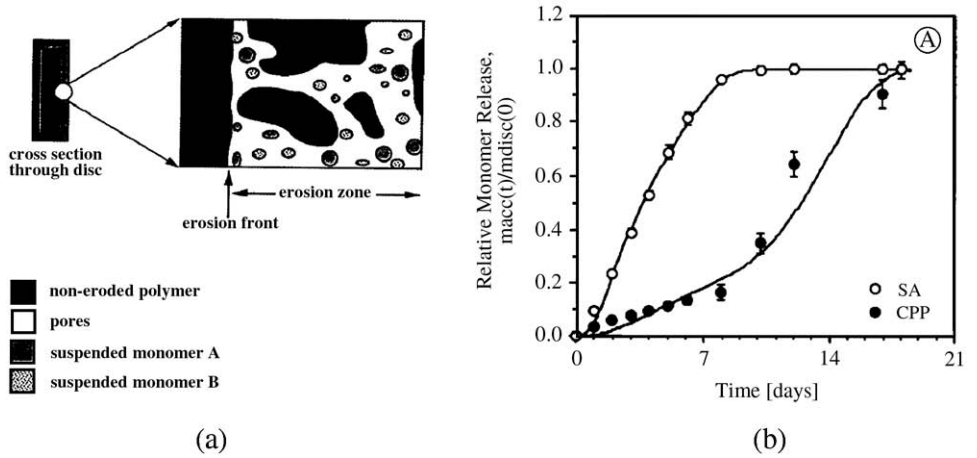

Fig. 15. (a) Schematic illustration of surface polymer degradation with monomer release mechanism incorporated; and (b) the model fitting to experimental data of CPP and SA monomers released from p(CPP-SA) 20:80 polymer matrix discs (reprinted from [78] with permission from Elsevier).

matrix porosity (ε) is updated for each time step according to the following equation:

$$\varepsilon(i\cdot\Delta x,t)=\frac{1}{n_y}\sum_{j=1}^{n_y}s(i,j)\qquad \text{for } 1\le i\le n_x \tag{91}$$

where $s(i,j)=\begin{cases}1 & \text{for 'eroded' pixels}\\ 0 & \text{for 'non}-\text{eroded' pixels.}\end{cases}$

As diffusion takes place in the x-direction, $i\cdot\Delta x$ is equal to x. In the above equation, $\varepsilon(x,t)$ is the discrete porosity distribution; n_x and n_y are the numbers of pixels in x and y direction in the grid, respectively; and $s(i,j)$ is a function that takes into account the status of a pixel to be either 'eroded' or 'non-eroded'. The porosity dynamically increases as mentioned by the increasing number of 'eroded' pixels. The matrix porosity affects the magnitude of the effective diffusion coefficient of the drug in the polymer matrix.

Since the monomer properties are found to be important to the erosion mechanism of *polyanhydrides*-based polymer matrix [75,77], the previous model is then developed in a more extensive detail by incorporating the monomer release [78]. Here, it turns out that the drug release profile is more correlated to the monomer release profile than the overall polymer molecular weight decrease due to erosion. The model is originally applied for the SA-CPP copolymer that is widely used at that time for the Gliadel® wafer. The schematic illustration of this modeling and its fitting results of monomer release are shown in Fig. 15. This block copolymer has been widely investigated to have the surface-eroding characteristic [77]. In such a system, the diffusion of monomer in polymer matrix is derived from Fick's second law of diffusion:

$$\frac{\partial}{\partial t}\left[C_i(x,t)\cdot\varepsilon(x,t)\right]=\frac{\partial}{\partial x}\left[D_{e,i}(C_i)\cdot\varepsilon(x,t)\cdot\frac{\partial C_i(x,t)}{\partial x}\right]+\frac{\partial S_i}{\partial t} \tag{92}$$

where $C_i(x,t)$ is the concentration of the diffusing SA or CPP monomer, $\varepsilon(x,t)$ is the porosity of each pixel, $D_{e,i}(C_i)$ is the effective diffusion coefficient of either monomer, and $\frac{\partial S_i}{\partial t}$ is the dissolution rate.

The complete species balances for monomer SA and CPP that include diffusion and dissolution processes are as follows:

$$\begin{aligned}\frac{\partial}{\partial t}C_{SA}(x,t)=&\frac{\partial C_{SA}(x,t)}{\partial x}\frac{\partial D_{e,SA}(C_{SA})}{\partial x}\\&+\frac{D_{e,SA}(C_{SA})}{\varepsilon(x,t)}\frac{\partial C_{SA}(x,t)}{\partial t}\frac{\partial\varepsilon(x,t)}{\partial x}\\&+D_{e,SA}(C_{SA})\frac{\partial^2 C_{SA}(x,t)}{\partial x^2}\\&+k_{SA}m_{SA}(x,t)[C_{SA,s}-C_{SA}(x,t)]\end{aligned} \tag{93}$$

$$\frac{\partial}{\partial t}C_{\mathrm{CPP}}(x,t) = \frac{\partial C_{\mathrm{CPP}}(x,t)}{\partial x}\frac{\partial D_{\mathrm{e,CPP}}(C_{\mathrm{CPP}})}{\partial x} + \frac{D_{\mathrm{e,CPP}}(C_{\mathrm{CPP}})}{\varepsilon(x,t)}\frac{\partial C_{\mathrm{CPP}}(x,t)}{\partial t}\frac{\partial \varepsilon(x,t)}{\partial x} + D_{\mathrm{e,CPP}}(C_{\mathrm{CPP}})\frac{\partial^2 C_{\mathrm{CPP}}(x,t)}{\partial x^2} + k_{\mathrm{CPP}}m_{\mathrm{CPP}}(x,t) \times \left\{\alpha\cdot 10^{-\beta[\mathrm{p}K_{\mathrm{a,SA}}-\log C_{\mathrm{SA}}(x,t)]^{1/2}} - C_{\mathrm{CPP}}(x,t)\right\} \quad (94)$$

where k_{SA} and k_{CPP} are the dissolution rate constants of SA and CPP crystals; m_{SA} and m_{CPP} are the mass of suspended SA and CPP crystals; $C_{\mathrm{SA,s}}$ and $\mathrm{p}K_{\mathrm{a,SA}}$ are the solubility and $\mathrm{p}K_{\mathrm{a}}$ value of SA, respectively.

A more detailed monomer modeling for surface-eroding homopolymers and copolymers tablets of CPP-SA and CPH-SA was developed by Kipper and Narasimhan [79]. This model accounts for the micro-phase separation between crystalline and amorphous regions and is conducted in the assumption of planar system with characteristic length scale of y. Therefore, the model sacrifices the geometrical effect for better understanding in monomer release to explain the polymer erosion. In addition, this model involves the monomers solubility changes and can be developed further to include the pH changes during erosion due to release of acidic monomers.

There are in total eight fractional changes due to the number of phases considered in the model (including the monomer phases), which are the fractions of amorphous polymer (f_{a1}, f_{a2}) and monomer (f_{ma1}, f_{ma2}) of components one and two as well as the fractions of crystalline polymer ($f_{\mathrm{c1}}, f_{\mathrm{c2}}$) and monomer ($f_{\mathrm{mc1}}, f_{\mathrm{mc2}}$) of components one and two. The transient equations for monomer are as follows:

$$\begin{aligned}\frac{\partial f_{\mathrm{ma1}}}{\partial \tau} &= f_{\mathrm{a1}} - f_{\mathrm{ma1}}\kappa_1\\ \frac{\partial f_{\mathrm{ma2}}}{\partial \tau} &= \gamma f_{\mathrm{a2}} - f_{\mathrm{ma2}}\kappa_2\\ \frac{\partial f_{\mathrm{mc1}}}{\partial \tau} &= \beta f_{\mathrm{c1}} - f_{\mathrm{mc1}}\kappa_1\\ \frac{\partial f_{\mathrm{mc2}}}{\partial \tau} &= \delta f_{\mathrm{c2}} - f_{\mathrm{mc2}}\kappa_2\end{aligned} \quad (95)$$

where the dimensionless time parameter (τ) is normalized by the degradation rate constant of amorphous polymer of type one ($\tau = \frac{tk_{\mathrm{a1}}}{\rho y}$), κ_1 and κ_2 are the dimensionless dissolution rates for polymer of types one and two, respectively, k_{a1} is the dissolution rate for amorphous polymer of component one, and ρ is the total density of the polymer. The degradation rate constants are normalized to that of amorphous polymer of type one by γ, β, and δ for the crystalline polymer of type one, amorphous polymer of type two, and crystalline polymer of type two, respectively.

The dimensionless dissolution rate for each monomer i (κ_i) is defined as follows:

$$\kappa_i = \frac{k_i(C_{\mathrm{sat},i} - C_i)}{k_{\mathrm{a1}}C_{\mathrm{sat},i}} \quad (96)$$

where k_i is the dissolution rate of monomer i and $C_{\mathrm{sat},i}$ is the saturation concentration of monomer i.

The dimensionless concentrations (χ_1 and χ_2) of the monomer of types one and two follow the diffusion equation with additional source term of dissolution from the pores as follows:

$$\begin{aligned}\frac{\partial \chi_1}{\partial \tau} &= \frac{(f_{\mathrm{ma1}} + f_{\mathrm{mc1}})\kappa_1\sigma}{\varepsilon} + D_1^*\frac{\partial^2 \chi_1}{\partial \xi^2}\\ \frac{\partial \chi_2}{\partial \tau} &= \frac{(f_{\mathrm{ma2}} + f_{\mathrm{mc2}})\kappa_2\sigma}{\varepsilon} + D_2^*\frac{\partial^2 \chi_2}{\partial \xi^2}\end{aligned} \quad (97)$$

where ε is the total porosity of the polymer, D_1^* and D_2^* are the dimensionless diffusivities of polymer type one and two, respectively, and σ is the dimensionless surface area per unit volume. $\xi = x/y$ is the dimensionless distance from the original surface of the polymer (y).

The total porosity of the polymer increases as the pore radius increases due to the monomer release. It is expressed as follows:

$$\frac{\partial \varepsilon}{\partial \tau} = \frac{8(1-\varepsilon)R^*}{\ell^2}\frac{\partial R^*}{\ell \tau} = \frac{8(1-\varepsilon)R^*}{\ell^2}[(f_{\mathrm{ma1}} + f_{\mathrm{mc1}})\kappa_1 + (f_{\mathrm{ma2}} + f_{\mathrm{mc2}})\kappa_2] \quad (98)$$

where R^* is the average dimensionless radius of the pore and ℓ is the dimensionless long-period of the crystalline lamellae ($\ell = l/y$), where l is the long-period of crystalline lamellae [79].

Finally, the cumulative polymer fractional mass loss is computed by integrating the porosity at a certain time point in the whole polymer matrix ($0 \le \xi \le \xi_{max}$). This can be expressed as follows:

$$\frac{M_{p,t}}{M_{p,\infty}} = \int_0^{\xi_{max}} \varepsilon(\tau, \xi) d\xi \tag{99}$$

The cumulative polymer fractional mass flow can be fitted to the result from experimental studies. Since several values can be taken from previous experimental studies, unknown parameters that are used for fitting purpose may give insights on the important mechanisms affecting the polymer erosion. The development of this model to include the exact geometry and the encapsulated drug release due to polymer erosion can be beneficial.

Interestingly, Siepmann et al. [58] applied a Monte-Carlo simulation to predict the drug release from bulk-erosion PLGA microspheres in a perfect sink medium with the experimentally determined initial drug loading (24% w/w). Due to symmetry condition, a quarter of the sphere is used and extended in the θ-direction to obtain a cylindrical 2D simulation domain. This assumption allows the simulation to be conducted in cylindrical coordinates. The quarter is divided into rectangular pixels and results in cylindrical rings when the rotation around the z-axis is done. Since there is no concentration gradient in θ coordinate, the drug diffusion in this domain is described by the Fick's second law for cylindrical coordinate without the θ-dependent.

Each pixel in the domain has a lifetime and as soon as a pixel is in contact with water, its lifetime ($t_{lifetime}$) starts decreasing as follows:

$$t_{lifetime} = t_{average} + \frac{(-1)^{\vartheta}}{\lambda} \ln\left(1 - \frac{\vartheta}{100}\right) \tag{100}$$

where $t_{average}$ is the average lifetime of the pixels, λ is a constant characterizing the type and physical state of the polymer, and ϑ is a random variable (integer between 0 and 99).

Given the initial status for each pixel, the status of each pixel at each time step is updated from the Monte-Carlo simulations that result in the increase of porosities in radial and axial direction, $\varepsilon(r,t)$ and $\varepsilon(z,t)$, respectively. They are calculated as follows:

$$\begin{aligned} \varepsilon(r,t) &= 1 - \frac{1}{n_z} \sum_{j=1}^{n_z} s(i(r), j, t) \\ \varepsilon(z,t) &= 1 - \frac{1}{n_r} \sum_{i=1}^{n_r} s(i, j(z), t) \end{aligned} \tag{101}$$

As a result of increasing porosity, diffusion coefficient of the drug also increases and is calculated as follows:

$$\begin{aligned} D_e(r,t) &= D_{crit}\varepsilon(r,t) \\ D_e(z,t) &= D_{crit}\varepsilon(z,t) \end{aligned} \tag{102}$$

where D_{crit} is the critical (maximum) diffusivity characterized for a specific drug–polymer interaction.

Their results also show that the above model provides a reasonable fitting to the *in vitro* 5-FU release rate from PLGA-based microparticles in a phosphate buffer solution with a pH value around 7.4.

5. Irradiation effect on drug release profile from polymeric microspheres

Irradiation sterilization, i.e., γ-irradiation, of pharmaceutical products is popular in recent years due to its ease of operation. Conventional sterilization processes, such as heat and chemical sterilizations often lead to degradation of polymer backbones and toxicological problems respectively. Dose of 25 kGy (2.5 Mrad) is essentially accepted to be satisfactory for pharmaceutical products sterilization. However, γ-irradiation sterilization is also known to alter the properties of drug delivery formulations. The other aspect that needs caution is that the radiation sterilization may form toxic degradation products though this possibility is still controversial.

Due to their biocompatibility, polyesters, which exhibit bulk-erosion behavior, are widely used as polymeric systems for drug delivery applications. They are essentially homo- or copolymer derived from monomers of lactic and glycolic acid. The family members of this type of polymer are PLA, *poly(glycolic acid)* (PGA), and the copolymer PLGA with different *lactide* to *glycolide* ratios. However, polyesters are prone to γ-irradiation due to a reduction in mechanical properties, which leads to chain scission [80]. The theory

of "cage effect" was also proposed where the scission of the polymer chain could be more dominant in the amorphous regions. PLA and PLGA are more susceptible to irradiation degradation than PGA even though the former is more resistant to hydrolytic degradation. This is due to the presence of the methyl group on lactic acid which sterically hinders the formation of radical pairs and increases the probability of degradation [81].

It was observed that the initial molecular weight distribution of polymer microspheres decreases substantially with the irradiation dose of 0 to 55 kGy [82]. When the first 15 kGy of irradiation was applied, slight decrease was observed in weight-average molecular weight (M_w) of 14% as compared to number-average molecular weight (M_n) of 26%. This observation was more pronounced for higher irradiation dose. Therefore, the increasing irradiation dose resulted in the increasing polydispersity index ($I=M_w/M_n$) of polymer. In contrast, this phenomenon was not observed by Volland et al. [83], Mohr et al. [84], and Yoshioka et al. [85,86] since the chain scission mechanism is a random process by γ-irradiation. Furthermore, Yoshioka et al. [85,86] suggested that irradiation up to 25 kGy has no significant changes in the glass transition temperature and the initial drug release rate.

In another study, Faisant et al. [87,88] correlated the 5-*fluorouracil* (5-FU) release profile from PLGA microspheres with irradiation effect (11–33 kGy) and proposed that the initial drug diffusivity is an exponential function of the irradiation dose (Fig. 16a). However, the dependence of the diffusivity on the irradiation dose was not significant and these studies concluded that the irradiation dose up to 25 kGy will not change the erosion behavior of PLGA polymer, but slightly alter the diffusional transport within the polymer matrix. This conclusion was supported by results from Montanari et al. [89] who observed that the decrease in M_w is negligible for irradiation dose below 15 kGy, while a 10%-decrease in M_w was observed for irradiation dose of 25 kGy, which is possibly caused by the increase of initial drug diffusivity. Fitting both non-cellular-automata model of Koizumi and Panomsuk [7] and cellular-automata model of Siepmann et al. [58] (Fig. 16b), the exponential dose-dependent initial diffusivity may be expressed in the following form:

$$D_0 = a\exp(bI) \tag{103}$$

where I is the irradiation dose, and a and b are fitting constants.

Since b is found to be in the order of 0.02 1/kGy in the range of 11–33 kGy irradiation for both fittings, it implies that the initial diffusivity is not a strong function of the irradiation dosage. This supports the previous experimental observation that, below 25 kGy irradiation, no significant change in PLGA erosion behavior is observed.

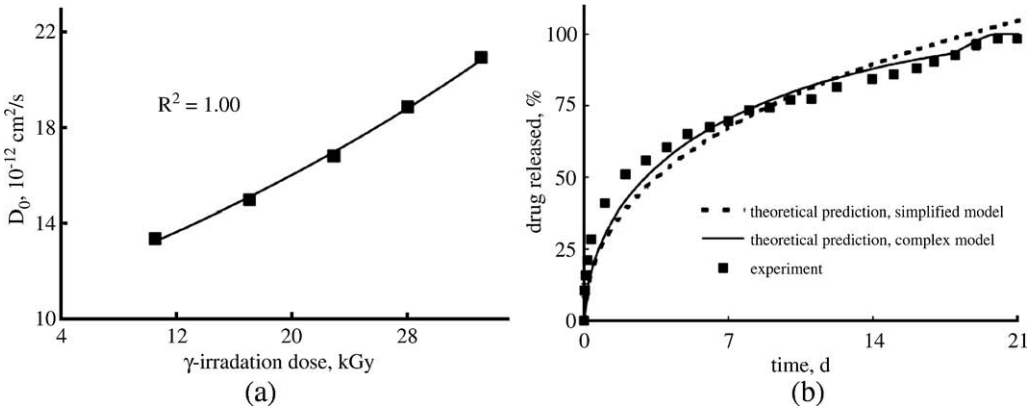

Fig. 16. (a) The dependence of the initial diffusivity of 5-FU in the PLGA microparticles on the applied γ-irradiation (^{60}Co source); and (b) experimental results (symbols) and model predictions (dotted line: Koizumi and Panomsuk [7] non-cellular-automata model, solid line: Siepmann cellular-automata model [58]) of 5-FU release profile from PLGA microparticles after exposure to 4.4 kGy γ-irradiation in phosphate buffer pH 7.4 (reprinted from [88] with permission from Elsevier).

6. Going to nanoscale: the implication on drug release mechanism

Biodegradable microparticulate systems have been well-studied for controlled release of various types of drugs, both hydrophobic and hydrophilic. In recent years, there is an obvious trend of increasing interest in development of nanoparticles for drug delivery applications especially in intravenous delivery. Nanoparticles may range from sizes 10 nm to 1000 nm [90] and include liposomes, micelles, polymer–drug conjugates, and polymer particles [91]. Novel fabrication processes have also been widely developed to produce nanoscale drug delivery systems. Fabrication techniques such as modified solvent evaporation methods [92,93], supercritical fluid techniques [94–96] and dialysis methods [97] were some of the feasible routes to achieve drug-loaded polymeric nanoparticles. For example, several fabrication methods have been adopted and developed for the controlled release of a model hydrophobic chemotherapeutic agent, *paclitaxel* in the form of nanoparticles in biodegradable polymer matrix. The various fabrication techniques and size range of particles obtained for *paclitaxel* delivery system are summarized in Table 1.

6.1. Drug targeting and biodistribution

One of the important applications of nanoparticles for drug delivery is a site-specific delivery [98]. Biodistribution of drug carriers is very much dependent on the size of the particles and the properties of the particle surfaces [91] in oral and intravenous delivery. Effect of the size of biodegradable micro and nanoparticles on gastrointestinal has been investigated in the studies by Desai et al. [99]. PLGA particles of size 100 nm, 500 nm, 1 μm and 10 μm were used for animal studies (rats) in situ. The uptake efficiency depends on the type of tissue, but generally the uptake efficiency of 100 nm size particles in intestinal tissue was higher as compared to the larger size microparticles. Histological studies showed that particles at 100 nm could diffuse through the submucosal layers while the larger sized particles (500 nm–10 mm) were found to be concentrated in the epithelial lining of the tissue. This provides insight to the design of nanoparticles for oral drug delivery systems.

For intravenous injection, nanoparticles are generally cleared from the blood rapidly and found to be concentrated in the spleen, liver and blood marrow [100]. To increase the blood circulation time of

Table 1
Summary of nanofabrication methods for a model hydrophobic drug of *paclitaxel*

Method	Group	Year	Materials	Particle size range (nm)	Remarks
Solvent evaporation	Chen et al. [102]	2001	Brij78+*paclitaxel* Poloxamer F68+*paclitaxel*	103.5±29.2 220±98	Solid lipid nanocores
Spray drying	Mu and Feng [103]	2001	PLGA+DPCC+cholesterol+*paclitaxel*	800–1000	–
Temperature induced phase transition	Lee et al. [104]	2002	F127[a] PLGA+*paclitaxel*	150–600	–
Interfacial deposition method	Fonseca et al. [105]	2002	PLGA+*paclitaxel*	120–160	–
Modified single emulsion/ solvent evaporation	Mu and Feng [106–108]	2002, 2003	PLGA+*paclitaxel* PLA+*paclitaxel*	300–900 600–1000	PVA, DPPC as emulsifier; vitamin E TPGS as emulsifier and matrix material
	Zhang and Feng [109]	2006	PLA–vitamin E TPGS copolymer+*paclitaxel*	290–333	–
Controlled solvent displacement	Potineni et al. [110]	2003	Poly **1**[b]+pluronic F-108+*paclitaxel*	100–150	w/o pluronic F-108, particle ~400 nm
Dialysis (self-assembled nanoparticles)	Xie and Wang [97]	2005	PLGA+*paclitaxel* PLA+*paclitaxel*	286–291 310	Vitamin E TPGS as emulsifier
	Kim et al. [111]	2006	HGC[c]+*paclitaxel*	200–416	–

[a] F127: *poly(ethylene oxide)–poly(propylene oxide)–poly(ethylene oxide)* triblock copolymer.
[b] Poly **1**: *poly(ethylene oxide)*-modified *poly(β-amino ester)*.
[c] HGC: Hydrophobically modified glycol chitosan.

nanoparticles, a major challenge would be to avoid its opsonization and uptake by phagocytic cells. Biodegradable long circulating polymeric nanospheres were developed using amphiphilic copolymers of PLGA or with *poly(ethylene glycol)* (PEG) in the studies by Gref et al. [101]. *In vivo* studies in mice showed an increase in blood circulation time as the molecular weight of PEG used increases. This is most likely due to an increase in the protective layer (PEG layer) thickness on the outer surface of the nanospheres which could better prevent opsonization. A corresponding reduction in liver uptake was also achieved.

6.2. Drug release from nanoparticles

6.2.1. Hydrophobic drugs

A major challenge in drug delivery for anticancer agents is the poor aqueous solubility of many anticancer drugs. Due to the low aqueous solubility of the drug and low diffusivity within the polymer matrix, the release profile is generally very slow. An example is in the delivery of a promising anticancer agent *paclitaxel* which is found to be useful against a wide spectrum of carcinomas, especially in breast and ovarian cancer. Its low aqueous solubility and high crystallinity make it difficult to be encapsulated in biodegradable microparticles at reasonably high drug loading (>30%) and the drug release by diffusion is generally very low.

The use of nanoparticles provides a solution to the slow release profile by providing a much larger surface area, but compromised with the slower diffusivity in the polymer matrix due to the more compact structures resulted from the fabrication techniques. For a monolithic system with uniform drug distribution with the polymeric matrix, release is generally governed by diffusion or erosion mechanisms. Drug release from common polymeric nanoparticles, such as PLA and PLGA, is mainly due to diffusion, drug dissolution and subsequently surface erosion or bulk degradation. The effective diffusion coefficient of drug follows the combined effects of diffusion through particle pores and diffusion through an intact polymer matrix and is a function of the tortuosity and porosity of the polymer.

Adopting the drug dissolution and diffusion model by Harland et al. [59] as described earlier in Eqs. (58)–(62), the effect of varying particle size on the drug release profile of micro and nanoscale particles can be investigated. For hydrophobic drugs, such as *paclitaxel* and *lidocaine*, estimated drug diffusion coefficient in PLA polymer matrix has been reported in literature ranging from 10^{-15} m^2/s [112] to 10^{-20} m^2/s [114] respectively. In a study by Kang and Schwendeman [115], the diffusion coefficient of a small hydrophobic probe in PLGA microparticles was measured using laser scanning confocal microscopy (LSCM) and estimated values of D_e from 3 to 10×10^{-16} m^2/s were obtained.

The release profile of highly hydrophobic drug from polymeric systems is mainly influenced by drug diffusion mechanism. For hydrophobic drug molecules, due to the very low drug solubility in aqueous medium, the dissolution constant will generally be very small. Drug dissolution mechanism has little effect on the drug release as the solubility is low and the dissolution rate constant (k) will be very small as compared to the diffusion rate. In this respect, even though one may expect the diffusion of drug from polymeric microspheres to be very slow, the time scale of diffusion due to relatively small size of nanoparticles is still smaller than that of dissolution and, therefore, the encapsulated drug is preferably released through diffusion in the polymer matrix. Table 2 summarizes the estimated time scales for drug release for diffusion coefficients of 10^{-15} to 10^{-20} m^2/s ranging from micro- to nanoparticles. In the case for a crystalline polymer matrix such as PLA, drug release is often very slow due to a corresponding low diffusion coefficient.

Table 2
Diffusional time scale (t/τ) using Harland's dissolution-controlled, diffusional drug release (Eq. (61)) from non-swellable polymeric microspheres

Hydrophobic drug	Effective diffusion coefficient, D_e (m^2/s)	
	$D_e=10^{-15}$	$D_e=10^{-20}$
	t/τ (s)	t/τ (s)
10 μm	2.5×10^{4}	2.5×10^{9}
1 μm	2.5×10^{2}	2.5×10^{7}
100 nm	2.5	2.5×10^{5}

Hydrophilic drug	Effective diffusion coefficient, D_e (m^2/s)		
	$D_e=10^{-11}$	$D_e=10^{-13}$	
	t/τ (s)	Di	t/τ (s)
10 μm	2.5	2.5×10^{-4}	2.5×10^{2}
1 μm	2.5×10^{-2}	2.5×10^{-6}	2.5
100 nm	2.5×10^{-4}	2.5×10^{-8}	2.5×10^{-2}

From a simple Fickian diffusion model, one may expect that the release profile to be significantly altered by changes in particle size as illustrated by the difference in diffusion time scale as shown in Table 2. However, this is not reflective of actual experimentally determined release profiles shown in many studies especially for hydrophobic drug release, for example in Liggins and Burt [112] for *paclitaxel* release from PLA polymer matrix and Siepmann et al. [69] for *lidocaine* release from PLGA polymer matrix. In fact, as shown earlier in Fig. 11, the release profile for microparticles ranging from 7.2 μm to 53 μm was not significantly different as predicted using the same effective diffusion coefficient. A better fit of the experimental release profiles was obtained using the mathematical model with the autocatalytic effect to account for the influence of particle size on drug diffusivity. It is found that the drug diffusivity decreases with decreasing size of microspheres since the small diffusion length scale allows acid and base molecules to travel from bulk medium to neutralize the autocatalytic effect. Furthermore, SEM analysis on the surface and cross-section of different size particles after suspension in physiological solution also showed a corresponding increase in the porosity of larger microparticles due to the more pronounced autocatalytic effect as earlier illustrated in Fig. 12.

Similar trends were also observed for the *in vitro* release profiles of *paclitaxel* from PLGA (75:25) polymer matrix for micro- and nanoparticles in the study by Mu and Feng where effective drug diffusion coefficient values of 10^{-21} and 10^{-22} m^2/s were estimated for average particle sizes of 1.95 μm [103] and 273 nm [108] respectively. The application of the diffusion model is still limited to fully explain the hydrophobic drug release. In Fig. 17, Fickian diffusion model was used to fit experimental data for *paclitaxel* release from PLA micro- and nanospheres. It is shown that for particles ranging from 310 nm to 105 μm although drug release tends to be faster for smaller particles, the change in release profile was not as significantly different as predicted using the Fickian diffusion model using a constant drug diffusion coefficient. The estimated drug diffusion coefficients used to fit the experimental data are shown in Fig. 17. Here, for a reduction of size from 35–105-μm microspheres to 310-nm nanospheres, the drug diffusion coefficient is found to be reduced from 8×10^{-17} to 8×10^{-21} m^2/s. Therefore, when using the diffusion model, one also has to consider the relationship between particle size and drug diffusion coefficient.

Another important characteristic to be highlighted is the effect of drug loading on the release profile. The diffusion model generally predicts the release profile based on the fraction of initial loaded drug released over time. However, in many studies, it was observed that the release profile is dependent on the drug loading in the polymer matrix. In Mu and Feng [107,108], the cumulative release percent of *paclitaxel* from PLGA nanospheres generally decreases with an increase in drug loading, and this is also in consistency with the

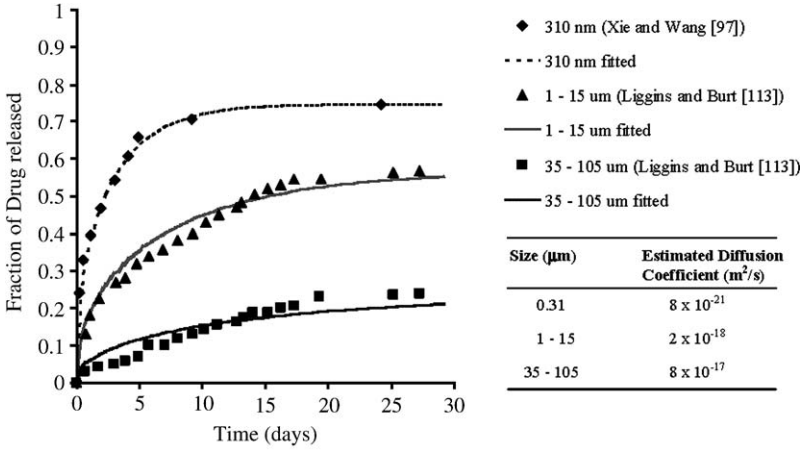

Size (μm)	Estimated Diffusion Coefficient (m^2/s)
0.31	8×10^{-21}
1 - 15	2×10^{-18}
35 - 105	8×10^{-17}

Fig. 17. Release profiles for *paclitaxel*-loaded microparticles ranging from 310 nm to 105 μm are modeled using a pure diffusion model. Release data are cited from Refs. [97] and [113].

observations by Polakovic et al. [114] and Gref et al. [101] for the release profiles of *lidocaine* from PLA and PLGA nanoparticles polymer matrices, respectively. Fig. 18 shows the experimental and fitted release profiles of *paclitaxel* from PLGA 5050 nanospheres from formulations with drug loading ranging from 2 to 12% w/w. It can be clearly observed that when drug loading was increased to 12%, the total fraction of drug release after a long time was much lower as compared to the lower drug loading formulations. The estimated effective diffusion coefficient for four different drug loading nanospheres was very close and ranged from 4 to 9×10^{-21} m^2/s. The possible explanation for this phenomenon is the encapsulation of drug as a molecularly dispersed phase within the polymer matrix at lower drug loadings. When the drug loading is high (e.g. at 30% w/w), the drug loading may exceed the drug solubility in the polymer matrix and small drug crystals will be embedded heterogeneously in the polymer matrix [101,114]. In this case, the release of drug will be much slower than predicted by the diffusion model.

Hence, in the design of controlled release devices for hydrophobic drugs, both factors of drug diffusion coefficient dependence on particle size and the effect of drug loading on fraction of drug available for diffusion from the polymer matrix play an important role.

6.2.2. Hydrophilic drugs

In contrast to the difficulties encountered in hydrophobic drug delivery of slow release, the release of drug from hydrophilic drugs such as proteins also poses a challenge in the control of the drug release profile. A large initial burst is often associated with polymeric controlled release devices for hydrophilic molecules, and this is followed by a phase of very slow drug release. The diffusion coefficient of a model protein drug *bovine serum albumin* (BSA) in polymer systems has been reported to be in the range of 10^{-11} m^2/s [116] to 10^{-13} m^2/s [117] which is typically much higher than the diffusion coefficient of hydrophobic molecules. Similarly, drug dissolution rate is also much higher for hydrophilic molecules as compared to hydrophobic molecules. A typical release profile for hydrophilic drug release from biodegradable polymer microspheres is illustrated in Fig. 13b. An initial burst is observed followed by a period of lag phase and subsequent release following polymer erosion. In contrast to the release profile of hydrophobic drugs which is mainly dominated by drug diffusion mechanism, the release of hydrophilic drugs and proteins is influenced by both drug diffusion and drug dissolution mechanisms. This is illustrated in the studies by Wong et al. [118] for sustained release of *human immunoglobulin G* (IgG) from biodegradable microspheres. Harland's diffusion and dissolution model for drug release was found to fit the actual release data better than for the pure diffusion model within the time frame where no bulk degradation was observed.

For smaller particle in the nanometer size range, drug will be released even more rapidly in less than

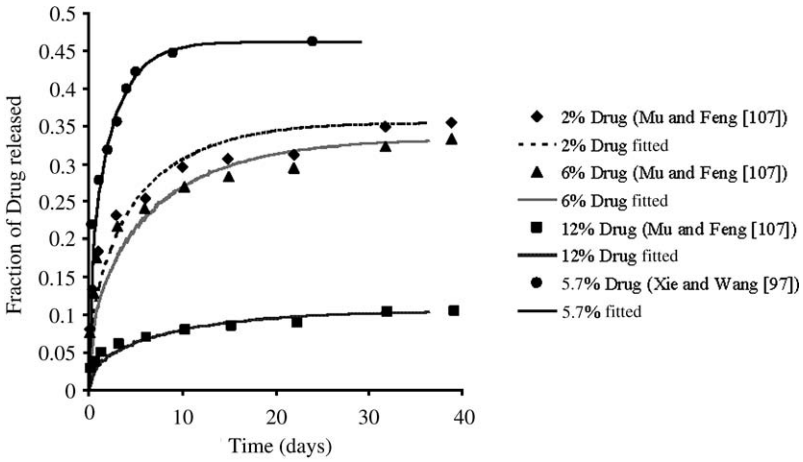

Fig. 18. Release profiles for different *paclitaxel*-loaded PLGA 50:50 nanoparticles ranging from 2% to 12% drug loadings. Effective diffusion coefficients used to fit the models ranged from 4 to 9×10^{-21} m^2/s.

1 ms. The approximated diffusion time scales as defined earlier in Eq. (61), for hydrophobic and hydrophilic drug release from different size particles are shown in Table 2. For both micro- and nanoscale particles, an initial burst phase can be predicted by the diffusion–dissolution model and observed in experimental data. This poses problems in applications where sustained delivery of drug over longer time periods is desired. The subsequent drug release may be modeled using semi-empirical models as described in Eq. (81).

One way to overcome this problem of initial burst effect from water-soluble molecules is the encapsulation of the drug in double-walled composite particles to dampen the initial burst effects to allow sustained release over a longer period of time. Double-walled microspheres have been fabricated for the sustained delivery of a water-soluble radiosensitizer drug, *etanidazole* [119]. A possible challenge in delivery of hydrophilic drug molecules would be the development of nanoscale particles capable of site-specific targeting with sustained release over a longer period of time. This may be achieved by the development of double-walled nanoparticles with a less permeable outer shell made of a hydrophobic matrix to control the initial burst effect. Surface modifications could be carried out to enhance the site-specific delivery of the nanoparticles.

7. Simulation of drug delivery in tissue: linking drug release profile and tissue elimination kinetics to predict temporal and spatial drug transport

In recent years, *in vitro* release profile of drug from controlled release devices has been combined with state-of-the-art computational fluid dynamics simulation to predict the spatial and temporal variation of drug transport in the living tissues. Macroscopically, the tissue, which can be either normal or tumor tissue, is ideally assumed as an isotropic porous medium, which is described by Darcy's law [120] for the balance of linear momentum in the tissue interstitium. The full-form of the momentum equation is expressed as follows:

$$\frac{\rho}{\varepsilon}\left(\frac{\partial \mathbf{v}}{\partial t}+\mathbf{v}\cdot\nabla\mathbf{v}\right)=-\nabla p_{\mathrm{i}}+\left(\frac{\mu}{\varepsilon}\right)\nabla^2\mathbf{v}+\rho\mathbf{f}-\left(\frac{\mu}{k}\right)\mathbf{v}-\frac{1}{2}C_{\mathrm{V}}\rho|\mathbf{v}|\mathbf{v} \quad (104)$$

where ρ is the density of the interstitial fluid, $\mathbf{v}$ is the convective velocity vector of the interstitial fluid, ε is the porosity of the tissue, μ is the mean viscosity of the interstitial fluid, $\mathbf{f}$ is the body force, k is the Darcy's permeability, and C_{V} is the inertial loss coefficient. The two terms on the left-hand side of Eq. (104) describe the transient and convective contributions, respectively. On the right-hand side of Eq. (104), the corresponding terms are the contribution by pressure gradient, viscous loss, body force, Darcy's resistance, and inertial loss, respectively.

The mass conservation (continuity) equation of the interstitial fluid can be formulated by considering the interstitial fluid source and sink in the tissue as described by Starling's law [121–123]:

$$\frac{\partial \rho}{\partial t}+\nabla\cdot(\rho\mathbf{v})=\rho(F_{\mathrm{V}}-F_{\mathrm{L}}) \quad (105)$$

where

$$F_{\mathrm{V}}=L_{\mathrm{p}}\left(\frac{S}{V}\right)[p_{\mathrm{v}}-p_{\mathrm{i}}-\sigma_{\mathrm{T}}(\pi_{\mathrm{v}}-\pi_{\mathrm{i}})]$$

$$F_{\mathrm{L}}=L_{\mathrm{p,L}}\left(\frac{S_{\mathrm{L}}}{V}\right)[p_{\mathrm{i}}-p_{\mathrm{L}}]$$

The right-hand side of the continuity equation is the application of Starling's law, where the two terms account for the fluid source from the blood vasculature and the fluid drainage (loss) to the lymphatic system, respectively. In the source term, L_{p} and $L_{\mathrm{p,L}}$ are the hydraulic conductivity of interstitial fluid from the vasculature to the interstitium and from the interstitium to the lymphatic system, respectively, (S/V) and (S_{L}/V) are the fluid exchange area per unit volume of the vasculature and lymphatic system, respectively, p_{v} and p_{L} are the vasculature and lymphatic pressure, respectively, p_{i} is the interstitial fluid pressure in the interstitium, σ_{T} is the osmotic reflective coefficient, π_{v} is the osmotic pressure of the vasculature, and π_{i} is the osmotic pressure of the interstitium. The variables in the sink term are also similar, except that hydraulic conductivity, surface area of exchange, and the pressures are specific to the lymphatic system.

To account for the drug distribution in the tissue, the species continuity equation is coupled with the momentum and overall continuity equations and solved simultaneously. The solute transport in biological

systems can be assumed to be a combination of convection and diffusion in the porous medium. Here, the concept of percolation theory for the solute transport in the porous medium [125,126] is applied with additional feature of solute elimination kinetics. In addition to the drug elimination due to degradation and uptake by the tissue cells, species conservation also involves the possible source of drug transported from the vasculature (F_s) and loss due to convective to the lymphatic system (F_{1s}), as shown in Fig. 19. For the drug (solute) transport, a diffusion/kinetics model is used as follows:

$$\frac{\partial C_i}{\partial t} = D_{e:tissue}\nabla^2 C_i - \nabla\cdot(r_F \mathbf{v} C_i) + F_s - F_{1s} - R(C_i) \quad (106)$$

where r_F is the retardation factor (the ratio of the drug velocity to the fluid velocity), $D_{e:tissue}$ and C_i are diffusion coefficient and concentration of drug molecules in the tissue interstitium, respectively. It is important to note that $D_{e:tissue}$ is different from the previous effective diffusivity in polymer matrix (D_e) since $D_{e:tissue}$ is used to account for the drug diffusivity in the tissue interstitium when it is assumed as a porous medium. On the right-hand side of Eq. (106), the first two terms account for the diffusion and convective contributions, the third and fourth terms describe the possible drug source and sink from the fluid exchange with the vasculature and lymphatic systems, and the last term is the rate of drug degradation and uptake in the tissue.

When solute transport is assumed to be the combination of convection, diffusion, and elimination kinetics, the prediction of transport parameter values, i.e. diffusion coefficient in the tissue and the elimination rate constant is also crucial. These two important transport parameters were initially determined in a coupled parameter of the diffusion/elimination modulus or Thiele modulus (ϕ_s) by fitting the species balance equation with the transient and spatial drug concentration obtained from *in vivo* animal experiments. This parameter can be uncoupled by conducting a separate diffusivity measurement in *ex vivo* tissue, in which the elimination can be assumed to be negligible, by using several techniques, i.e. integrative optical imaging [127], fluorescence recovery after photobleaching (FRAP) [128], and multiphoton microscopy [129]. Recently, some developments for *in vivo* diffusivity measurements have been made [128–132], even though a new and accurate model and its assumptions should be carefully employed to obtain the effective diffusivity without possible contribution by drug elimination during experimental time scale.

This review section will be sub-sectioned based on the targeted tissue for drug delivery. The rationale behind this classification is the differences in the nature of tissues such that different considerations must be taken into account. Each sub-section will discuss the development of the modeling works of drug delivery in the respective targeted tissue of interest. The mathematical models developed in this

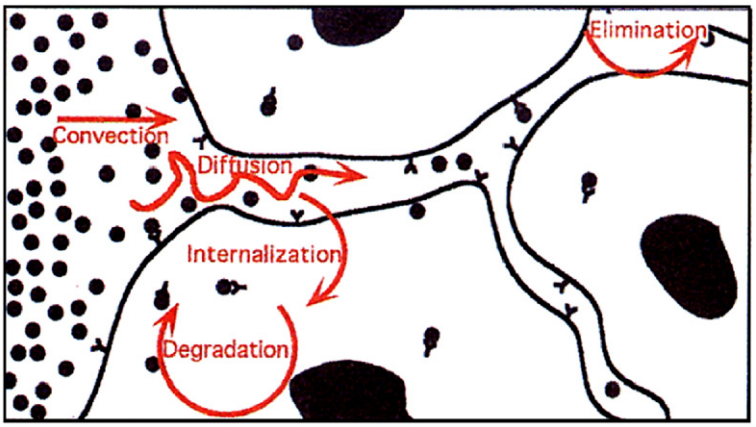

Fig. 19. The solute transport mechanisms in the tissue, given by convection of fluid, diffusion, elimination in the extracellular space, receptor- and non-receptor-based cells internalization, and intracellular elimination (reprinted from [124] with kind permission from Springer Science and Business Media).

area are mostly about the drug release from polymer implants that have certain characteristics of release profile. The discussion of the drug penetration and dominant transport mechanism will be highlighted.

7.1. Simulation of drug delivery in brain

The administration of drug in brain tissue or central nervous system (CNS) poses a challenge to overcome the very selective permeability of the blood capillaries, which is widely known as the blood–brain barrier (BBB). The BBB exists due to capillaries that have continuous lining of endothelial cells held together by tight junctions. Therefore, non-lipid solutes, either drug or protein, enter the brain slower as compared to other tissues. In addition, since most of the targeted Drug Delivery in the brain tissue is aimed to treat the brain tumor, there exists an additional barrier that needs to be overcome. It is the presence of elevated interstitial fluid pressure in the tumor that reduces the driving force of the solutes to be extravasated into the brain tissue from the blood vasculatures [123]. Since these two barriers are difficult to overcome for drug to penetrate the vasculature in the brain tissue, several invasive approaches of localized drug delivery, i.e. polymer implants and localized injection become more popular. Even for the site-specific implantation of controlled drug delivery devices, such as polymer implants, the high interstitial fluid pressure barrier, when tumor tissue is present, still poses a challenge of reducing the extent of drug reaching the tumor region due to the outward flow of interstitial fluid.

Saltzman and Radomsky [133] first developed a diffusion/kinetics model for the drug release from polymer implants into brain tissue. The transport is assumed to be mainly by diffusion, whereas the complex elimination reactions due to irreversible metabolism, reversible binding to the fixed tissue components, and capillaries partitioning, are finally simplified to be first-order kinetics. The complex and simplified forms of the elimination term are given by:

$$-R(C_i) = k_{BBB}\left(\frac{C_i}{\varepsilon} - C_{pL}\right) + \frac{V_{max}C_i}{K_m + C_i} + k_e C_i \approx k_{app} C_i \tag{107}$$

where k_{BBB} is the permeability of the BBB (defined based on extracellular matrix drug concentration), C_{pL} is plasma concentration, V_{max} and K_m are Michaelis–Menten parameters, k_e is the first-order elimination constant due to non-enzymatic reactions, and k_{app} is the lumped first-order elimination rate constant.

On the right-hand side, the first term designates the drug loss due to the BBB permeability, the second and third terms are the drug elimination due to the enzymatic and non-enzymatic processes, respectively. Since the drug permeability of the BBB is low ($C_{pL} \ll C_i$) and the concentration of the solute in the brain is very low so that the enzymatic process is in the order of first-order magnitude ($C_i \ll K_m$), the overall reaction can be assumed to be a first-order kinetics with an apparent elimination rate constant (k_{app}).

This model was applied to describe the *in vivo* drug release from the implant in the rat [134], rabbit [135], and monkey brain tissues [136]. In these models, the aforementioned one-dimensional diffusion-and-kinetics models are used for *carmustine* delivery from polymer implants with diffusion process as the main mechanism. In the absence of the convective or bulk flow, the only fitting parameter is the Thiele modulus (ϕ_s), as given below:

$$\phi_s = a\sqrt{\frac{k_{app}}{D_e}} \tag{108}$$

where a is the length scale of the polymer geometry.

In brief, high ϕ_s results in a steeper local concentration gradient due to the rapid elimination when drug diffuses in the extracellular matrix. Assuming the steady-state solution, the experimental data of drug spatial distribution fit well to the model's prediction. Here, the steady-state assumption is valid over the period of study since the mean steady-state ϕ_s is close to the transient ϕ_s. An example of the fitting result for *carmustine* distribution in rat brain is shown in Fig. 20. In addition, the summary of these works has been also nicely described in the literature [137].

However, this simplified model may not be valid for the case when the influence of convective flow is significant, i.e., when vasogenic edema takes place [138–140]. Vasogenic edema is the condition of significant increase of production of fluid in the extracellular space (ECS) of the brain due to a surgical trauma that damages the BBB and hence increases the

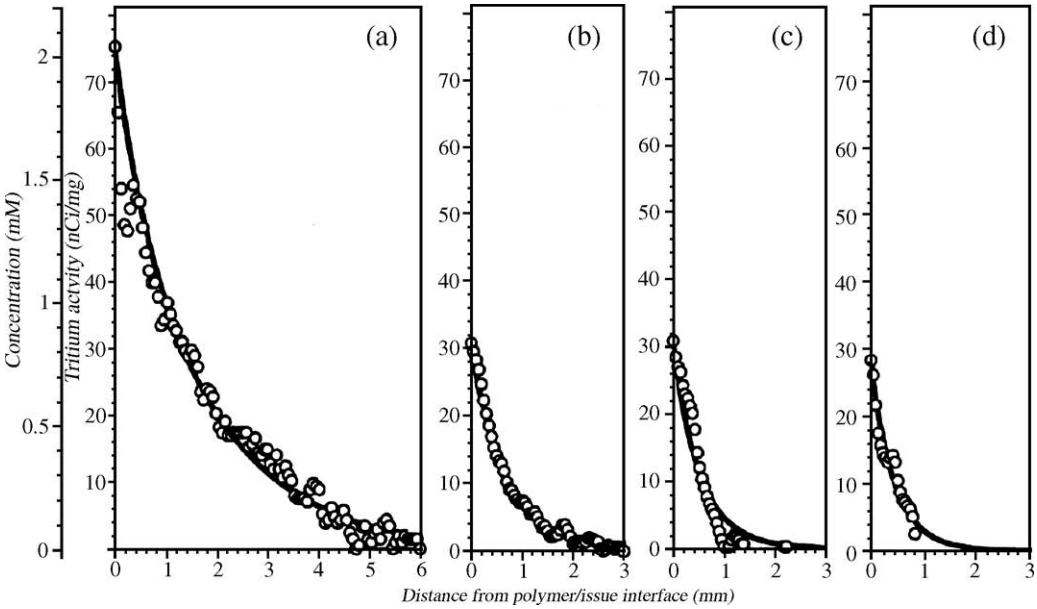

Fig. 20. *Carmustine* concentration profile in the rat brain tissue in the vicinity of a polymer implant at time point of (a) day 1, (b) day 3, (c) day 7, and day 14. The experimental results are denoted by symbols, whereas the steady-state diffusion/kinetic model with fitted ϕ_s for each time point is shown in solid lines (reprinted from [134] with kind permission from Springer Science and Business Media).

blood capillaries permeability. Thus, at the site of edema, there is a substantial increase of pressure gradient that leads to the bulk flow, which may carry the drug released from the implant site. This hypothesis is also bolstered by simulation results that showed the importance of the convective flow when edema takes place that causes a deeper penetration of *carmustine*.

Kalyanasundaram et al. [141] utilized the finite element method to develop a two-dimensional (2D) model of drug delivery in rabbit brain (Fig. 21). The grid for this model uses realistic brain geometry and incorporated the differences in transport properties of the white and gray matters, the effect of ventricle at the boundary, and the effect of edema, which may cause a significant increase in interstitial fluid pressure in the brain. The ventricle, in which approximately half of the total cerebrospinal fluid (CSF) is produced in the brain (besides from blood vessels), becomes an internal boundary to provide an escape route for the drug through the bulk flow of interstitial fluid. As the white matter has more regular arrangement of nerve fibers than in gray matter, the transport resistance in the white matter is relatively lower than in the gray matter. The model drug used in this 2D simulation is *interleukin*-2 (IL-2), which is administered via both bolus and microspheres injection as a comparison study. The pressure and velocity profiles are tracked from magnetic resonance imaging (MRI) after contrast agent administration. In the modeling perspective, this study has included the flow in porous medium using the extended form of Darcy's law and a constant lumped parameter in the species balance due to clearance into capillary and enzymatic elimination. However, the transient flow profile in the brain and its influence on drug penetration were not described in detail.

The three-dimensional simulation of human brain tumor of primitive neuroectodermal tumor (PNET) was initiated by Wang et al. [142,143]. Here, the simulation study is aimed to analyze and compare several *carmustine* delivery techniques to a real human brain tumor case, i.e. systemic administration (injection) and controlled release from polymer. Using a simplified geometry of an isolated tumor, the simulation is conducted in computational fluid dynamics software package to solve simultaneously continuity, momentum, and drug species equations. For instance, the

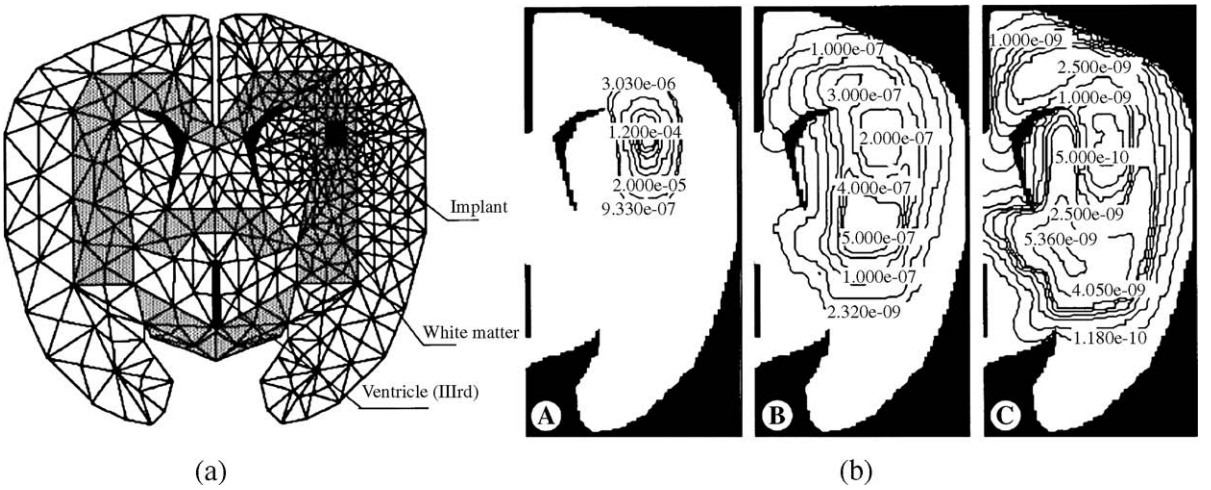

Fig. 21. (a) The 2D finite element meshes of the rabbit brain (1 mm anterior to the bregma). The grid contains 800 triangular elements and includes the implant and different brain regions (white matter, gray matter, and ventricle). (b) The IL-2 distribution profile (in g/cm^3) involving diffusion, convective transport, and edema effect at time point of hour 1 (A), hour 6 (B), and hour 12 (C) (reprinted from [141] with permission from The American Physiological Society).

drug source term (F_s) in Eq. (106) is modeled by the following:

$$F_s = F_v(1-\sigma)C_v + PS/V(C_v - C_i)Pe_v/(e^{P_{ev}}-1) \tag{109}$$

where σ and C_v are the osmotic reflection coefficient and drug concentration in the vascular space, respectively. P is the transcapillary permeability of the drug molecule. The transcapillary Peclet number (Pe_v) is given by:

$$P_{ev} = \frac{F_v(1-\sigma)}{PS/V} \tag{110}$$

This model examines in detail the contribution of convective transport of macromolecular and small molecular drugs in the vicinity of tumor and reproduced Baxter and Jain's model prediction for elevated pressure profile in the tumor. However, the transport properties are only distinguished in terms of tumor and normal brain tissue and the possible effect of edema has not been incorporated. Simulation results suggest that, since the penetration depth of *carmustine* is very short due to high elimination rate, the polymer implantation approach provided higher mean concentration, longer exposure time, and reduced systemic toxicity as compared to bolus injection treatment. This study provides insight that the computer simulation can be employed to optimize the type and dosage of drug delivery in the tissue before any experimental work is conducted for validation. Using a 2D simplified geometry of PNET together with discrete placement of Gliadel® wafer discs, the simulation to investigate the transient interstitial fluid flow due to surgical cavity with the presence of post-surgery edema was conducted by Teo et al. [144]. The study evaluated the impact of surgical excision of tumor on the resulting transient interstitial fluid flow field and efficiency of drug delivery. It further suggests that the presence of the post-surgery edema increases the interstitial pressure and fluid velocity, thereby causing higher relative toxicity in the surrounding normal tissue.

Tan et al. [145,146] improved the 3D human brain tumor model by reconstructing the 3D isolated tumor geometry from a magnetic resonance image (MRI) and incorporating the effect of vasogenic edema (Fig. 22). In both studies, the model drug is a radiosensitizer, *etanidazole*. Since there is no functioning lymphatics in the brain, F_{1s} is also negligible ($F_{1s} \sim 0$). In view of the order of magnitude for Pe_v, a simplified expression for F_s is used. The

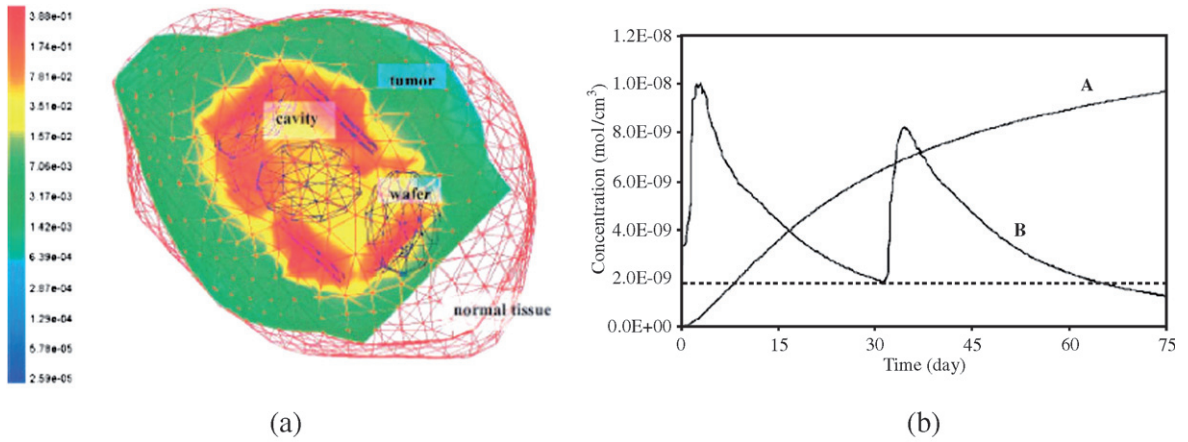

Fig. 22. (a) Contour plot of *etanidazole* concentration (in kg/m^3) in a planar cut-section parallel to the *z*-axis at hour 20; and (b) mean *etanidazole* concentration profiles for zero-order release system (A) and double-burst release system (B). The dotted lines represent the fictitious minimum threshold concentration of *etanidazole* (reprinted from [145] with permission from Wiley-Liss, Inc., a subsidiary of John Wiley & Sons, Inc. Copyright © 2003).

constitutive equations for F_s and R terms in Eq. (104) for various regimes are given by:

$$F_{s,\text{etanidazole}} = \left\{ \begin{array}{ll} S_0 e^{-t/t_r} & \text{in wafers} \\ -\dfrac{PS}{V} C & \text{in tumor and tissues} \\ 0 & \text{in cavity} \end{array} \right\}$$

$$R_{\text{etanidazole}} = \left\{ \begin{array}{ll} k_{\text{app,cavity}} C & \text{in cavity} \\ k_{\text{app,tissue}} C & \text{in tumor and normal tissues} \\ 0 & \text{elsewhere} \end{array} \right\} \quad (111)$$

where S_0 and t_r can be obtained by fitting experimental *etanidazole* release profile.

In the first study, the different mechanisms of drug release from polymer implants, i.e. linear and double-burst release systems, were investigated [145]. The simulation results suggest that the double-burst release system provided a higher drug penetration depth and reasonably similar therapeutic index as compared to those of linear release system. In this case, the therapeutic index is defined as the ratio of mean drug concentration in the tumor region to that of the normal tissue region.

The second study by Tan et al. [146] emphasized on the effect of the surgical opening on the delivery efficiency of drug and polymer implants (Fig. 23). It is shown that the drug efficacy was significantly lowered for open tumor case due to the convective transport of interstitial fluid to the open site. This leads to the non-uniform distribution of the drug in the tumor zone; thus, eventually decreases the drug therapeutic index. However, since in both studies the model geometry is the isolated tumor, the overall picture of the fluid flow in the brain, e.g. the contribution of fluid flow from ventricle, has not been taken into account.

The drug simulation in brain tissue poses great challenges to provide more meaningful results for biomedical applications. They include the incorporation of the accurate determination of geometric reconstruction and transport parameters by fitting to the model firstly with the normal case. In the former case, the automatic reconstruction of normal tissue and tumor geometry from medical images, i.e. magnetic resonance imaging (MRI) and computed tomography (CT) scan, is now possible owing to recent development of biomedical imaging software. This can be utilized to generate an actual modeling grid that allows a patient-specific modeling work to be conducted. In the latter case, the difficulty to obtain transport parameters experimentally can be overcome by fitting these parameters to the model with actual modeling grid owing to accurate boundary conditions of physiological variables, such as ventricular (*choroid plexus*) pressure, which are easier to measure experimentally. In addition, different therapy strategies, i.e. polymer implant, site-specific direct injection, systemic administration from vasculature,

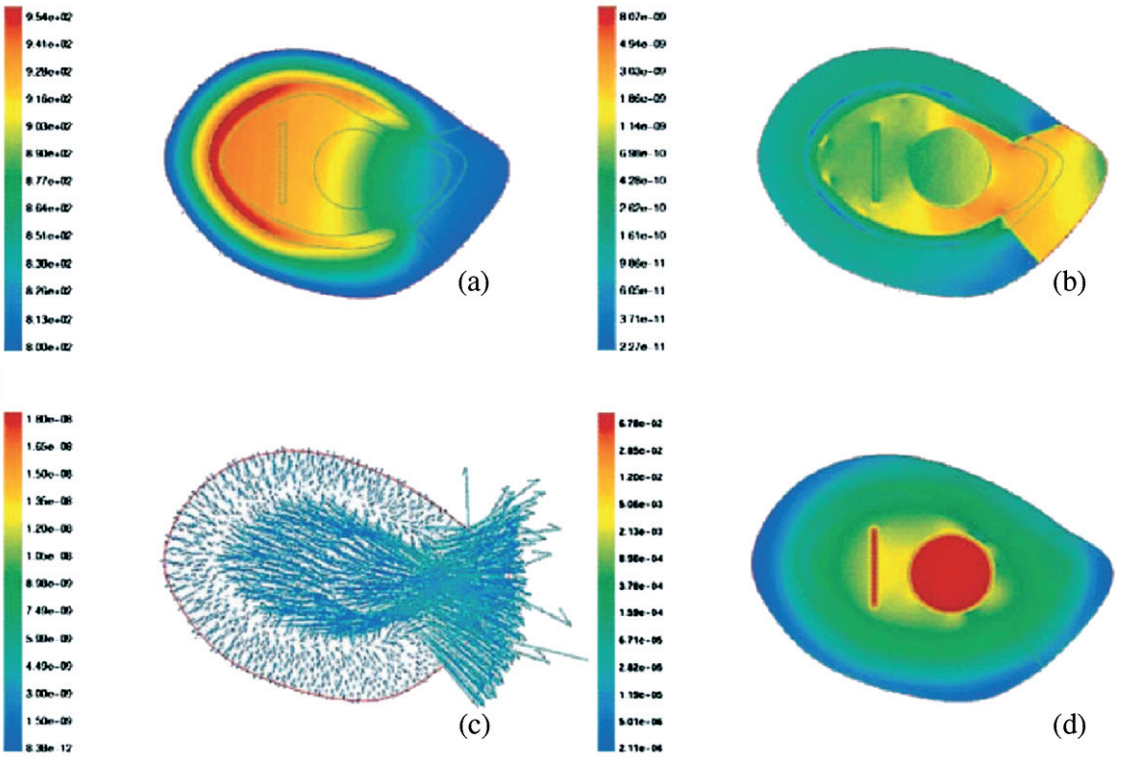

Fig. 23. (a) Pressure (Pa) and (b) velocity (m/s) contour plots at hour 20; (c) the velocity (m/s) vector plot showing the fluid loss due to surgical opening; and (d) drug distribution (kg/m^3) contour plot at hour 20 (reprinted from [146] with permission from Wiley-Liss, Inc., a subsidiary of John Wiley & Sons, Inc. Copyright © 2003).

also give variations to the modeling works in tissue drug delivery.

7.2. Simulation of drug delivery in liver

An example of drug delivery in liver is given by the trans-catheter oily chemoembolization for the treatment of *hepatoma*. The procedure involves the insertion of a catheter through an opening in the groin of the patient into the hepatic artery or its branches. The tube is then guided up the artery until it reaches the *hepatoma* in the liver. The anticancer drug *doxorubicin* is mixed with *lipiodol*, an oily contrast medium, and is injected through the tube into the blood capillaries. Here, one simulation study of doxorubicin delivery to *hepatoma* was performed by Goh et al. [147]. The model also utilizes computational fluid dynamics to solve the pressure and velocity profile in the liver tissue. However, the drug is released from trans-catheter administration via branches of hepatic artery. The transient vascular pressure (p_v) is assumed to be a step function followed by a decreasing exponential function, which can be written as follows:

$$p_v = p_{v,0}\left[1 + A\exp\left(\frac{t}{t_c}\right)\right] \tag{112}$$

In this equation, $p_{v,0}$ is the initial vascular pressure, A is the fraction increase from the initial vascular pressure due to injection of the drug and fluid, and t_c is the time-constant of decay, which depends on the tumor vasculature. The term A can be estimated for a bed of uniform parallel capillaries where the pressure drop in a laminar blood flow is related to the mean capillary flow velocity and capillary density for a given bulk flow rate. Furthermore, the plasma pharmacokinetics of *doxorubicin* is obtained from the literature data and

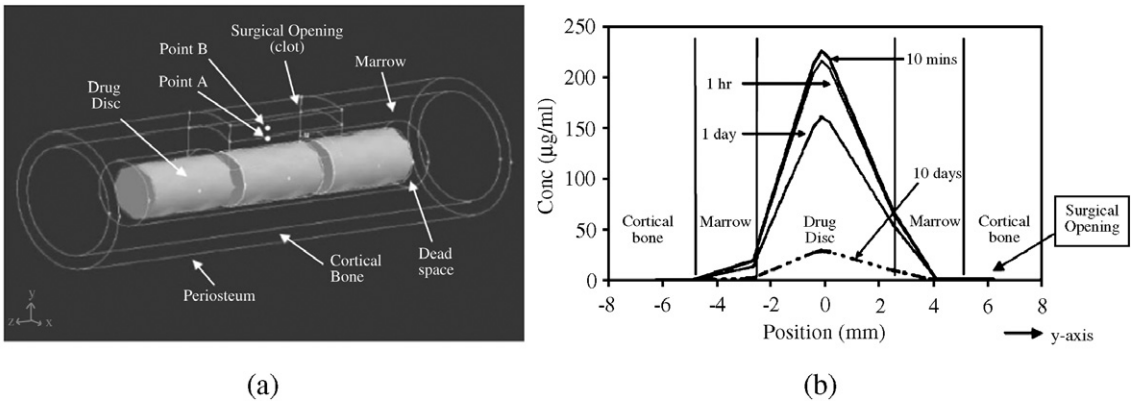

Fig. 24. (a) Simulation geometry of femur segment with implantation of PLGA drug discs; and (b) the *gentamycin* concentration profile released from the discs along the line $x=0$ in the *xy*-plane at different time points after the implantation (reprinted from [147] with permission from Wiley-Liss, Inc., a subsidiary of John Wiley & Sons, Inc. Copyright © 2001).

fitted as piecewise-smooth functions for the temporal variation of *doxorubicin* concentration.

This mathematical model is used to evaluate the sensitivity of the following few physiology and operating parameters for actual clinical treatments, such as therapeutic index, injection rate, extent of angiogenesis, lymphatic drainage, and DNA binding kinetics. It is found that, in the trans-catheter treatment, increasing the injection volume does not result in a substantial drug concentration increase in the tumor, core, and normal tissues. This is due to the small volume injection compared to fluid extravasation from the blood vessel so that the fluid volume acts as a "perfectly-stirred vessel" that dissolves the drug at a very rapid time without increasing its extravasation rate. Diffusion is the main mechanism of transport in the interstitium for free doxorubicin molecules. A smaller vascular exchange area results in lower interstitial drug concentration. Lymphatic drainage in the tumor causes negligible reductions in the mean concentrations in all three different zones. Cellular metabolism and DNA binding kinetics also decrease the mean concentrations of drug by about 15 to 40% respectively, as compared to the baseline case.

7.3. Simulation of drug delivery in bone

Lee et al. [148] developed a simulation model for antibiotic (*gentamycin*) delivery to bone tissue for *osteomyelitis* treatment that was delivered by either biodegradable polymer (PLGA) discs or non-biodegradable polymer *poly(methylmethacrylate)* (PMMA) beads (Fig. 24). In this simulation, effect of the clotting process due to surgical trauma is investigated. The clotting process is modeled by varying Darcy's permeability with time (anisotropic in nature, relatively higher permeability is observed in the axial direction), where the initial permeability is assumed to be comparable to that of *in vitro* gel and the final permeability is predicted to be the cortical bone axial permeability.

The simulation model provides quantitative predictions for the region of effective therapy for *gentamycin* concentration greater than MIC (minimum inhibitory concentration) and relates this to the contribution of various transport properties and interstitial fluid distribution. Comparison between the baseline simulation and the implantation of PLGA discs and PMMA beads is also investigated where the results show a comparable overall increase in drug concentration in all zones. It is shown that the implantation of PMMA beads into the bone led to higher mean concentration in the marrow that may be due to the difference in the geometry between the disc and the bead. The study performs sensitivity analysis on two different formulations of discs. One of them is fabricated from pure PLGA 50:50 only while the other has 30% *b-tricalcium phosphate* blended in it. The salient feature of both release profile is that they are biphasic, exhibiting an initial burst followed by a second burst about 3 weeks later. However, the differences between the two profiles include the amount of initial burst and

the time when the second burst takes place. However, PMMA carriers are not biodegradable, and have to be surgically removed at the end of treatment, causing unnecessary additional trauma to patient. In contrast, PLGA discs do not involve any second surgery for removal.

7.4. Challenges ahead the simulation of drug delivery in tissue

Since the patient validation for tissue modeling is still not fully attainable at least until now, the modeling plays a role in suggesting the appropriate release profile in order to optimize the therapeutic efficiency of an agent. This refers to the highest toxicity for the targeted tissue (e.g. tumor) and the least for the surrounding normal tissue. The simulation results can also be reverted back to provide recommendation on the required (optimized) release profile at the drug device fabrication stage. Here, there are two important issues that have to be addressed. Firstly, it is important to fit the modeling concept and results to the existing normal tissue fluid flow data. It can be achieved by allowing some undetermined variables that are difficult to obtain experimentally to fit the baseline (normal) case of the tissue fluid flow. Secondly, the emerging capability of medical imaging equipment and software to create a patient-specific simulation grid is also crucial. The patient-specific simulation grid can provide a patient-specific recommendation in terms of required dosage and release profile.

The emerging adjunct therapies for tumor treatment (besides chemotherapy), i.e. radiotherapy and anti-angiogenic therapy, become an important area where the modeling effort can play a crucial role. Radiotherapy helps the chemotherapeutic agent eliminates the tumor cells when patient undergoes irradiation after surgery. Qin et al. [149] suggested that irradiation induced the opening of BBB and, when it was combined with chemotherapy, helped enhance the survival rates by 200% (means that the patient with combined therapy had three times longer survival time) with statistically significant improvement. Several studies suggest that irradiation improves the hydraulic conductivity of BBB by increasing the fluid production from blood vessels [150] and decreasing the interstitial drug diffusion in the tumor tissue due to an increase in its collagen content [151]. Theoretically, the former will reduce the drug delivery efficacy as the additional convective effect will "wash" the drug away from the targeted site. On the other hand, the latter can help control the drug penetration confined only in smaller region, i.e. tumor. Here, the CFD simulation can be used to optimize the interplay effect of the irradiation to the Drug Delivery efficacy, for instance, by the scheduling of irradiation and chemotherapy treatments.

On the other hand, the anti-angiogenic therapy is one of the most recent important strategies to combat tumor since theoretically it will help inhibit the blood vessel vascularization that is required for tumor growth. Jain [152] hypothesized that the anti-angiogenic therapy normalized the tumor vascularization so it inhibited the tumor growth and helped the Drug Delivery to the tumor site. Kunkel et al. [153] confirmed the inhibition of *glioma* growth in intracranially implanted animal tumor models, in which tumor volume is reduced by 59% as compared to the control. It was also suggested that the interstitial fluid pressure decreases in subcutaneously implanted U87 (*glioblastoma*) tumor in nude mice [154]. From the transport perspective, this concept can be interpreted as the reduced convective effect from the tumor site, thereby, increasing the chemotherapy efficiency in the tumor site. This particular effect is also interesting to be investigated through future simulation studies.

8. Conclusions

The mathematical model and simulation of drug release from polymeric microspheres have developed and evolved to various approaches and concepts. Based on the nature of the polymeric matrices used and the behavior during drug release, these models can be distinctly categorized to diffusion-controlled, swelling-controlled, and erosion-controlled systems. For all types of systems, chemical reactions and mass transfer processes, which are affected by polymer and drug type, device size, shape, composition, and encapsulation techniques, are crucial in controlling the drug release. In this case, the choice of an appropriate mathematical model for a specific drug delivery system has to be carried out with caution.

Both molecular-level study (e.g. diffusivity, drug–polymer interaction parameters) and macroscopic study (e.g. drug release profile, molecular weight decrease profile) are important to integrate the understanding of drug release mechanisms from polymeric systems with mathematical model development. The challenges posed here are to test the drug release in the *in vivo* condition. The surrounding environment, such as pH, osmotic pressure, and tissue elimination, will influence the drug release profile, especially for bioerodible polymeric systems, in which the degradation process would be strongly affected. One may expect that, especially for bioerodible polymer matrix system, the *in vivo* release is faster than *in vitro* release as degradation rate is enhanced due to enzymatic reactions. Other important challenge that has been addressed in this review is to account for the possibility of altering the drug release profile by applying the sterilization procedures, i.e. γ-irradiation.

Even though the use of simple empirical or semi-empirical models is sufficient, the detailed mechanism regarding the drug release process is not fully elucidated. Therefore, there is still room for improvement for mechanistic model to highlight the important drug release mechanism for different systems. In this case, when reliable and detailed information on drug release process is available, mechanistic models are the best to apply. However, it does not mean that the more complex the mechanistic model is, the better it is. The most ideal model is the simplest model that is able to satisfy the theory of step-by-step drug release mechanisms for general cases and highlight the important process affecting the drug release profile.

Future drug delivery modeling efforts would be mainly focused on the drug transport in tissue after it is released from systemic administration or implanted polymeric devices. Linked to the concept of computational fluid dynamics, the modeling involves the complex interplay of possible processes of drug diffusion and convective transport in extracellular matrices, drug extravasation from blood vessels (when the device is systematically administered), tissue elimination by lymphatic system, and intracellular internalization and degradation. In this case, the *in vitro* drug release profile may not be appropriate for this purpose of modeling as the realistic physiological condition may substantially change the mechanism of drug release.

Acknowledgements

This work was supported by Science and Engineering Research Council (SERC), Singapore and National University of Singapore under the grant number R279-000-208-305. The authors are grateful to Professor Kenneth A. Smith (Department of Chemical Engineering, MIT) for helpful discussion on this project. We would also thank J. Xie and L.K. Lim for their technical support in the course of this study.

References

[1] K.W. Leong, R. Langer, Polymeric controlled Drug Delivery, Advanced Drug Delivery Reviews 1 (1987) 199–233.
[2] J.-M. Vergnaud, Controlled Drug Release of Oral Dosage Forms, Ellis Horwood Limited, Chichester, 1993.
[3] J. Crank, The Mathematics of Diffusion, 2nd ed., Clarendon Press, Oxford, 1975.
[4] R.W. Baker, H.K. Lonsdale, Controlled release: mechanisms and rates, in: A.C. Tanquarry, R.E. Lacey (Eds.), Controlled Release of Biologically Active Agents, Plenum Press, New York, NY, 1974, pp. 15–71.
[5] R. Baker, Controlled Release of Biologically Active Agents, John Wiley & Sons, 1987.
[6] T. Higuchi, Mechanism of sustained-action medication: theoretical analysis of rate of release of solid drugs dispersed in solid matrices, Journal of Pharmaceutical Sciences 52 (1963) 1145–1149.
[7] T. Koizumi, S.P. Panomsuk, Release of medicaments from spherical matrices containing drug in suspension: theoretical aspects, International Journal of Pharmaceutics 116 (1995) 45–49.
[8] D.S. Cohen, T. Erneux, Controlled drug release asymptotics, SIAM Journal on Applied Mathematics 58 (4) (1998) 1193–1204.
[9] P.I. Lee, Diffusional release of a solute from a polymeric matrix — approximate analytical solutions, Journal of Membrane Science 7 (1980) 255–275.
[10] D.R. Paul, S.K. McSpadden, Diffusional release of a solute from a polymer matrix, Journal of Membrane Science 1 (1976) 33–48.
[11] M.J. Abdekhodaie, Y.-L. Cheng, Diffusional release of a dispersed solute from a spherical polymer matrix, Journal of Membrane Science 115 (1996) 171–178.
[12] M.J. Abdekhodaie, Y.-L. Cheng, Diffusional release of a dispersed solute from planar and spherical matrices into finite external volume, Journal of Controlled Release 43 (1997) 175–182.
[13] X.Y. Wu, Y. Zhou, Studies of diffusional release of a dispersed solute from polymeric matrixes by finite element method, Journal of Pharmaceutical Sciences 88 (10) (1999) 1050–1057.
[14] Y. Zhou, X.Y. Wu, Theoretical analyses of dispersed-drug release from planar matrices with a boundary layer in a finite medium, Journal of Controlled Release 84 (2002) 1–13.

[15] Y. Zhou, X.Y. Wu, Modeling and analysis of dispersed-drug release into a finite medium from sphere ensembles with a boundary layer, Journal of Controlled Release 90 (2003) 23–26.
[16] J. Siepmann, A. Peppas, Modeling of drug release from delivery systems based on hydroxypropyl methylcellulose (HPMC), Advanced Drug Delivery Reviews 48 (2001) 139–157.
[17] B. Narasimhan, Mathematical models describing polymer dissolution: consequences for Drug Delivery, Advanced Drug Delivery Reviews 48 (2001) 195–210.
[18] P. Costa, J.M.S. Lobo, Modeling and comparison of dissolution profiles, European Journal of Pharmaceutical Sciences 13 (2001) 123–133 P.I.
[19] Lee, N.A. Peppas, Prediction of polymer dissolution in swellable controlled-release systems, Journal of Controlled Release 6 (1987) 207–215.
[20] T. Alfrey Jr., E.F. Gurnee, W.G. Lloyd, Diffusion in glassy polymers, Journal of Polymer Science. Part C 12 (1966) 249–261.
[21] R.W. Korsmeyer, S.R. Lustig, N.A. Peppas, Solute and pentrant diffusion in swellable polymers. I. Mathematical modeling, Journal of Polymer Science. Polymer Physics Edition 24 (1986) 395–408.
[22] R.W. Korsmeyer, E. von Meerwall, N.A. Peppas, Solute and penetrant diffusion in swellable polymers. II. Verification of theoretical models, Journal of polymer science. Polymer physics edition 24 (1986) 409–434.
[23] P.L. Ritger, N.A. Peppas, A simple equation for description of solute release. I. Fickian and non-Fickian release from non-swellable devices in the form of slabs, spheres, cylinders or discs, Journal of Controlled Release 5 (1987) 23–26.
[24] P.L. Ritger, N.A. Peppas, A simple equation for description of solute release. II. Fickian and anomalous release from swellable devices, Journal of Controlled Release 5 (1987) 37–42.
[25] H. Kim, R. Fassihi, Application of binary polymer system in drug release rate modulation. 2. Influence of formulation variables and hydrodynamic conditions on release kinetics, Journal of Pharmaceutical Sciences 83 (1997) 323–328.
[26] J.L. Ford, K. Mitchell, P. Rowe, D.J. Armstrong, P.N.C. Elliott, C. Rostron, J.E. Hogan, Mathematical modeling of drug release from hydroxypropylmethylcellulose matrices: effect of temperature, International Journal of Pharmaceutics 71 (1991) 95–104.
[27] N.A. Peppas, J.J. Sahlin, A simple equation for the description of solute release. III. Coupling of diffusion and relaxation, International Journal of Pharmaceutics 57 (1989) 169–172.
[28] R.T.C. Ju, P.R. Nixon, M.V. Patel, Drug release from hydrophilic matrices. 1. New scaling laws for predicting polymer and drug release based on the polymer disentanglement concentration and the diffusion layer, Journal of Pharmaceutical Sciences 84 (12) (1995) 1455–1463.
[29] R.T.C. Ju, P.R. Nixon, M.V. Patel, D.M. Tong, Drug release from hydrophilic matrices. 2. A mathematical model based on the polymer disentanglement concentration and the diffusion layer, Journal of Pharmaceutical Sciences 84 (12) (1995) 1464–1477.
[30] J.S. Papanu, D.S. Soane, A.T. Bell, D.W. Hess, Transport models for swelling and dissolution of thin polymer films, Journal of Applied Polymer Science 38 (1989) 859–885.
[31] P. Colombo, R. Bettini, P. Santi, A.D. Ascentiis, N.A. Peppas, Analysis of the swelling and release mechanisms from Drug Delivery systems with emphasis on drug solubility and water transport, Journal of Controlled Release 39 (1996) 231–237.
[32] R.S. Harland, A. Gazzaniga, M.E. Sangalli, P. Colombo, N.A. Peppas, Drug–polymer matrix swelling and dissolution, Pharmaceutical Research 5 (1988) 488–494.
[33] U. Conte, P. Colombo, A. Gazzaniga, M.E. Sangalli, A. La Manna, Swelling-activated Drug Delivery systems, Biomaterials 9 (1988) 489–493.
[34] B. Narasimhan, N.A. Peppas, Molecular analysis of Drug Delivery systems controlled by dissolution of the polymer carrier, Journal of Pharmaceutical Sciences 86 (3) (1997) 297–304.
[35] J.S. Vrentas, C.M. Vrentas, Energy effects for solvent self-diffusion in polymer–solvent systems, Macromolecules 26 (1993) 1277–1281.
[36] J.S. Vrentas, C.M. Vrentas, Solvent self-diffusion in rubbery polymer–solvent systems, Macromolecules 27 (1994) 4684–4690.
[37] J.S. Vrentas, C.M. Vrentas, Solvent self-diffusion in glassy polymer–solvent systems, Macromolecules 27 (1994) 5570–5576.
[38] P.J. Flory, J. Rehner, Statistical mechanics of cross-linked polymer networks. II. Swelling, The Journal of Chemical Physics 11 (1943) 521–526.
[39] J. Siepmann, H. Kranz, R. Bodmeier, N.A. Peppas, HPMC-matrices for controlled Drug Delivery: a new model combining diffusion, swelling, and dissolution mechanisms and predicting the release kinetics, Pharmaceutical Research 16 (11) (1999) 1748–1756.
[40] J. Siepmann, N.A. Peppas, Hydrophilic matrices for controlled Drug Delivery: an improved mathematical model to predict the resulting drug release kinetics (the "sequential layer" model), Pharmaceutical Research 17 (10) (2000) 1290–1298.
[41] J. Siepmann, A. Sterubel, N.A. Peppas, Understanding and predicting Drug Delivery from hydrophilic matrix tablets using the "sequential layer" model, Pharmaceutical Research 19 (3) (2002) 306–314.
[42] J. Siepmann, H. Kranz, N.A. Peppas, R. Bodmeier, Calculation of the required size and shape of hydroxypropyl methylcellulose matrices to achieve desired drug release profiles, International Journal of Pharmaceutics 201 (2000) 151–164.
[43] A.G. Hausberger, P.P. DeLuca, Characterization of biodegradable poly(D,L-lactide-co-glycolide) polymers and microspheres, Journal of Pharmaceutical and Biomedical Analysis 13 (6) (1995) 747–760.
[44] N. Kumar, R.S. Langer, A.J. Domb, Polyanhydrides: an overview, Advanced Drug Delivery Reviews 54 (2002) 889–910.
[45] F. Von Burkersroda, L. Schedl, A. Göpferich, Why degradable polymers undergo surface erosion or bulk erosion, Biomaterials 23 (2002) 4221–4231.

[46] C.N. Satterfield, C.K. Colton, W.H. Pitcher Jr., Restricted diffusion in liquids within fine pores, AIChE Journal 19 (3) (1973) 628–635.
[47] W.M. Deen, Hindered transport of large molecules in liquid-filled pores, AIChE Journal 33(9) 1409–1425.
[48] W. Weibull, A statistical distribution of wide applicability, Journal of Applied Mechanics 18 (1951) 293–297.
[49] F. Langenbucher, Linearization of dissolution rate curves by the Weibull distribution, Journal of Pharmacy and Pharmacology 24 (1972) 979–981.
[50] G.K. Vudathala, J.A. Rogers, Dissolution of fludrocortisones from phospholipid coprecipitates, Journal of Pharmaceutical Sciences 82 (1992) 282–286.
[51] A. Dokoumetzidis, V. Papadopoulou, P. Macheras, Analysis of dissolution data using modified versions of Noyes–Whitney equation and the Weibull function, Pharmaceutical Research 23 (2) (2006) 256–261.
[52] H.B. Hopfenberg, Controlled release from erodible slabs, cylinders, and spheres, in: D.R. Paul, F.W. Harris (Eds.), Controlled Release Polymeric Formulations, ACS Symposium Series, vol. 33, American Chemical Society, Washington, 1976, pp. 26–31.
[53] A.W. Hixson, J.H. Crowell, Dependence of reaction velocity upon surface and agitation, Industrial and Engineering Chemistry Research 23 (1931) 923–931.
[54] S.K. El-Arini, H. Leuenberger, Dissolution properties of praziquantel–PVP systems, Pharmaceutica Acta Helvetiae 73 (2) (1998) 89–94.
[55] D.O. Cooney, Effect of geometry on the dissolution of pharmaceutical tablets and other solids: surface detachment kinetics controlling, AIChE Journal 18 (2) (1972) 446–449.
[56] M. Zhang, Z. Yang, L.L. Chow, C.H. Wang, Simulation of drug release from biodegradable polymeric microspheres with bulk and surface erosions, Journal of Pharmaceutical Sciences 92 (10) (2003) 2040–2056.
[57] D. Larobina, G. Mensitieri, M.J. Kipper, B. Narasimhan, Mechanistic understanding of degradation in bioerodible polymers for Drug Delivery, AIChE Journal 48 (12) (2002) 2960–2970.
[58] J. Siepmann, N. Faisant, J. Benoit, A new mathematical model quantifying drug release from bioerodible microparticles using Monte Carlo simulations, Pharmaceutical Research 19 (12) (2002) 1885–1893.
[59] R.S. Harland, C. Dubernet, J.-P. Benoit, N.A. Peppas, A model of dissolution-controlled, diffusional drug release from non-swellable polymeric microspheres, Journal of Controlled Release 7 (1988) 207–215.
[60] J. Heller, R.W. Baker, Theory and practice of controlled Drug Delivery from bioerodible polymers, in: W. Baker (Ed.), Controlled Release of Bioactive Materials, Academic Press, New York, 1980, pp. 1–18.
[61] A.G. Thombre, K.J. Himmelstein, A simultaneous transport-reaction model for controlled Drug Delivery from catalyzed bioerodible polymer matrices, AIChE Journal 31 (5) (1985) 759–766.
[62] A. Charlier, B. Leclerc, G. Couarraze, Release of mifepristone from biodegradable matrices: experimental and theoretical evaluations, International Journal of Pharmaceutics 200 (2000) 115–120.
[63] C. Raman, C. Berkland, K. Kim, D.W. Pack, Modeling small-molecule release from PLG microspheres: effects of polymer degradation and nonuniform drug distribution, Journal of Controlled Release 103 (2005) 149–158.
[64] J. He, C. Zhong, J. Mi, Modeling of drug release from bioerodible polymer matrices, Drug Delivery 12 (2005) 251–259.
[65] J.F. Fitzgerald, O.I. Corrigan, Mechanisms governing drug release from poly α-hydroxy aliphatic esters, diltiazem base release from poly-lactide-co-glycolide delivery systems, in: M. A. El-Nokaly, D.M. Piatt, B.A. Charpentier (Eds.), Polymeric Delivery Systems, Properties and Applications, ACS Symposium Series, vol. 520, American Chemical Society, Washington, 1993, pp. 311–326.
[66] J. Siepmann, N. Faisant, J. Akiki, J. Richard, J.P. Benoit, Effect of the size of biodegradable microparticles on drug release: experiment and theory, Journal of Controlled Release 96 (2004) 123–134.
[67] R. Wada, S.-H. Hyon, Y. Ikada, Kinetics of diffusion-mediated drug release enhanced by matrix degradation, Journal of Controlled Release 37 (1995) 151–160.
[68] T. Ehtezazi, C. Washington, Controlled release of macromolecules from PLA microspheres: using porous structure topology, Journal of Controlled Release 68 (2000) 361–372.
[69] J. Siepmann, K. Elkharraz, F. Siepmann, D. Klose, How autocatalysis accelerates drug release from PLGA-based microparticles: a quantitative treatment, Biomacromolecules 6 (2005) 2312–2319.
[70] R.P. Batycky, J. Hanes, R. Langer, D.A. Edwards, A theoretical model of erosion and macromolecular drug release from biodegrading microspheres, Journal of Pharmaceutical Sciences 86 (12) (1997) 1464–1477.
[71] E. Shen, R. Pizsczek, B. Dziadul, B. Narasimhan, Microphase separation in bioerodible copolymers for Drug Delivery, Biomaterials 22 (2001) 201–210.
[72] K. Zygourakis, Development and temporal evolution of erosion fronts in bioerodible controlled release devices, Chemical Engineering Science 45 (8) (1990) 2359–2366.
[73] K. Zygourakis, P.A. Markenscoff, Computer-aided design of bioerodible devices with optimal release characteristics: a cellular automata approach, Biomaterials 17 (2) (1996) 125–135.
[74] A. Gopferich, R. Langer, Modeling of polymer erosion, Macromolecules 26 (1993) 4105–4112.
[75] A. Gopferich, R. Langer, The influence of microstructure and monomer properties on the erosion mechanism of a class of polyanhydrides, Journal of Polymer Science. Part A, Polymer Chemistry 31 (1993) 2445–2458.
[76] A. Gopferich, R. Langer, Modeling of polymer erosion in three dimensions: rotationally symmetric devices, AIChE Journal 41 (10) (1995) 2292–2299.
[77] A. Gopferich, Mechanisms of polymer degradation and erosion, Biomaterials 17 (2) (1996) 103–114.
[78] A. Gopferich, R. Langer, Modeling monomer release from bioerodible polymers, Journal of Controlled Release 33 (1995) 55–69.

[79] M.J. Kipper, B. Narasimhan, Molecular description of erosion phenomena in biodegradable polymers, Macromolecules 38 (2005) 1989–1999.
[80] C.C. Chu, N.D. Campbell, Scanning electron microscopic study of the hydrolytic degradation of poly(glycolic acid_suture, Journal of Biomedical Materials Research 16 (4) (1982) 417–430.
[81] M.B. Sintzel, A. Merkli, C. Tabatabay, R. Gurny, Influence of irradiation sterilization on polymers used as drug carriers — a review, Drug Development and Industrial Pharmacy 23 (9) (1997) 857–878.
[82] A.G. Hausberger, R.A. Kenley, P.P. DeLuca, Gamma irradiation effects on molecular weight and in vitro degradation of poly(D,L-lactid-co-glycolide microparticles, Pharmaceutical Research 12 (6) (1995) 851–856.
[83] C. Volland, M. Wolff, T. Kissel, The influence of terminal gamma-sterilization on captopril containing poly(D,L-lactide-co-glycolide) microspheres, Journal of Controlled Release 31 (1994) 293–305.
[84] D. Mohr, M. Wolff, T. Kissel, Gamma irradiation for terminal sterilization of 17β-estradiol loaded poly(D,L-lactide-co-glycolide) microparticles, Journal of Controlled Release 61 (1999) 203–217.
[85] S. Yoshioka, Y. Aso, T. Otsuka, S. Kojima, The effect of γ-irradiation on drug release from poly(lactide) microspheres, Radiation Physics and Chemistry 2 (1995) 281–285.
[86] S. Yoshioka, Y. Aso, S. Kojima, Drug release from poly(DL-lactide) microspheres controlled by γ-irradiation, Journal of Controlled Release 37 (1995) 263–267.
[87] N. Faisant, J. Siepmann, P. Oury, V. Laffineur, E. Bruna, J. Haffner, J.P. Benoit, The effect of gamma-irradiation on drug release from bioerodible microparticles: a quantitative treatment, International Journal of Pharmaceutics 242 (2002) 281–284.
[88] N. Faisant, J. Siepmann, J. Richard, J.P. Benoit, Mathematical modeling of drug release from bioerodible microparticles: effect of gamma-irradiation, European Journal of Pharmaceutics and Biopharmaceutics 56 (2003) 271–279.
[89] L. Montanari, M. Costantini, E.C. Signoretti, L. Valvo, M. Santucci, M. Bartolomei, P. Fattibene, S. Onori, A. Faucitano, B. Conti, I. Genta, Gamma irradiation effects on poly(DL-lactide-co-glycolide) microspheres, Journal of Controlled Release 56 (1998) 219–229.
[90] K.S. Soppimath, T.M. Aminabhavi, A.R. Kulkarni, W.E. Rudzinski, Biodegradable polymeric nanoparticles as Drug Delivery devices (review), Journal of Controlled Release 70 (2001) 1–20.
[91] J.P. Vasir, M.K. Reddy, V.D. Labhasetwar, Nanosystems in drug targeting: opportunities and challenges, Current Nanoscience 1 (2005) 47–64.
[92] T. Niwa, H. Takeuchi, T. Hino, N. Kunou, Y. Kawashima, Preparations of biodegradable nanospheres of water-soluble and insoluble drugs with D,L-lactide/glycolide copolymer by a novel spontaneous emulsification solvent diffusion method and the drug release behavior, Journal of Controlled Release 25 (1993) 89–98.
[93] C. Fonseca, S. Simoes, R. Gaspar, Paclitaxel-loaded PLGA nanoparticles: preparation, physiochemical characterization and in vitro anti-tumoral activity, Journal of Controlled Release 83 (2002) 273–286.
[94] P. Chattopadhyay, R.B. Gupta, Supercritical CO_2 based production of magnetically responsive micro- and nanoparticles for drug targeting, Industrial and Engineering Chemistry Research 41 (2002) 6049–6058.
[95] T.W. Randolph, A.D. Randolph, M. Mebes, S. Yeung, Sub-micrometer-sized biodegradable particles of poly (L-lactic acid) via the gas antisolvent spray precipitation process, Biotechnology Progress 9 (1993) 429–435.
[96] D.J. Jarmer, C.S. Lengsfeld, T.W. Randolph, Manipulation of particle size distribution of poly(L-lactic acid) nanoparticles with a jet-swirl nozzle during precipitation with a compressed antisolvent, Journal of Supercritical Fluids 27 (2003) 317–336.
[97] J. Xie, C.H. Wang, Self-assembled biodegradable nanoparticles developed by direct dialysis for the delivery of paclitaxel, Pharmaceutical Research 22 (12) (2005) 2079–2090.
[98] R.A. Roman, A. Naik, Y.N. Kalia, R.H. Guy, H. Fessi, Skin penetration and distribution of polymeric nanoparticles, Journal of Controlled Release 99 (2004) 53–62.
[99] M.P. Desai, V. Labhasetwar, G.L. Amidon, R.J. Levy, Gastrointestinal uptake of biodegradable microparticles: effect of particle size, Pharmaceutical Research 13 (12) (1996) 1838–1845.
[100] L.B. Peppas, Recent advances on the use of biodegradable microparticles and nanoparticles in controlled drug delivery, International Journal of Pharmaceutics 116 (1995) 1–9.
[101] R. Gref, Y. Minamitake, M.T. Peracchia, V. Trubetskoy, V. Torchilin, R. Langer, Biodegradable long-circulating polymeric nanospheres, Science 263 (1994) 1600–1603.
[102] D.B. Chen, T.Z. Yang, W.L. Lu, Q. Zhang, In vitro and in vivo study of two types of long-circulating solid lipid nanoparticles containing paclitaxel, Chemical and Pharmaceutical Bulletin 49 (11) (2001) 1444–1447.
[103] L. Mu, S.S. Feng, Fabrication, characterization and in vitro release of paclitaxel (Taxol®) loaded poly (lactic-co-glycolic acid) microspheres prepared by spray drying technique with lipid/cholesterol emulsifiers, Journal of Controlled Release 76 (2001) 239–254.
[104] K.E. Lee, B.K. Kim, S.H. Yuk, Biodegradable polymeric nanospheres formed by temperature-induced phase transition in a mixture of poly(lactide-co-glycolide) and poly(ethylene oxide)–poly(propylene oxide)–poly(ethylene oxide) triblock copolymer, Biomacromolecules 3 (2002) 1115–1119.
[105] C. Fonseca, S. Simoes, R. Gaspar, Paclitaxel-loaded PLGA nanoparticles: preparation, physicochemical characterization and in vitro anti-tumoral activity, Journal of Controlled Release 83 (2002) 273–286.
[106] L. Mu, S.S. Feng, Vitamin E TPGS used as emulsifier in the solvent evaporation extraction technique for fabrication of polymeric nanospheres for controlled release of paclitaxel (Taxol®), Journal of Controlled Release 80 (2002) 139–144.
[107] L. Mu, S.S. Feng, PLGA/TPGS nanoparticles for controlled release of paclitaxel: effects of the emulsifier and drug loading ratio, Pharmaceutical Research 20 (11) (2003) 1864–1872.
[108] L. Mu, S.S. Feng, A novel controlled release formulation for the anticancer drug paclitaxel (Taxol®): PLGA nanoparticles

containing vitamin E TPGS, Journal of Controlled Release 86 (2003) 33–48.
[109] Z. Zhang, S.S. Feng, Nanoparticles of poly(lactide)/vitamin E TPGS copolymer for cancer chemotherapy: synthesis, formulation, characterization and in vitro release, Biomaterials 27 (2006) 262–270.
[110] Potineni, D.M. Lynn, R. Langer, M.M. Amiji, Poly(ethylene oxide)-modified poly(b-amino ester) nanoparticles as a pH-sensitive biodegradable system for paclitaxel delivery, Journal of Controlled Release 86 (2003) 223–234.
[111] J.H. Kim, Y.S. Kim, S. Kim, J.H. Park, K. Kim, K. Choi, H. Chung, S.Y. Jeong, R.W. Park, I. Kim, I.C. Kwon, Hydrophobically modified glycol chitosan nanoparticles as carriers for paclitaxel, Journal of Controlled Release 111 (2006) 228–234.
[112] R.T. Liggins, H.M. Burt, Paclitaxel loaded poly(L-lactic acid) microspheres: properties of microspheres made with low molecular weight polymers, International Journal of Pharmaceutics 222 (2001) 19–33.
[113] R.T. Liggins, H.M. Burt, Paclitaxel loaded poly(L-lactic acid) microspheres II: the effect of processing parameters on microsphere morphology and drug release kinetics, International Journal of Pharmaceutics 281 (2004) 103–106.
[114] M. Polakovic, T. Gorner, R. Gref, E. Dellacherie, Lidocaine loaded biodegradable nanospheres II. Modelling of drug release, Journal of Controlled Release 60 (1999) 169–177.
[115] C. Kang, S.P. Schwendeman, Determination of diffusion coefficient of a small hydrophobic probe in poly (lactide-co-glycolide) microparticles by laser scanning confocal microscopy, Macromolecules 36 (2003) 1324–1330.
[116] S.R. Van Tomme, B.G. De Geest, K. Braeckmans, S.C. De Smedt, F. Siepmann, J. Siepmann, C.F. van Nostrum, W.E. Hennick, Mobility of model proteins in hydrogels composed of oppositely charged dextran microspheres studied by protein release and fluorescence recovery after photobleaching, Journal of Controlled Release 110 (1) (2005) 67–78.
[117] Y. Zhang, C.C. Chu, Biodegradable dextran–polylactide hydrogel network and its controlled release of albumin, Journal of Biomedical Materials Research 54 (1) (2000) 1–11.
[118] H.M. Wong, J.J. Wang, C.H. Wang, In vitro sustained release of human immunoglobulin G from biodegradable microspheres, Industrial and Engineering Chemistry Research 40 (2001) 933–948.
[119] T.H. Lee, F.J. Wang, C.H. Wang, Double-walled microspheres for the sustained release of a highly water soluble drug: characterization and irradiation studies, Journal of Controlled Release 83 (2002) 437–452.
[120] J.F. Gross, A.S. Popel, Mathematical models of transport phenomena in normal and neoplastic tissue, in: H.I. Peterson (Ed.), Tumor Blood Circulation, CRC Press, Boca Raton, 1979, pp. 169–183.
[121] E.H. Starling, On the absorption of fluids from the connective tissue spaces, Journal of Physiology 19 (1986) 312–326.
[122] F.E. Curry, Mechanics and thermodynamics of transcapillary exchange, in: E.M. Renkin, C.C Michel (Eds.), Handbook of Physiology, Section 2: the Cardiovascular System), Amer. Physiol. Soc., Bethesda, 1984, pp. 309–374.
[123] L.T. Baxter, R.K. Jain, Transport of fluid and macromolecules in tumors. I. Role of interstitial pressure and convection, Microvascular Research 37 (1989) 77–104.
[124] M.F. Haller, W.M. Saltzman, Localized delivery of proteins in the brain: can transport be customized? Pharmaceutical Research 15 (3) (1998) 377–385.
[125] R.G. Larson, L.E. Scriven, H.T. Davis, Percolation theory of two phase flow in porous media, Chemical Engineering Science 36 (1981) 57–73.
[126] W.M. Saltzman, R. Langer, Transport rates of proteins in porous materials with known microgeometry, Biophysical Journal 55 (1989) 163–171.
[127] C. Nicholson, L. Tao, Hindered diffusion of high molecular weight compounds in brain extracellular microenvironment measured with integrative optical imaging, Biophysical Journal 65 (1993) 2277–2290.
[128] W.M. Saltzman, M.L. Radomsky, K.J. Whaley, R.A. Cone, Antibody diffusion in human cervical mucus, Biophysical Journal 66 (1993) 508–515.
[129] M. Stroh, W.R. Zipfel, R.M. Williams, W.W. Webb, W.M. Saltzman, Diffusion of nerve growth factor in rat striatum as determined by multiphoton microscopy, Biophysical Journal 85 (2003) 581–588.
[130] D.K. Binder, M.C. Papadopoulos, P.M. Haggie, A.S. Verkman, In vivo measurement of brain extracellular space diffusion by cortical surface photobleaching, The Journal of Neuroscience 24 (37) (2004) 8049–8056.
[131] R.G. Thorne, S. Hrabětová, C. Nicholson, Diffusion of epidermal growth factor in rat brain extracellular space measured by integrative optical imaging, Journal of Neurophysiology 92 (2004) 3471–3481.
[132] R.G. Thorne, C. Nicholson, In vivo diffusion analysis with quantum dots and dextrans predicts the width of brain extracellular space, PNAS 103 (14) (2006) 5567–5572.
[133] W.M. Saltzman, M.L. Radomsky, Drugs released from polymers: diffusion and elimination in brain tissue, Chemical Engineering Science 46 (10) (1991) 2429–2444.
[134] L.K. Fung, M. Shin, B. Tyler, H. Brem, W.M. Saltzman, Chemotherapeutic drugs released from polymers: distribution of 1,3-bis(2-chloroethyl)-1-nitrosurea in the rat brain, Pharmaceutical Research 13 (5) (1996) 671–682.
[135] J.F. Strasser, L.K. Fung, S. Eller, S.A. Grossman, W.M. Saltzman, Distribution of 1,3-bis(2-chloroethyl)-1-nitrosurea and tracers in the rabbit brain after interstitial delivery by biodegradable polymer implants, The Journal of Pharmacology and Experimental Therapeutics 275 (3) (1995) 1647–1655.
[136] K.W. Fung, M.G. Ewend, A. Sills, E.P. Sipos, R. Thompson, M. Watts, O.M. Colvin, H. Brem, W.M. Saltzman, Pharmacokinetics of interstitial delivery of carmustine, 4-hydroperoxycyclophosphadime, and paclitaxel from a biodegradable polymer implant in the monkey brain, Cancer Research 58 (1998) 672–684.
[137] A.B. Fleming, W.M. Saltzman, Pharmacokinetics of the carmustine implant, Clinical Pharmacokinetics 41 (6) (2002) 403–419.
[138] H.J. Reulen, R. Graham, M. Spatz, I. Klatzo, Role of pressure gradients and bulk flow in dynamics of vasogenic

brain edema, Journal of Neurosurgery 46 (1) (1977) 24–35.
[139] T. Nagashima, B. Horwitz, S.I. Rapoport, A mathematical model for vasogenic brain edema, Advances in Neurology 52 (1990) 317–325.
[140] T. Nagashima, T. Shirakuni, S.I. Rapoport, A two-dimensional, finite element analysis of vasogenic brain edema, Neurologia Medico-Chirurgica (Tokyo) 30 (1990) 1–9.
[141] S. Kalyanasundaram, V.D. Calhoun, K.W. Leong, A finite element model for predicting the distribution of drugs delivered intracranially to the brain, American Journal of Physiology—Regulatory, Integrative and Comparative Physiology 273 (1997) 1810–1821.
[142] C.H. Wang, J. Li, Three-dimensional simulation of IgG delivery to tumors, Chemical Engineering Science 53 (20) (1998) 3579–3600.
[143] C.H. Wang, J. Li, C.S. Teo, T. Lee, The delivery of BCNU to brain tumors, Journal of Controlled Release 61 (1999) 21–41.
[144] C.S. Teo, W.H.K. Tan, T. Lee, C.H. Wang, Transient interstitial fluid flow in brain tumors: effect on Drug Delivery, Chemical Engineering Science 60 (2005) 4803–4821.
[145] W.H.K. Tan, F.J. Wang, T. Lee, C.H. Wang, Computer simulation of the delivery of etanidazole to brain tumor from PLGA wafers: comparison between linear and double burst release systems, Biotechnology and Bioengineering 82 (3) (2003) 278–288.
[146] W.H.K. Tan, T. Lee, C.H. Wang, Simulation of intratumoral release of etanidazole: effects of the size of surgical opening, Journal of Pharmaceutical Sciences 92 (2003) 773–789.
[147] Y.M.F. Goh, H.L. Kong, C.H. Wang, Simulation of the delivery of doxorubicin to hepatoma, Pharmaceutical Research 18 (6) (2001) 761–770.
[148] C.G. Lee, Y.-C. Fu, C.H. Wang, Simulation of gentamicin delivery for the local treatment of osteomyelitis, Biotechnology and Bioengineering 91 (5) (2005) 622–635.
[149] D. Qin, G. Ou, H. Mo, Y. Song, G. Kang, Y. Hu, X. Gu, Improved efficacy of chemotherapy for glioblastoma by radiation induced opening of blood–brain barrier: clinical results, International Journal of Radiation Oncology, Biology, Physics 51 (2001) 959–962.
[150] M.V. Vulpen, H.B. Kal, M.J.B. Taphoorn, S.Y. El Sharouni, Changes in blood–brain barrier permeability induced by radiotherapy: implications for timing of chemotherapy? (Review), Oncology Reports 9 (2002) 683–688.
[151] C.A. Znati, M. Rosenstein, T.D. McKee, E. Brown, D. Turner, W.D. Bloomer, S. Watkins, R.K. Jain, Y. Boucher, Irradiation reduces interstitial fluid transport and increases the collagen content in tumors, Clinical Cancer Research 9 (2003) 5508–5513.
[152] R.K. Jain, Normalization of tumor vasculature: an emerging concept in antiangiogenic therapy, Science 307 (2005) 58–62.
[153] P. Kunkel, U. Ulbricht, P. Bohlen, M.A. Brockmann, R. Fillbrandt, D. Stavrou, M. Westphal, K. Lamszus, Inhibition of glioma angiogenesis and growth in vivo by systemic treatment with a monoclonal antibody against vascular endothelial growth factor receptor-2, Cancer Research 61 (2001) 6624–6628.
[154] R.T. Tong, Y. Boucher, S.V. Kozin, F. Winkler, D.J. Hicklin, R.K. Jain, Vascular normalization by vascular endothelial growth factor receptor 2 blockade induces a pressure gradient across the vasculature and improves drug penetration in tumors, Cancer Research 64 (2004) 3731–3736.